UNIVERSITÀ DEGLI STUDI DI PADOVA

DIPARTIMENTO DI INGEGNERIA DELL'INFORMAZIONE

DIPARTIMENTO DI INGEGNERIA DELL'INFORMAZIONE

CORSO DI LAUREA MAGISTRALE IN BIOINGEGNERIA

Effect of tibiofemoral malalignment on the contralateral hip forces in patients with unicompartmental osteoarthritis during daily motor activities: a musculoskeletal modeling analysis

Relatore: Prof. Zimi Sawacha

Laureando: Mattia Meggiolaro

Correlatore: Ing. Giordano Valente, PhD

ANNO ACCADEMICO 2021 – 2022

11 Luglio 2022

ABSTRACT

Osteoarthritis (OA) is a degenerative disease which affects articulations, in particular knees and vertebrae, and regards about 50% of people over 60. It leads to the formation of new connective and bone tissue around the area of interest, resulting in increased pain for the subject.

Tibiofemoral malalignment leads to a worsening of the OA. It consists in a deviation of the mechanical axis of the leg, resulting in modified loads distributions between medial and lateral compartments of the knee. In particular, varus malalignment, which characterizes the patients of this study, exhibits a medial translation of the axis and a consequent increment of the medial load.

In this field, High Tibial Osteotomy (HTO) represents an ideal option, especially for young patients. This surgical technique modifies the limb alignment with a consequent unloading of the damaged compartment, reducing the pain and the progression of osteoarthritis. However, HTO is currently the least performed intervention.

The aim of this thesis was to evaluate the correlation between the tibiofemoral malalignment angle in the target limb and the hip contact forces in the contralateral limb, in patients with unicompartmental knee osteoarthritis during daily activities. This project is the continuation of a previous work carried out by the colleague Nicolò Caredda, which focused on the correlation between tibiofemoral angle and knee contact loads, by distinguishing the medial and lateral components. Both of them are part of a bigger study, which is carried out at Rizzoli Orthopaedic Institute of Bologna whose aim is to evaluate how an accurately planned HTO affects the progression of knee osteoarthritis by analysing the quality of cartilage and subchondral bone in people with varus tibiofemoral alignment, by combining biomechanical and medical imaging approach.

Nineteen patients with early-stage medial osteoarthritis, who were indicated for HTO, were studied within this thesis. Subjects were randomly divided into a control and an operation group, characterized by conservative therapies and surgery, respectively, and for each of them gait analysis data were collected from 3 motor activities (walking, stair ascent and stair descent) through a stereophotogrammetric system, a set of markers, 2 force platforms and 8 EMG sensors for each limb.

First, by using subject-specific anthropometric data, a generic musculoskeletal (MSK) model was scaled within OpenSim, which is an open-source software that permits to create and analyse MSK models, and then simulate different motor activities. The tibiofemoral malalignment angle was calculated by processing RX images through the software HTO-Rplus, specifically created to plan this type of surgery. Within OpenSim, an inverse dynamic problem based on optimization was solved to compute the internal joints contact forces and muscle activations.

In the post-processing phase, the relationship between tibiofemoral malalignment and contralateral hip contact forces was evaluated through a linear correlation analysis. Then, statistical parametric mapping in a nonparametric two-tailed unpaired t-tests ($\alpha = 0.05$), and Mann-Whitney U-test ($\alpha = 0.05$) were used to study the differences between the contralateral and target limbs, throughout the gait cycles and on the force peaks, respectively. The last part of this thesis evaluates the ground reaction forces recorded during the gait analysis sessions using the force platforms, and validates the results through a comparison between muscle activations computed via OpenSim, and EMG signals across the activity cycle.

The analysis of the results reported a weak correlation between tibiofemoral malalignment in the target limb and hip contact loads in the contralateral limb, although some significant correlations were found if considering the two limbs separately. Moreover, peak force distribution and contact forces analysis highlighted a statistically significant difference between target and contralateral limbs, in favor of the latter, which was emphasized in more demanding tasks. This could be due to an antalgic compensation strategy adopted to relieve the pain in the target limb. Muscle activations showed good matching with EMG signals, except on few occasions.

However, this study has some limitations. Musculoskeletal models do not specify knee contact point locations, which have been demonstrated to affect the precision of the estimated joint loads; in addition, the calculation of the tibiofemoral angle within the software HTO-RPlus, can present a high inter- and intra-user variability. More data are needed to confirm this trend, and future developments will focus on the comparison between pre- and post-HTO contact loads, to evaluate the effectiveness of high tibial osteotomy as treatment for unicompartmental knee osteoarthritis.

CONTENTS

1. INTRODUCTION

Among the various forms of arthritis, osteoarthritis (OA) is the most common one. It consists of a degenerative joint disease which leads to the degradation of the cartilage and the consequent formation of bone spurs, resulting in pain and decreasing the capacity to perform even the simplest movements, like walking or stair ascending and descending. The knee joint is particularly affected by this disease, reporting an incidence of 16% and 23% in individuals aged 15+ and 40+ respectively (39) and typically presents the OA in the medial site, hence taking the name of unicompartmental knee osteoarthritis. Aging and overweight are the main factors which could lead to its development, but tibiofemoral alignment play a crucial role, too. Since there is currently no cure for the OA, prevention and early diagnosis are fundamental. Conservative therapies represent the first choice to treat the disease, however, surgery is necessary once the formers are no more helpful.

Total or unicompartmental knee arthroplasty were the most common surgical procedures, but in the last few decades high tibial osteotomy (HTO) became a valid substitute, in particular in treating symptomatic unicompartmental OA. Among these techniques, the latter is the only one that maintains the biological knee, by adding or removing a bone wedge and redistributing the load within the joint. Moreover, HTO delays the need for knee arthroplasty and allows young and fit patients to return to active lives.

The genu varus condition, which characterize the patients analysed in this thesis, causes the shifting of the load distribution toward the medial compartment, resulting in a worsening of the medial OA. Thus, the evaluation of the joint contact loads and the muscle forces and activation, and their correlation with the tibiofemoral alignment, may help the planning of an ideal HTO procedure. Here, musculoskeletal models make possible to evaluate these biomechanical quantities, otherwise not calculable with direct physical experiments, thus better assessing the patient's condition.

The aim of this thesis was to evaluate the correlation between the tibiofemoral malalignment in the target limb and the hip contact forces in the contralateral limb during daily activities. This study extends the findings of a previous experience, which analysed the effect of tibiofemoral angle in load distribution between the medial al lateral compartments in the knee joint. Both of them are included within a wider project carried out at the Rizzoli Institute of Bologna, whose goal is to evaluate the impact of high tibial osteotomy in preventing the progression of the disease in medial knee osteoarthritis, by quantifying the effect on cartilage

and subchondral bone through the use of a combined biomechanical and medical imaging approach.

Focusing on this thesis, the background chapter provides the basic information to understand and introduce the fields behind this project. We start describing the anatomy of the knee in all its components, specifying the elements that characterize the osteoarthritis of the joint and its stages, with a focus on its correlation with the mechanical axis of the lower limb. Then, we explain in detail how HTO works, the opening- and closing-wedge techniques, the ideal patient for this type of operation, and the current limitations. In the end, we introduce the musculoskeletal (MSK) modelling approach, starting from the basics aspects of motion capture up to the application and creation of MSK models within OpenSim.

In chapter 3, the workflow and the dataset used for this project are described. First, we illustrate a brief overview of the 19 patients which took part to this study, by reporting their general anthropometric information in a table. Then, we focus on the gait analysis experimental setup, by analysing all the components used within the stereophotogrammetry acquisition, starting from the cameras, the force platforms, the EMG sensors and the markers set, and reporting a schematic view of walking, ascending and descending tasks performed by the subjects. Thus, we describe in detail the software HTO-RPlus, developed inside the Bioengineering and Computing Laboratory (BIC), where this thesis took place, and studied to simulate the entire process of the surgery. At the end, it returns the value of the tibiofemoral malalignment angle. With this information and the data collected from the sessions of gait analysis, we scaled a generic model and simulate the patients' motor tasks within OpenSim, whose entire workflow is deeply reported. In the last part, we describe data post-processing through Matlab, including the statistical analysis, which consisted in statistical parametric mapping, using nonparametric two-tailed unpaired t-tests ($\alpha = 0.05$), Mann-Whitney U-test ($\alpha = 0.05$), and boxplot distributions, and the model validation, by comparing the muscle activations estimated via OpenSim and the recorded EMG signals. The obtained results are then showed in chapter 4.

In the last two chapter we discuss our outcomes, by evaluating our research question and comparing our results with those obtained in the previous thesis mention before, taking into consideration only the medial compartment of the knee joint, since it showed similar values and pattern. Finally, we sum up our experience, its aim and its limitation, and we report some future improvements which could lead to more precise and reliable results.

2. BACKGROUND

2.1 THE KNEE ANATOMY

The knee is the largest and one of the most complex joints of the human body (*Figure 1*). It is a synovial bicondylar hinge joint between the condyles of the femur and those of the tibia, and with the patella anteriorly (*Figure 4 - Left*) (1). It is composed of three functional compartments: the patellofemoral articulation, the medial and the lateral tibiofemoral articulations linking the femur with the tibia. The joint is bathed in a synovial fluid which is contained inside the synovial membrane called joint capsule.

The knee is functionally considered to be a hinged joint, whereby the distal section of the femur rolls and glides over the tibial surface. This approximation is due to the fact that the main movement performed by the joint is the flexion-extension in sagittal plane (7). However, it also permits a small amount of internal-external rotation of the tibia with respect to the femur, particularly when the knee is flexed, and the foot is off the ground. The relatively poor degree of interlocking of the articular surfaces makes it liable to strains and dislocations (1).

In details, the stability of the knee structure and the alignment of the bone components through movements, as in the other joints, is guarantee by the combination of a ligamentous, tendinous and muscular component which limits movements and protect the articular capsule.

Figure 1 – The knee joint

2.1.1 Ligaments of the knee

Ligaments are fibrous connective tissue that connect bones to other bones and, as tendons, are made of connective tissue (*Figure 2*). Without its ligaments, the knee would show excessive motion that could damage the bones at the joint. In particular, there are two types of ligaments: intracapsular and extracapsular ligaments.

The first group includes the cruciate ligaments and the transverse ligament: the anterior cruciate ligament extends from the lateral condyle of femur to the anterior intercondylar area, preventing knee iper-extension caused by the excessive forward movement of the tibia; the posterior cruciate ligament stretches from the medial condyle of femur to the posterior intercondylar area, preventing the excessive forward sliding of the femur; the transverse ligament stretches from the lateral meniscus to the medial meniscus (4).

The second group includes the collateral ligaments and the patellar ligament: the medial collateral ligament extends from the medial epicondyle of the femur to the medial tibial condyle, supporting the knee when excessive loads are applied to the opposite side; the lateral collateral ligament is equivalent to the medial one, but located in the outer side of the knee; the patellar ligament connects the patella to the tuberosity of the tibia (5).

Thus, cruciate ligaments guarantee antero-posterior stability of the knee and collateral ligaments the medio-lateral one.

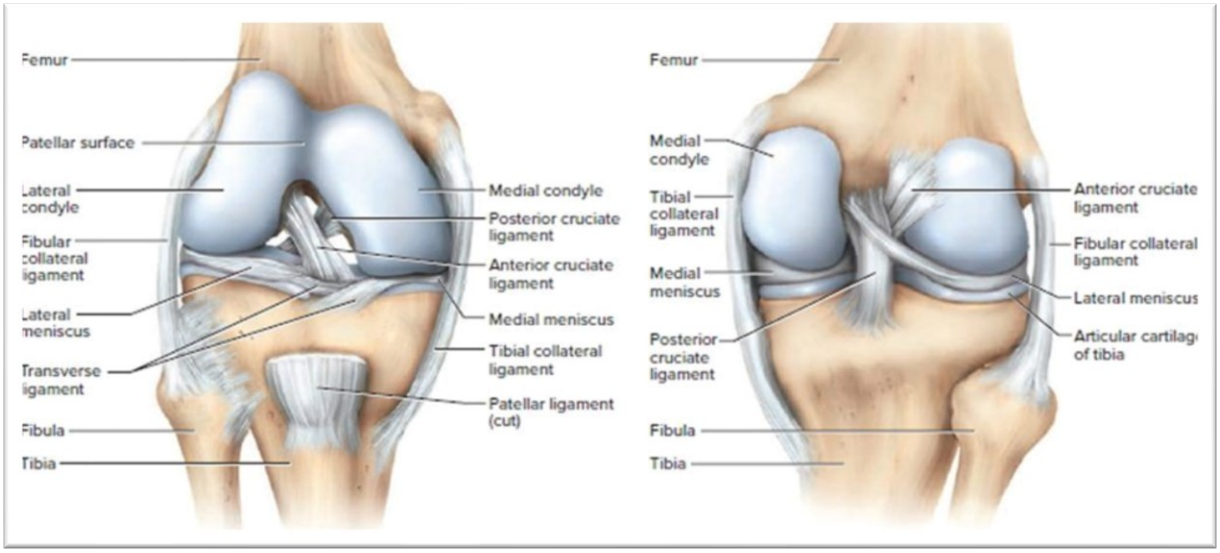

Figure 2 – Anterior (Left) and Posterior (Right) view of right knee joint

2.1.2 Muscles and Tendons of the knee

While ligaments connect one bone to another, tendons connect muscles to bones. Ligaments and menisci provide for static stability, muscles and tendons for dynamic stability.

The muscles (*Figure 3*) involved in the flexion action are the hamstrings, which include the semitendinosus, the semimembranosus and the bicep femoris, the gastrocnemii, the gracilis, the sartorius, the popliteus. The quadriceps femoris and the tensor fascia lata, instead, cause the extension of the joint. In particular, quadriceps group is made up of four individual muscles, which are the rectus femoris and the vasti medialis, lateralis and intermedius. These muscles combine to form the quadriceps tendon which attaches to the patella; then the patellar tendon joins the patella to the tibia. The function of the kneecap is to increase the efficiency of the quadriceps contractions (7). The muscles involved in medial rotation are the semitendinosus, the semimembranosus, the gracilis, the sartorius and the popliteus while the biceps femoris acts in lateral rotation. The insertion points and the geometrical characteristics such as volume and fibers length, make some of these muscles more relevant than other by generating a higher force.

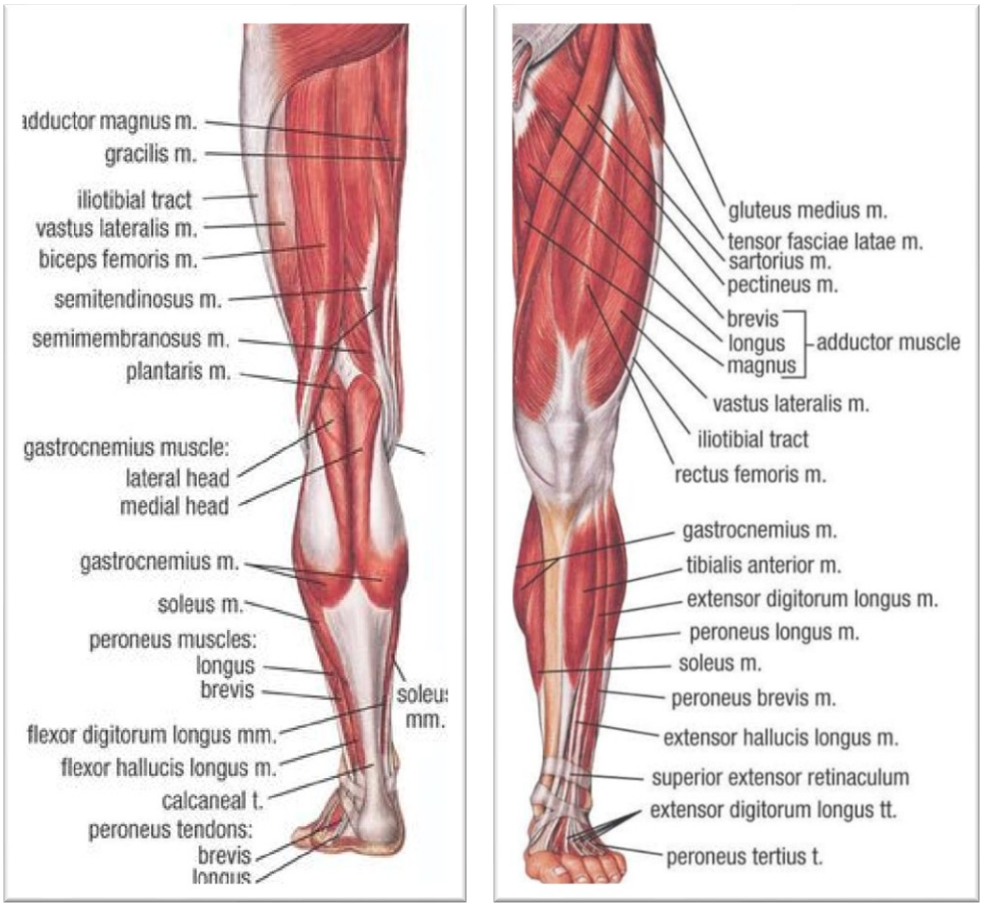

Figure 3 – Muscles of the lower limb (Posterior and Anterior view)

2.1.3 Cartilage of the knee

Cartilage is a thin, elastic tissue that protects the bone and makes sure the joint surfaces can slide easily over each other. In the knee there are two types of joint cartilage: fibrous cartilage, located in the menisci, and hyaline cartilage (*Figure 4 - Left*) (2). The knee has two menisci, medial and lateral (*Figure 4 - Right*). They consist in crescent-shaped discs that act as a cushion so that bones can move through their range of motion without rubbing against each other. They also improve balance and stability and guarantee a correct weight distribution between the femur and the tibia (3,6).

However, cartilage wears over the years due mechanical stress and lack of synovial fluid and nutrients supply, and it has a very limited capacity for self-restoration. The newly formed tissue will generally consist of a large part of fibrous cartilage of lesser quality than the original hyaline cartilage. As a result, new cracks and tears will form over time (2).

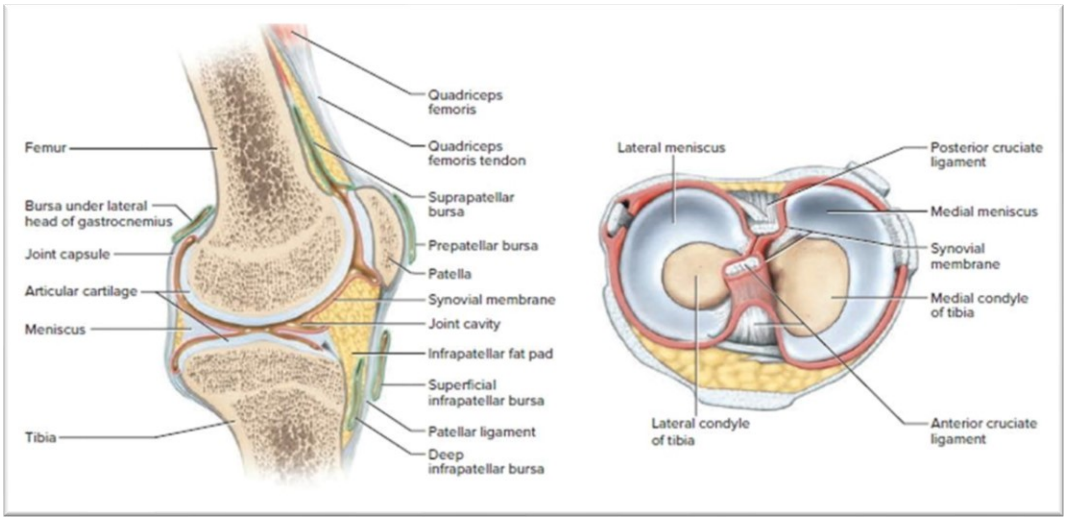

Figure 4 – Sagittal section (Left) and Superior view (Right) of knee joint

2.2 MECHANICAL AND ANATOMICAL AXES OF LOWER LIMBS

In defining genu varus and genu valgus condition, knee alignment is expressed relative to some reference axis or plane and measurements will depend on what is selected as reference system (9). On normal weight bearing anteroposterior radiographs, the vertical axis, which extends from the centre of the pubic symphysis straight to the ground, is used as reference axis from which other axes are determined (8).

The Mechanical Axis (MA) of the lower limb (*Figure 5*) is a straight line from the centre of the femoral head to the centre of the ankle joint (9). It consists of two parts: the femoral MA,

which goes from the head of the femur to the intercondylar notch of the distal part of the same bone, and the tibial MA, which runs from the centre of the tibial plateau to the middle of the tibiotalar joint (8,9). To quantify the frontal plane alignment the most commonly used measure is the mechanical femorotibial angle, which is defined as the angle between the mechanical axes of the femur and tibia. The frontal plane distance between the MA of the lower limb and the knee joint center is less used (13,21). In a neutral limb, the mechanical axes of the femur and tibia lie along that of the limb, which has an approximately 3° slope compared with that of the vertical axis (8).

The Anatomic Axis (AA) of the lower limb (*Figure 5*) is related to the intramedullary canals. Also in this case, it can be divided into two components: the femoral AA, which is a line drawn proximal to distal in the intramedullary canal bisecting the femur; it can be also represented as a line uniting a point at the centre of the femoral shaft with a point 10 cm above the knee joint, which is equally spaced between the medial and the lateral cortex. The tibial AA is represented in the same way as the femur one (8,13). On a weight-bearing radiograph, the lateral angle between the anatomic axes of the femur and the tibia is called the femorotibial angle, and it is approximately 178° in men and 175° in women (8).

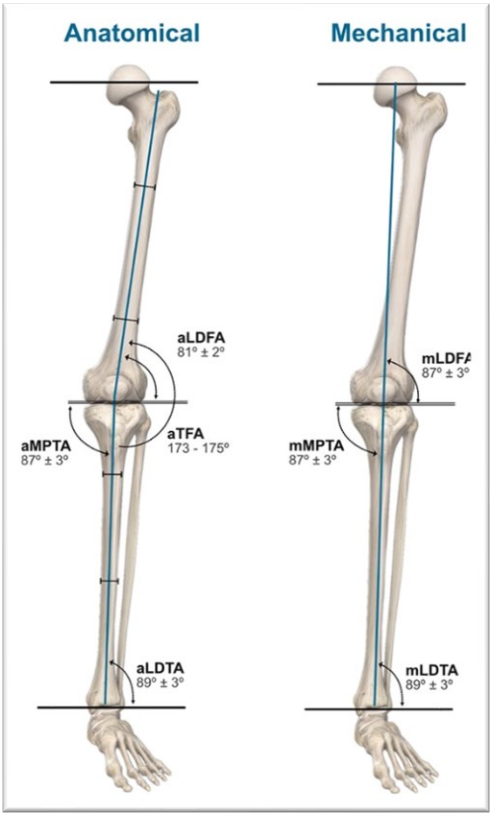

Figure 5 – Mechanical and Anatomical axes of lower limbs

In the case of genu varus and genu valgus condition (*Figure 6*), mechanical axes of the femur and the tibia don't correspond to the generic MA of the lower limb but form an angle at the knee that indicates the extent of mechanical malalignment (14). A normal knee joint presents a naturally 2° to 3° varus condition with respect to the mechanical axis of the limb (8). In particular, if the MA passes medially to the knee center, the subject presents a genu varus condition, which shift the load to the medial compartment; if the MA passes laterally, the subject presents a genu valgus condition, and the load is shifted to the lateral compartment (14). Typically, during the stance phase of the gait cycle, the medial compartment shares a greater percentage of the total load across the joint, that reach 73% and 65% in the first and second axial force peak, respectively, and this increases by 5% for each additionally degree of varus deformity (15).

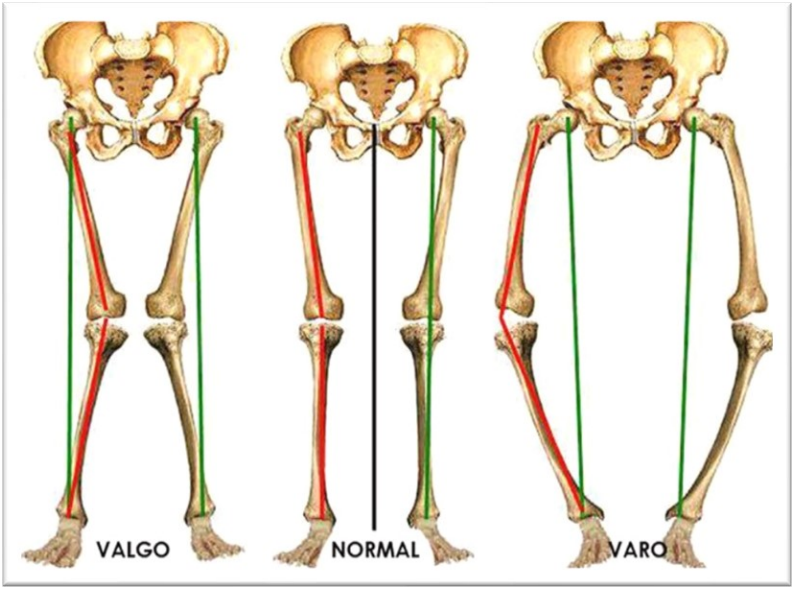

Figure 6 – Comparison between valgus, normal and varus tibiofemoral alignment

Even if the aim of the different alignment techniques is to restore a neutral alignment of the knee, several studies reported that in healthy nonarthritic patients, this condition has the least incidence: Hsu et al (10) noted that among 120 normal subjects, only the 2.2% had a 0° angle with respect to the MA; Bellmans et al (11) studied a group of 250 healthy asymptomatic adults finding 32% of men and 17% of women with a natural genu varus deformity of 3° or more; Fahlman et al (12) examined 143 participants and reported that approximately 50% of them had both knee with varus condition, 21% both valgus and only 11% both straight knees. The rest had a different inclination in the two lower limbs.

2.3 OSTEOARTHRITIS OF THE KNEE

Osteoarthritis (OA) is the most common form of arthritis, affecting people of all ethnic groups, men and women, although it occurs more commonly in women (33,38). It is a type of degenerative joint disease and it is typically the results of wear and tear and progressive loss of articulation cartilage (34). This causes the bones of the joint to rub more closely, resulting in pain and stiffness, decreasing the ability to move and leading to the formation of bone spurs (35) (*Figure 7*).

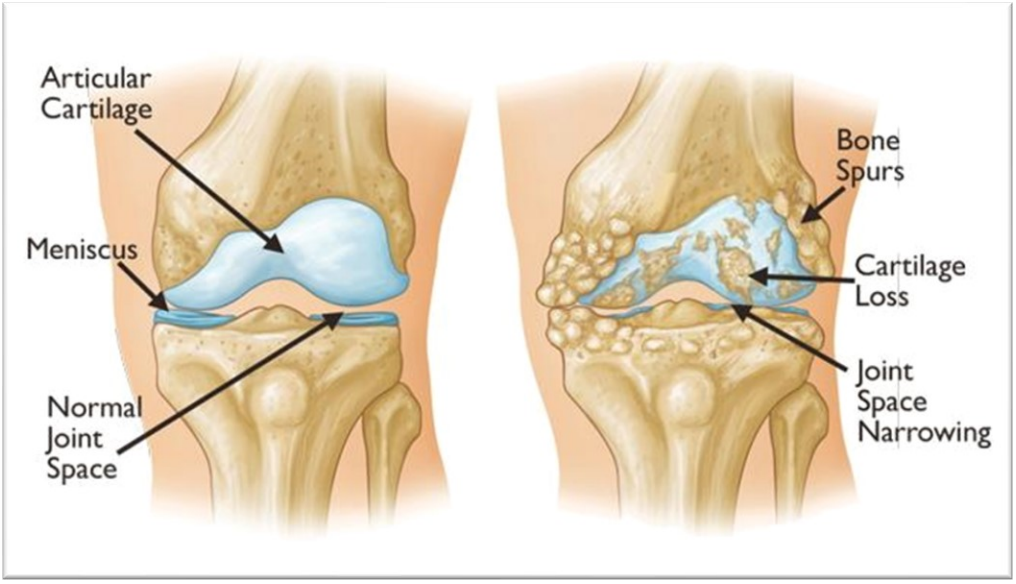

Figure 7 – Healthy knee (left) and osteoarthritic knee (right)

Most frequently OA develops in the absence of a known cause of joint degeneration, in this case it is called Primary or Idiopathic OA and it is typically associated with aging and deterioration (34,36). Instead, when osteoarthritis occurs because of known reasons it is named secondary OA. Possible causes of secondary knee osteoarthritis are obesity, joint hypermobility or instability, malposition of the joint (varus/valgus posture), previous injury to the joint (fractures), congenital defects or metabolic causes (36).

Among these factors, aging and overweighting are the most common and affecting, so knee OA incidence will continue to increase as life expectancy and obesity rises. A recent study carried out by Cui et al. in 2020 found out that knee OA prevalence was 16% and 23% in individuals aged 15+ and 40+ respectively, the ratio was 1.69 in females and 1.39 in males (39) and the prevalence rises to 40% for people older than 70 years (34).

In 2016, Reyes Carlen et al. (40) studied the correlation between body weight and the progression of OA. Compared to normal-weight subjects (BMI<25kg/m^2), being overweight

or obese increased the risk of OA at hip, knee and hand sites, especially at the knee. In overweight ($25kg/m^2<BMI<30kg/m^2$), grade I ($30kg/m^2<BMI<35kg/m^2$) and grade II ($35kg/m^2<BMI<40kg/m^2$) obesity subjects, this risk rises by a factor of 2, 3.1 and 4.7, respectively (40). The mechanical overload of the weight-bearing joint or the activation of metabolic factors contributing to the joint damage, have both been proposed as possible mechanism to explain how weight increases the risk of knee OA (41).

In general, in the healthy knee, articular cartilage that covers the articular surfaces of bones is maintained in a state of equilibrium of chemical reaction (37), which is guarantee by the action of chondrocytes, the only cells found in healthy cartilage (42). These cells deal with the synthesis of collagen and proteoglycans, which are components of the extracellular matrix of the cartilage, and the synthesis of proteolytic enzymes responsible for the disruption of the formers. Thus, preserving the homeostasis. OA results from failure of chondrocytes in maintaining the equilibrium between the synthesis and the degradation of these extracellular matrix components (43). Consequently, a series of phenomena develop in cascade (37):

1. Disorganised pattern of collagen, and loss of articular cartilage elasticity.
2. Cracking of the cartilage and erosion of the articular surface.
3. Damaged cartilage cannot recover.
4. Cartilage has completely worn away.
5. Bony surfaces appear and new osteophytes develop.

Nowadays osteoarthritis has no cure, so prevention and early diagnosis play a huge role. For this reason, it becomes very important to identify as soon as possible the symptoms and the degree of progress of the disease (37). Osteoarthritis is classified in 5 grades, based on cartilage condition (*Figure 8*):

- Grade 0: healthy knee.
- Grade 1: absence of pain and very minor bone spur growth.
- Grade 2: greater bone spur growth but the cartilage remains at a healthy stage. Pain and joint stiffness only after a prolonged effort.
- Grade 3: moderate OA. The pain becomes more frequent, and the cartilage shows evident damage.
- Grade 4: severe OA. The space between the bones is very small and the cartilage is almost completely absent. This causes pain during any simple movement of the joint (37).

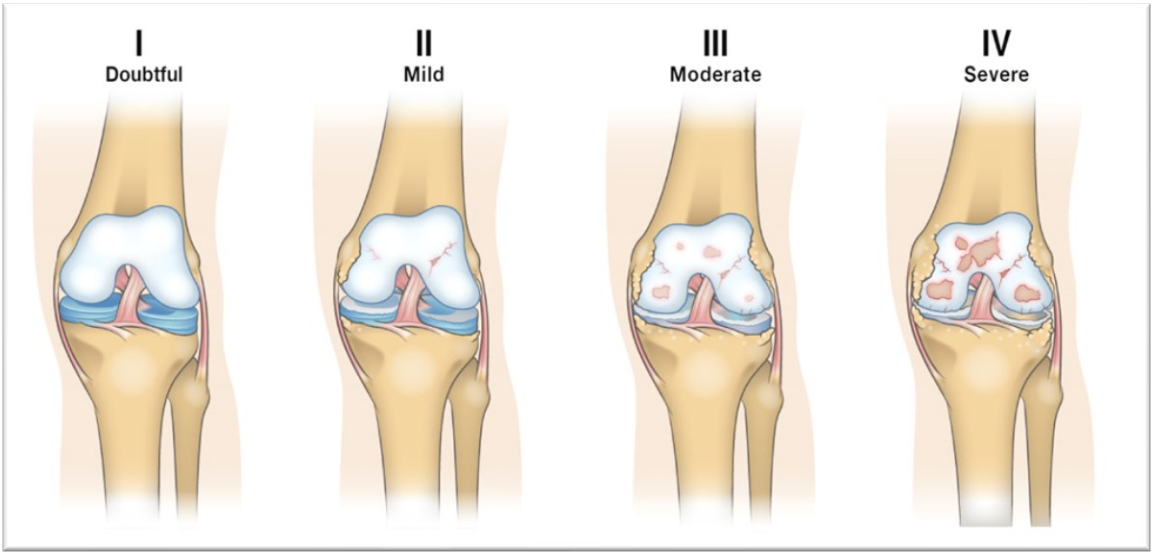

Figure 8 – Stages of knee osteoarthritis

When the degradation of the cartilage is localized to one of the compartments of the knee, and typically to the medial site, it is called unicompartmental knee osteoarthritis (*Figure 9*). This condition is often associated with varus malalignment which causes a mechanical overload of the internal compartment of the knee and consequent meniscal disruption.

Figure 9 – Unicompartmental knee osteoarthritis

The initial treatment of OA always begins with conservative modalities and moves to surgical treatment once conservative methods are no longer effective. The formers do not alter the disease process, but they can decrease the pain and the disability of the subject (34,37). Among them, patient education and physical therapy have shown to be the best treatment, along with drug therapy that includes analgesics and anti-inflammatory medications. As

reported, overweight is one of the main causes of osteoarthritis progression, so weight loss is valuable in all stages of knee OA (34).

When medical treatments are ineffective or have been exhausted, surgery may be helpful, especially with advanced OA. The type of surgical treatment depends on many factors, including patient's age, overall health, and severity of condition. Surgery options are:

- Osteotomy
- Unicompartmental Knee Arthroplasty (UKA) (*Figure 10 - right*)
- Total Knee Arthroplasty (TKA) (*Figure 10 - left*)

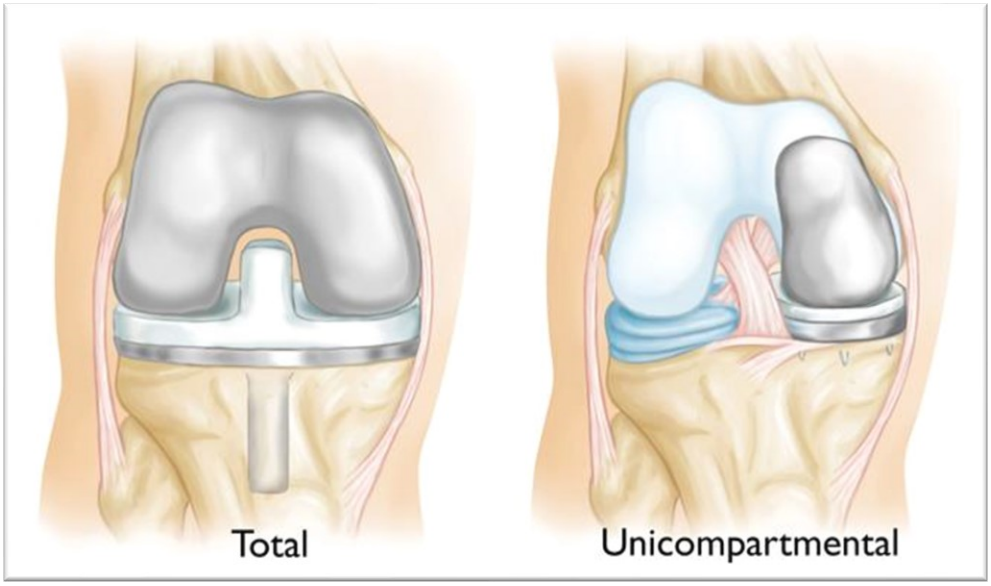

Figure 10 – Total Knee Arthroplasty (TKA) (left) and Unicompartmental Knee Arthroplasty (UKA) (right)

2.4 HIGH TIBIAL OSTEOTOMY

High Tibial Osteotomy (HTO) is a surgical procedure used to treat symptomatic unicompartmental OA associated with knee malalignment (16) and implies the shifting of the weight-bearing line in the coronal plane (17) (*Figure 11*).

Mostly associated with the correction of varus malalignment in medial unicompartmental osteoarthritis knee (18), the aim of the procedure is to unload the medial arthritic compartment, by shifting the loading line to the healthier contralateral side and producing a postoperative slightly valgus alignment (23,24). This leads to a load redistribution in the tibial plateau, which results in decreasing the pain in the diseased compartment and in slowing down the degenerative progression of cartilage (25). The ultimate result is to avoid or

postpone total knee arthroplasty (TKA) (34) and preserving, in this way, the original joint (17-20).

HTO technique has gained relevance only in the last few decades (16). In the 1970s, knee arthroplasty (KA) surgery was mostly used since osteotomies, like HTO or distal femoral osteotomy (DFO), were more demanding than KA and associated with less predictable outcomes and significant complications (18,26). However, as patients with OA are getting younger and want to return to demanding physical activity, aspect in which KA lacks, HTO has received renewed attention (26).

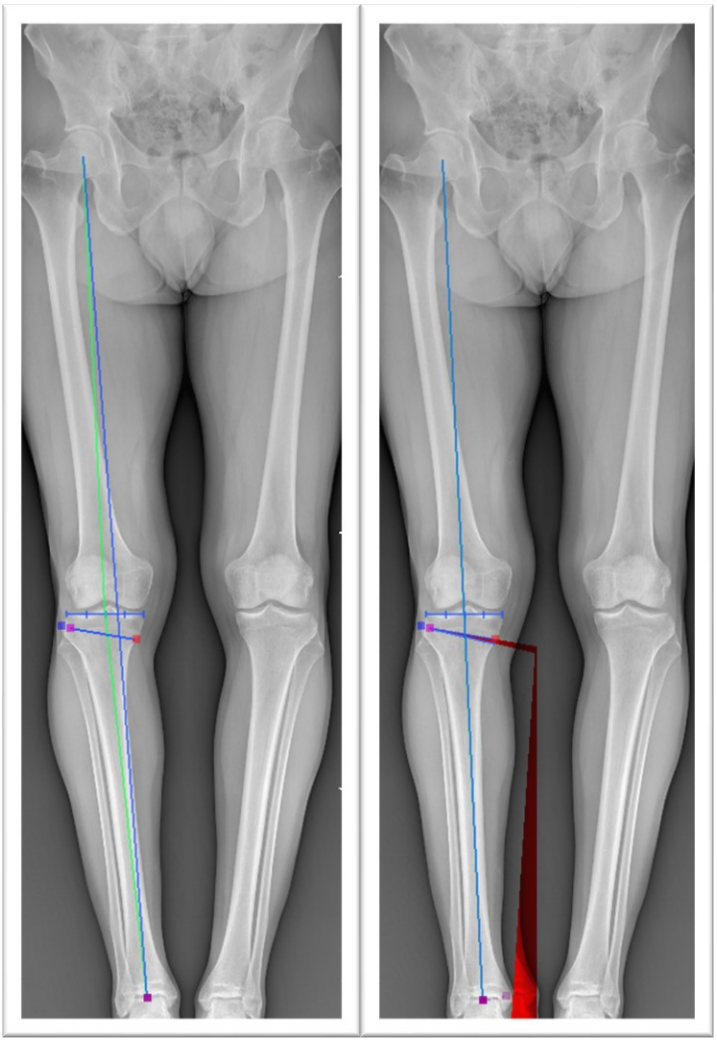

Figure 11 – Pre-operative (left) and post-operative (right) planning within HTO-RPlus software

2.4.1 Techniques

In general, two types of HTO procedures can be adopted for both varus and valgus malalignment: opening-wedge (OW), where a bone wedge is added, and closing-wedge (CW), where a bone wedge is removed (23).

In genu varus condition, the two techniques are adopted to shift the mechanical limb laterally and thus unloading the medial side (21). They are defined as medial OW (MOW) and lateral CW (LCW) (*Figure 12*), both operating at the proximal tibia. Valgus malalignment, in the other hand, involves the same techniques at the distal femur (21). According to recent studies, OW-HTO has higher accuracy and better survival at ten years, a wider range of motion and less soft-tissue dissection with respect to CW-HTO, but both procedures present advantages and disadvantages that depend on the situation (19). Indeed, LCW technique was originally the first choice in genu valgus condition, mainly for direct bone-to-bone contact. However, the meticulous preoperative process, the possibility of damaging the peroneal nerve and the necessity for fibular osteotomy, have made this technique less popular nowadays (21).

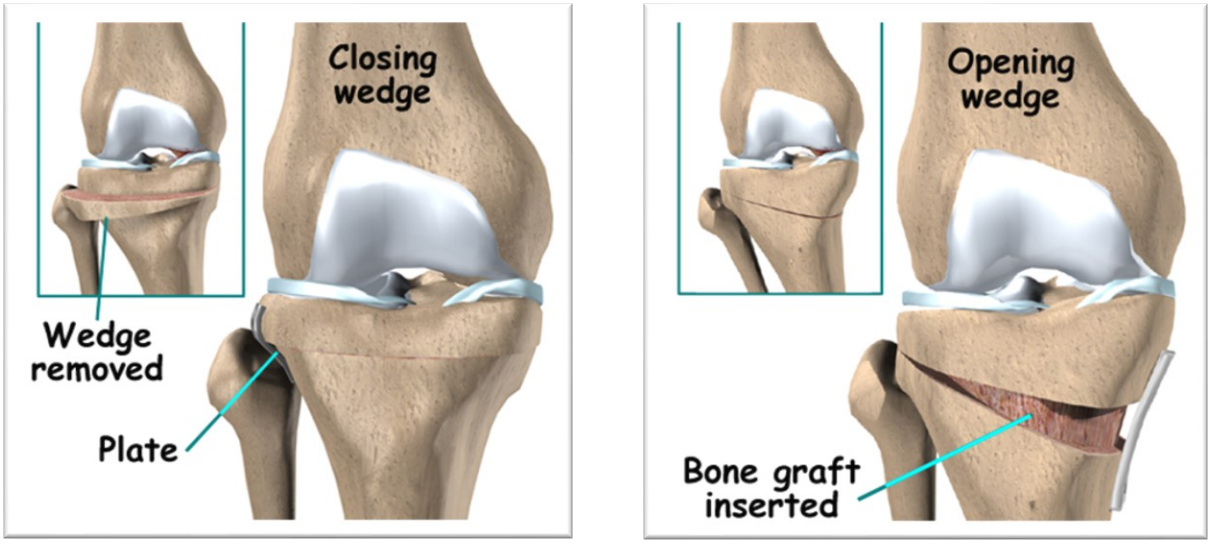

Figure 12 – Lateral Closing Wedge HTO (left) and Medial Opening Wedge HTO

2.4.2 Ideal patient and preoperative planning

HTO surgery is a useful technique only in appropriately selected patients with unicompartmental OA (27,28). The ideal candidate for this operation must be a non-smoking, non-obese (BMI<30 Kg/m^2) young active patient (40 to 60 years), with mild to moderate unicompartmental osteoarthritis and with intact cartilage and meniscus in the contralateral compartment (20-22). Knee joint must have a good range of motion (29), without ligamentous instability and the angle of misalignment must be less than 15° (18,23).

In preoperative evaluation, radiography is crucial (16). A complete preoperative planning should include weight-bearing AP, PA flexion and focalized knee radiographs. Furthermore, the condition of cartilage and meniscus should be evaluated through MRI images before the surgical procedure (21). Radiography also plays an important role in the postoperative period, evaluating the patient's condition and highlighting any complications (16).

2.4.3 Outcomes and limitations

The recent interest in osteotomies around the knee is also due to the improvements in the surgical technique and in the careful subject selection. This allowed most HTO patients to return to sport and work activities in 10-22 weeks, with the same or higher workload, reporting a significant decrease in pain (26). Both MOW and LCW technique have shown good clinical and radiographic outcomes: Hantes et al (30) reported a 95% survival rate of the native joint for MOW technique at 12.3 years and according to Berruto et al (31), 97% of patients have shown good results at 12.6 years after LCW procedure. However, Duivenvoorden et al (32) in 2014 found LCW-HTO had a higher rate of total knee arthroplasty (22%) with respect to MOW-HTO (8%) at 6 years. In general, survival rates for high tibial osteotomy reaches 87-99% at 5 years and 66-84% at 10 years (20,26).

In the other hand, the failure of the surgical procedure can be linked to a variety of factors, mostly concern cortical hinge fractures, infections, not perfect union of bone tissue and damage of the peroneal nerve (21), which depend on the OW or CW techniques. Thus, despite the renewed interest, high tibial osteotomy still causes some complications which are closely related to the biomechanics of the HTO (23).

2.5 MUSCULOSKELETAL MODELING APPROACH

2.5.1 Basic aspects of motion capture

Motion Capture is the process of recording the movement of the human body or objects, for an immediate or delayed analysis. The information can be a simple standing of the body in the space as well as complex deformations of the face. For this reason, it finds different fields of application, like medical, military and entertainment areas (45). Over the years, motion capture has undergone several changes and improvements driven by the need to have more and more accurate data and a more versatile and less intrusive instrumentation. There are several ways of acquiring movement (44):

- *Optical systems*: based on tracking passive (reflected light) or active (own light) markers placed on specific body landmarks through a set of cameras (stereophotogrammetric system). This technique requires long preparation and postprocessing to clean the data, so it’s a bit time-consuming.
- *Non-optical systems*: movement is acquired by a series of sensors attached to the body. Electromagnetic systems and inertial systems belong to this category.

The former are based on small electric coils within an electromagnetic field; the latter on accelerometers, gyroscopes and magnetometers (46).

- *Markerless systems*: combine 3D cameras with infrared and ultrasonic sensors, which permit to extract joint and body segments from the general human figure, without wearing any equipment.

In research and in clinical medicine fields, the main application of motion capture is gait analysis (*Figure 13*), which studies human movement from a biomechanical point of view and provides clinicals with information not directly observable (46). This technique proves very important not only in sports or biomechanical research, but also in evaluating post-surgery rehabilitation (48) and in diagnosing and monitoring physical and mental diseases. Generally, in this latter case, patients share similar gait anomalies (49), which can be useful in facing and treating diseases like Cerebral Palsy (50) and Parkinson (51).

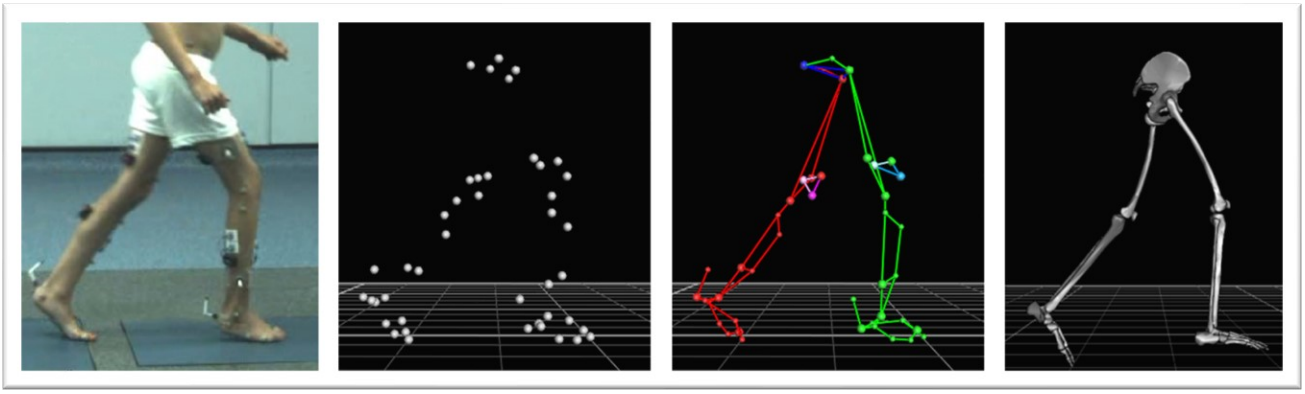

Figure 13 – Steps of gait analysis with optical system

2.5.2 Musculoskeletal modeling and OpenSim

Musculoskeletal (MSK) models have been developed to derive information that direct physical experiments could not provide, like muscle forces and activations or joint contact loads, thus having a broader understanding of subject's condition (47). Especially in the clinical and rehabilitation field, for patients with gait impairment due to mental and physical anomalies, MSK modelling guarantees more safety and non-invasiveness, with the opportunity to study different therapies or surgical interventions (52,54), by perturbing model characteristics and avoiding a direct consequence on the patient (55).

Moreover, the combination of direct measurements in cadavers and the more recent MRI in vivo acquisition, gives the possibility of creating an increasingly precise subject specific MSK model (47,56), which permits to study a specific therapy or surgery for the patients, but also to obtain more reliable biomechanics results in the research field.

Musculoskeletal models can be developed, modified, and simulated within OpenSim (57) (*Figure 14*).

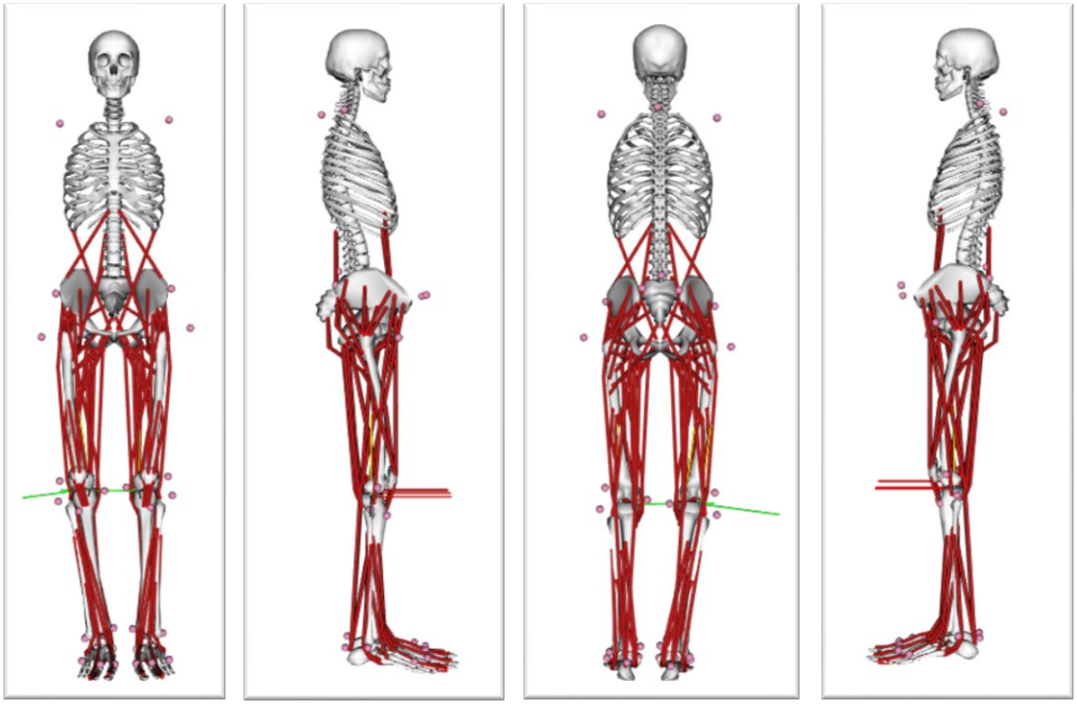

Figure 14 – example of musculoskeletal model developed within OpenSim

OpenSim is an open-source software which permits to the users to create and analyse a subject specific musculoskeletal model, with desired characteristics (55), and then simulating different motion tasks for various purposes, from research to rehabilitation, from prevention of injury to planning or post-surgery analysis, and many others. In general, OpenSim MSK models are divided into several parts: bodies, joints, forces/muscles and constraints (53) (*Figure 15*).

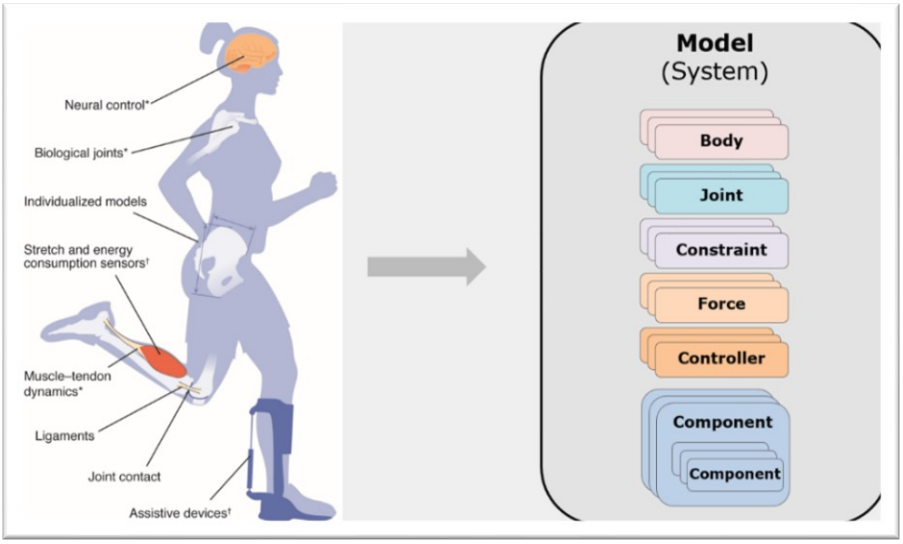

Figure 15 – Conceptual scheme of a model within OpenSim

The core software and the graphical user interface (GUI) (*Figure 16*) are written in C++ and Java, respectively. The GUI allows the user to visualize and modify MSK model and its movements, but also to create new ones through the software features. Moreover, with the application programming interface (API) it is possible to increase the software potential, by interfacing OpenSim with programming software like C++, Phyton and Matlab (53).

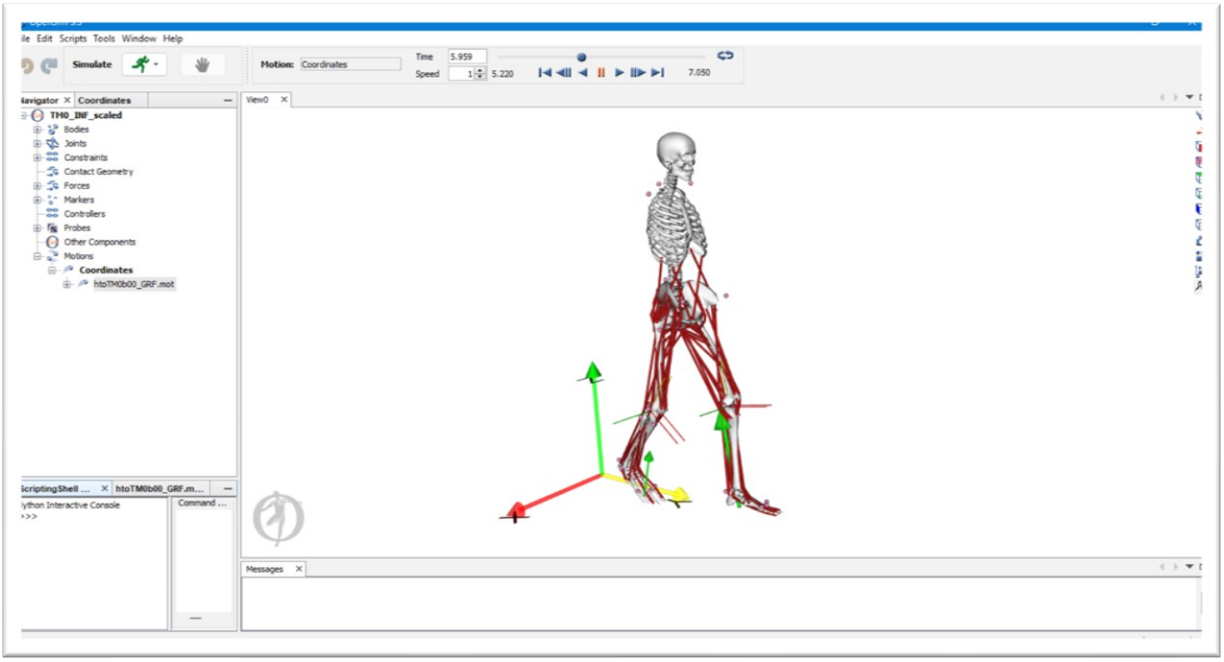

Figure 16 – Graphical User Interface (GUI) inside OpenSim

However, the most important aspect of OpenSim is represented by its community. Researchers from different institutes collaborate with each other by exchanged, analyzing, and improving MSK models and simulations, thus building a large, shared library (53,57).

2.5.3 Inverse problem analysis within OpenSim

Depending on the research question, OpenSim presents a specific path (58). In this chapter the typical structure of an inverse problem analysis is described, which is the same workflow followed for this project. All the details are taken from the OpenSim guide (53).

Scaling

Scaling process turns a generic musculoskeletal model into a subject-specific model, by minimizing the distances between virtual markers, in the generic model, and experimental markers, tracked by gait analysis system. Virtual markers and experimental markers share the same anatomical positions (*Figure 18*). The scale tool takes as input arguments the generic musculoskeletal model and the experimental markers trajectories during a static trial of few

seconds, while the subject is wearing a specific marker set. As output, it returns the scaled model which best represents the patient's anthropometric characteristics (*Figure 17*).

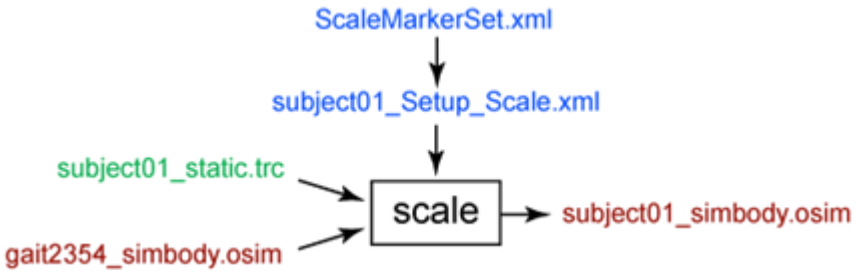

Figure 17 – Inputs and outputs of the scaling tool

The distances between experimental markers with respect to the corresponding distances of virtual markers, define the scaling factors, which are used to scale model's geometry. These factors can be manually specified, or they can be measurement-based, or both of them (47). The masses and the inertial properties of the segments are scaled by specifying the patient's weight and preserving mass distribution as input. The latter guarantees that the sum of their masses equals the subject's one.

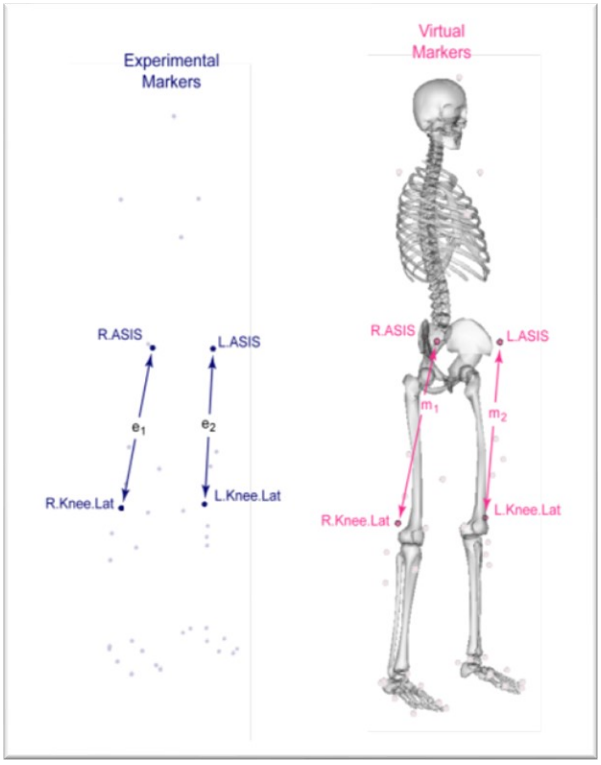

Figure 18 – Experimental markers vs. virtual markers

It is then possible to evaluate graphically the result, by visualizing the "Messages" window of the GUI, and checking the marker errors, which indicate the distance between virtual and experimental markers. A good scaling is characterized by a maximum marker error and an RMS error which should be less than 2 cm and 1 cm, respectively. After that, virtual markers

can be moved to improve their fitting and markers weightings can be modified to define which experimental marker requires a better match with respect to the others (typically those positioned in palpable bony landmark). The iterative cycle repeats by checking again the "Messages" window, until we are satisfied with the result.

Inverse kinematic

Inverse Kinematics (IK) Tool requires as input the scaled musculoskeletal model, defined with the Scaling Tool, and the file with the experimental marker trajectories of a specific trial. The aim is to match the virtual markers with the experimental ones for each frame of the motion to best replicate the movement of the patient. IK returns as output the coordinates and joint angles during the task (*Figure 19*). The best matching is the one that minimizes a sum of weighted squared errors of markers.

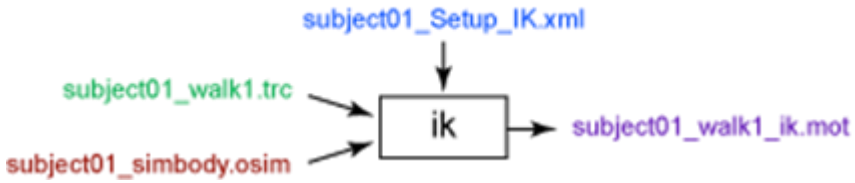

Figure 19 – Inputs and outputs of the IK tool

IK output will be used in the subsequent phases of the workflow, therefore it is necessary to derive an accurate result. As in the previous tool, "Messages" window is useful at this scope. In this case, maximum marker error and RMS should be less than 2-4 cm and 2 cm, respectively. This leads the user to eventually modify the weights of the markers and, if necessary, redo the Scaling process.

Inverse Dynamics

The Inverse Dynamics (ID) Tool computes the forces and torques at each joint through the motion. It requires as input the scaled musculoskeletal model, the IK motion file and the External Loads file, which data derive from force platforms used inside the Gait Analysis Laboratory (*Figure 20*).

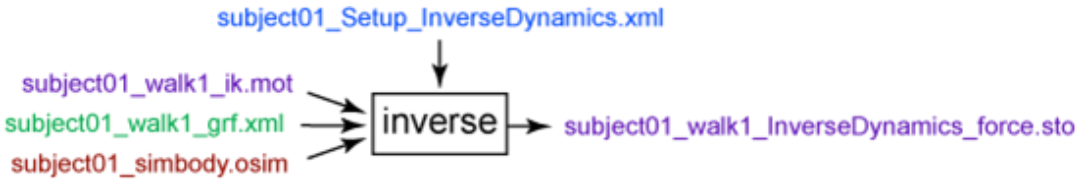

Figure 20 – Inputs and outputs of the ID tool

In ID analysis, it is good practise to filter the data, since noise id amplified by differentiation. The equation of motion, expressed as mass-dependent relationship between force and acceleration (F=m*a), is solved by ID Tool in the inverse dynamics sense and it is reported below.

$$\underbrace{\mathbf{M}(\mathbf{q})\ddot{\mathbf{q}} + \mathbf{C}(\mathbf{q},\dot{\mathbf{q}}) + \mathbf{G}(\mathbf{q})}_{\text{knowns}} = \underbrace{\tau}_{\text{unknowns}}$$

Equation of motion

The known terms in the left side are used to solve the equations of motion for the unknown generalized forces in the right side of the equation.

Static Optimization

Static Optimization (SO) Tool follows ID analysis and resolves the net joint moments into individual muscle forces by minimizing the sum of squared (or higher power) muscle activations.

$$J = \sum_{m=1}^{n} (a_m)^p$$

SO objective function

Input data for SO analysis are the same of the previous tool (*Figure 21*) and even in this case is good practise to filter them. However, model muscles are unable to produce enough force to satisfy the Newton law F=m*a, and this causes a dynamic inconsistency between the estimated model accelerations and the measured ground reaction forces. For this reason, residual actuators are used to compensate this gap. Generally, they are appended to the first free joint of the model, which is typically the ground-pelvis, and one actuator is necessary for each degree of freedom of the joint (Point and Torque Actuators). However, high values of residuals are not realistic: residual forces should be lower than 5% of maximum external force magnitude and residual moments 1% or less of COM height times the magnitude of the measured net external forces (58).

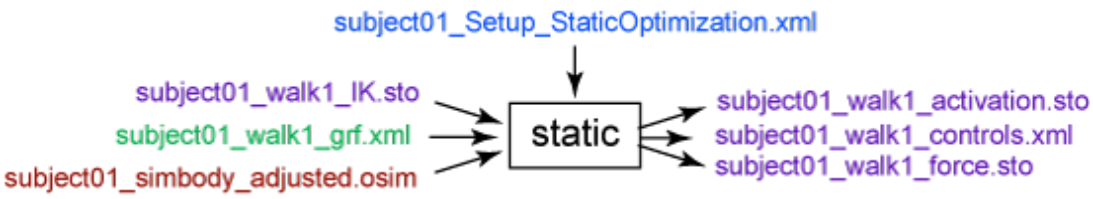

Figure 21 – *Inputs and outputs of the SO tool*

Joint Reaction Analysis

Joint Reaction Analysis (JRA) is a procedure under the Analyze Tool. It solves the internal forces and moments at each joint, by considering all the loads acting on the model. Reaction loads act in the center of the joint and by default, they are defined on the child body in the ground reference system but also on the parent body in the child, parent or ground reference system.

With respect to ID analysis, which only considers the model motion and external forces, JRA analysis also takes into account the contributions of all muscles, motors and actuators to calculate joints loads.

JRA Tool requires as input the scaled model, the IK motion file, the actuators, the external loads and the force file given by the Static Optimization. The analysis returns a storage file containing three forces and three moments components for each joint, defined on child or parent body in the child, parent or ground reference system.

3. MATERIALS AND METHODS

This script studies the correlation between tibiofemoral misalignment angle and the contralateral hip forces in patients with unicompartmental osteoarthritis (OA) during daily motor activities. The thesis is the prosecution of a previous elaborate carried out by Nicolò Caredda within the same laboratory, which concentrated on knee joint loads by distinguishing the medial and the lateral compartment. They are both parts of a wider project, whose purpose is to evaluate the impact of high tibial osteotomy (HTO) surgical procedure in preventing the progression of OA in the medial compartment of the knee joint, due to genu varus condition.

In this thesis, we considered 19 patients with characteristic tibiofemoral malalignment and at a different stage of unicompartmental OA. For each of them, 3 motor tasks were tested in gait analysis sessions and RX images were used to compute the varus angle through HTO-RPlus software. The combination of medical images and patients' masses allowed us to create subject-specific models, which were used in OpenSim to simulate the motion data collected through gait analysis and then, to evaluate the biomechanics of the hip joint.

Subsequently, outputs from OpenSim were postprocessed in Matlab. Firstly, data were filtered, resampled and normalized in the subject's body weight (BW) to compare patients with each other. Secondly, we analysed and plotted the correlation between the varus angle in the target limb and the peak of the contact forces in the contralateral limb. The mean values and boxplot of the peaks at hip joint were evaluated for each task, too.

Lastly, we examined our results through a statistical analysis, by applying statistical parametric mapping (spm) and Mann-Whitney U-tests, and we validated them by comparing EMG signals, which were collected during gait analysis sessions, with corresponding muscles activation, computed within model simulation in Open.

3.1 PATIENTS

Table 1 reports the 19 patients which have been analysed in this thesis. The whole HTO project plans to study 50 subjects, however, as it's still at an early phase, for some of them all the data haven't been collected yet. The group includes 15 males and 4 females, with an average age of 52.3 (±7.5) and a body mass index (BMI) that goes from 20.4 kg/m^2 (normal weight) to 35.7 kg/m^2 (grade II obesity), with most of them being overweight (40).

Subject	Age	Weight [kg]	BMI [kg/m^2]	Gender	Group	Target	Contralateral	Side
BA	39.7	93.7	27.1	M	C	4.4°	6.8°	R
BC	60.8	83.3	27.5	M	C	5.6°	7.1°	L
BCA	61.3	58.0	21.8	F	O	8.5°	4.0°	R
BN	57.2	89.6	31.0	M	O	10.9°	10.2°	L
BS	46.5	66.2	23.5	M	O	7.2°	3.5°	L
BSE	47.0	88.1	26.0	M	O	7.0°	8.1°	R
CA	58.7	80.5	25.1	M	O	9.3°	6.1°	L
CC	62.0	66.9	25.5	M	C	5.3°	2.9°	R
CG	53.8	93.7	34.0	M	O	11.8°	6.1°	R
CGC	53.6	112.4	35.1	M	O	2.6°	-2.1°	R
CL	52.9	97.7	27.9	M	O	14.0°	10.4°	L
GF	62.3	65.1	21.8	M	O	5.5°	5.2°	R
LC	52.0	70.9	25.4	F	C	2.4°	1.4°	R
MR	46.3	80.1	26.8	M	O	9.8°	6.6°	R
PL	48.6	55.5	20.4	F	O	6.7°	4.2°	L
SA	46.0	119.7	31.5	M	O	13.4°	7.0°	L
SEA	38.1	67.4	23.3	M	C	8.1°	8.1°	R
TM	59.8	67.8	23.5	F	O	7.7°	0.4°	R
UI	47.4	105.6	35.7	M	O	6.8°	5.5°	R
mean (SD)	**52.3 (7.5)**	**82.2 (18.4)**	**27.0 (4.6)**	/	/	**7.7° (3.2)**	**5.3° (3.2)**	/

Table 1 – Subjects' characteristics

All the subjects are affected by symptomatic early medial osteoarthritis, with varus tibiofemoral malalignment of 7.7° (±3.2) and 5.3° (±3.2) in both target and contralateral limb, respectively (12). Moreover, being young and active people, they represent the ideal patient for high tibial osteotomy (21) and were recruited after the surgeon consultant.

Before data collection, subjects were randomly divided into a Control and an Operative group, with the aim of a post-operative analysis of the experimental results. The first group is treated with a conservative therapy, the second one undergoes the surgical operation. However, for some patients with excessive pain and progression of osteoarthritis at the knee, the surgeon can decide for the osteotomy, even if she/he was selected for the conservative therapy.

Finally, for each subject, medical images and gait analysis data were collected. RX (panoramic and Rosenberg), CBCT and MRI were used to compute tibiofemoral misalignment angles through HTO-RPlus software, and to evaluate the progression of the disease at knee joint. Instead, marker trajectories, ground reaction forces and EMG signals allowed to create a subject-specific model via OpenSim, whose results were then analysed and processed in Matlab to focus the attention on hip joint loads and muscle forces and activations, and to perform a statistical analysis.

3.2 GAIT ANALYSIS EXPERIMENTAL SETUP

The aim of this thesis was to evaluate the effect of tibiofemoral malalignment on hip contact forces, especially on the contralateral limb, during daily motor activity. For this reason, subjects were tracked through a stereophotogrammetric system while performing 3 motor tasks of daily life (walking, stair ascending and stair descending).

The motion capture setup used in this experience is an optical system which consists of:

- A set of markers
- Several 2D cameras
- 2 force platforms
- 16 EMG sensors

We applied passive markers in specific body landmark by following the IORgait protocol, defined by Leardini et al. (60) in 2007, which was proposed for the analysis of pelvis and lower limb motion in impaired children and involves the attachment of 22 skin markers as reported in *Figure 22*. Using a specific protocol, we can reduce uncertainties regarding

markers mispositioning and thus enhancing the reliability of outputs. However, results inaccuracies may also regard instrumentals errors, due to bad reconstruction of markers position in global frame, and skin movement artefacts, due to the relative movement of the markers with respect to the underlying bone. While the formers can be filtered, the latter are associated with the presence of soft tissues, and they increase with subject's BMI and movement. This error cannot undergo a filtering process, but it can be minimized by choosing those locations in which the displacement between marker and bone is minimal (59). Thus, based on Leardini protocol, we positioned 11 reflecting markers in each lower limb, 4 in the pelvis and 4 in upper body portion, corresponding to 30 total markers which were then recorded by a Vicom cameras system during patients' motion (69).

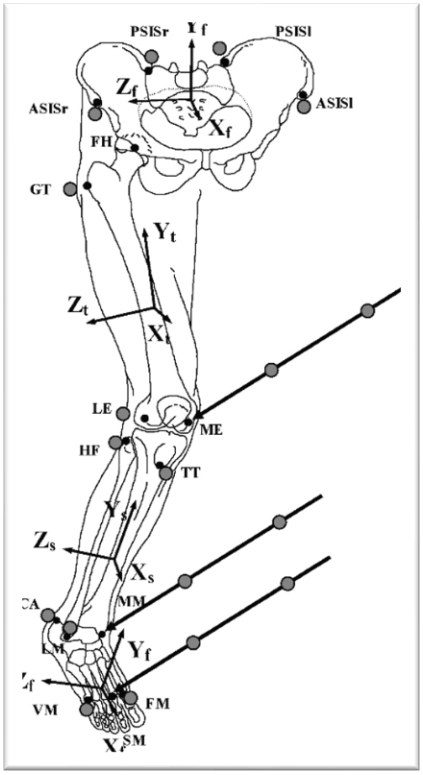

Figure 22 – IORgait protocol

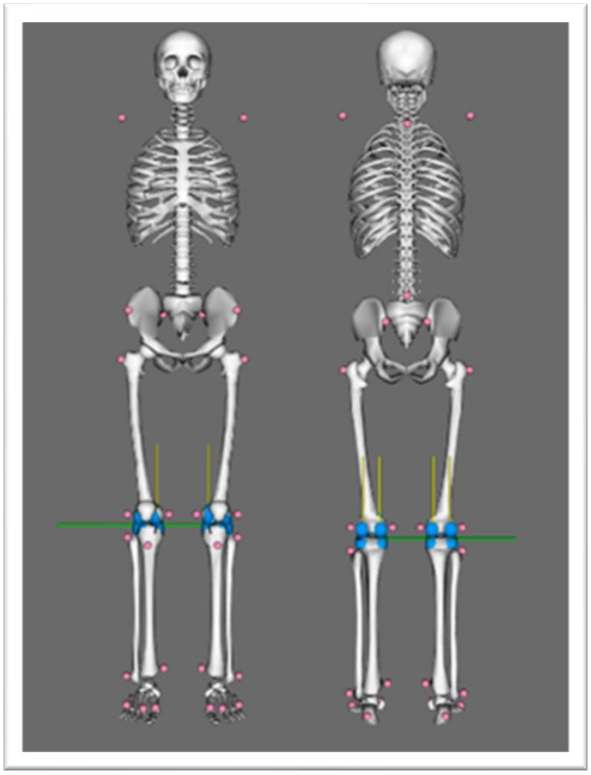

Figure 23 – Markers set used for this project

The complete markers set used in this project is shown in *Figure 23* and listed below:

- A (R&L) – *Acromion*
- C7 - 7th *cervical vertebra*
- L5 - 5th *lumbar vertebra*
- PSIS (R&L) – *posterior iliac spine*
- ASIS (R&L) – *anterior iliac spine*
- GT (R&L) – *great trochanter*
- LE (R&L) – *lateral epicondyle*

- ME (R&L) – *medial epicondyle*
- HF (R&L) – *proximal tip head fibula*
- TT (R&L) – *tibial tuberosity*
- LM (R&L) – *lateral malleolus*
- MM (R&L) – *medial malleolus*
- CA (R&L) – *tendon insertion on calcaneus*
- FM (R&L) – *first metatarsal head*
- SM (R&L) – *second metatarsal head*
- VM (R&L) – *fifth metatarsal head*

2 force platforms and 16 EMG sensors, 8 for each lower limb, completed the experimental setup. Trough each motor task, schematized in *Figure 24* and *Figure 25*, the former computed the ground reaction forces during the bearing phase and the latter used surface electrodes to record the EMG signals, which were then used to validate the subject-specific musculoskeletal models. The analysed muscles are listed below:

- GMED – *gluteus medius*
- ES – *erector spinae*
- RF – *rectus femoris*
- VML – *vastus medialis*
- BFLH – *bicep femoris long head*
- STEND – *semitendinosus*
- GASTMH – *gastrocnemius medial head*
- TA – *tibialis anterior*

Once the experimental setup was settled, patients successfully repeated each motor task for 5 times. In the other hand, standing position was maintained for several seconds and performed in two different ways: one with both feet on the second platform and one with a foot in each platform. The first one allowed us to compute a precise weight value for all the subjects.

During walking and stair ascending tasks, patients positioned the right foot on the first platform and the left foot on the second platform, while in stair descending task the association was inverted, since the subjects were asked to perform the last two tasks subsequently, to prevent them from getting tired.

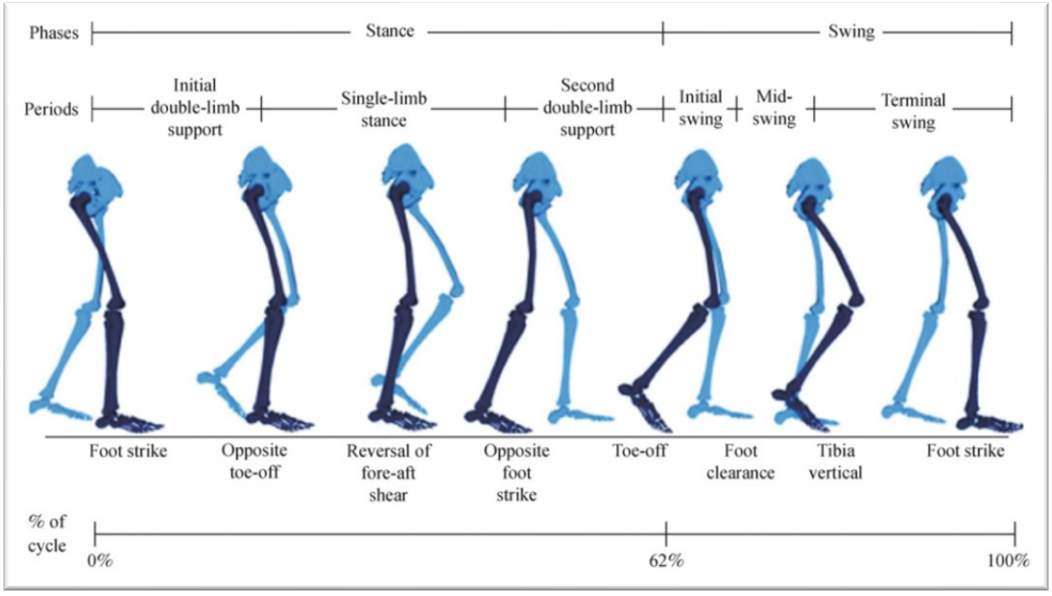

Figure 24 – Gait cycle

All trials were performed at a regular self-selected speed by each subject and were contemporary observed by a technician, to ensure a perfect position of both feet on the platforms but not influencing the patient' gait.

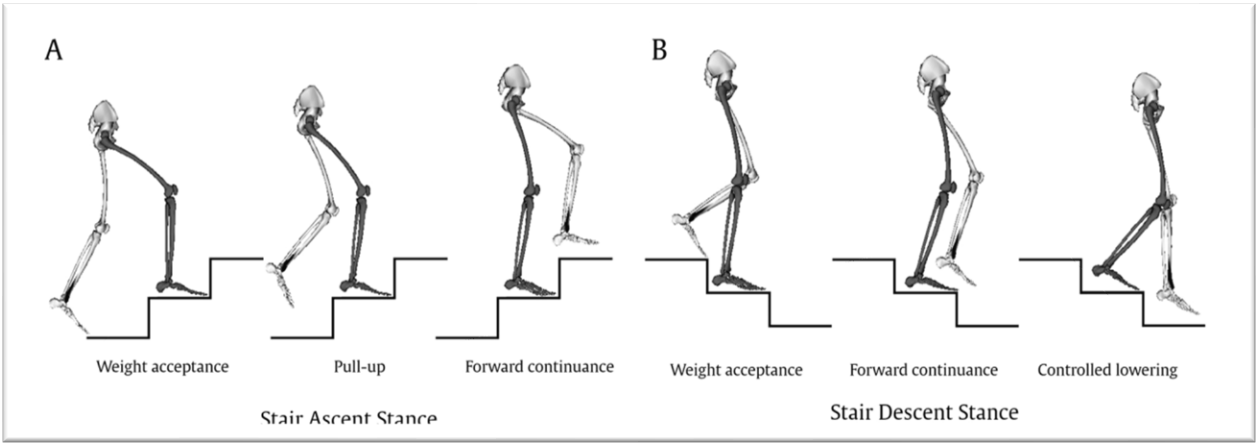

Figure 25 – Stair ascending (A) and stair descending (B)

3.3 LERNER MUSCULOSKELETAL MODEL

As said before, this script is the prosecution of a previous experience carried out in the same laboratory, which investigated how varus tibiofemoral malalignment influences the knee contact forces on medial and lateral compartment. At the beginning, it has been evaluated if creating a subject-specific model for each patient or to scale a generic one. Several papers report scaled models are too approximative, in particular if considering paediatric or pathological subjects (62,65), and they lack accuracy in estimating joint reaction loads and

muscles forces (63). In the other hand, an ever-greater specificity of the musculoskeletal model leads to more reliable and precise outcomes, confirmed by Lerner et al. (61) and by Lenaerts et al. (64), who evaluated increasing degrees of accuracy in their knee and hip joints models, respectively. However, considering the large dataset used in this project, consisting of 50 patients at the end of the acquisition, the creation of a subject-specific MSK model for each patient would take too long as well as an high experience with specific creation software (66). For this reason, it has been decided to scale a generic model.

The choice fell on the model presented by Lerner et al. (61), whose structure allows to compute separately the medial and lateral component of knee contact forces, which is fundamental for the thesis carried out by Nicolò, but at the same time it allows to evaluate the hip contact forces, which is the focus of this script. In this way, it has been possible to consider two different research questions on the same model, and contemporary saving time. *Figure 26* illustrates the model's structure, which is then described in detail.

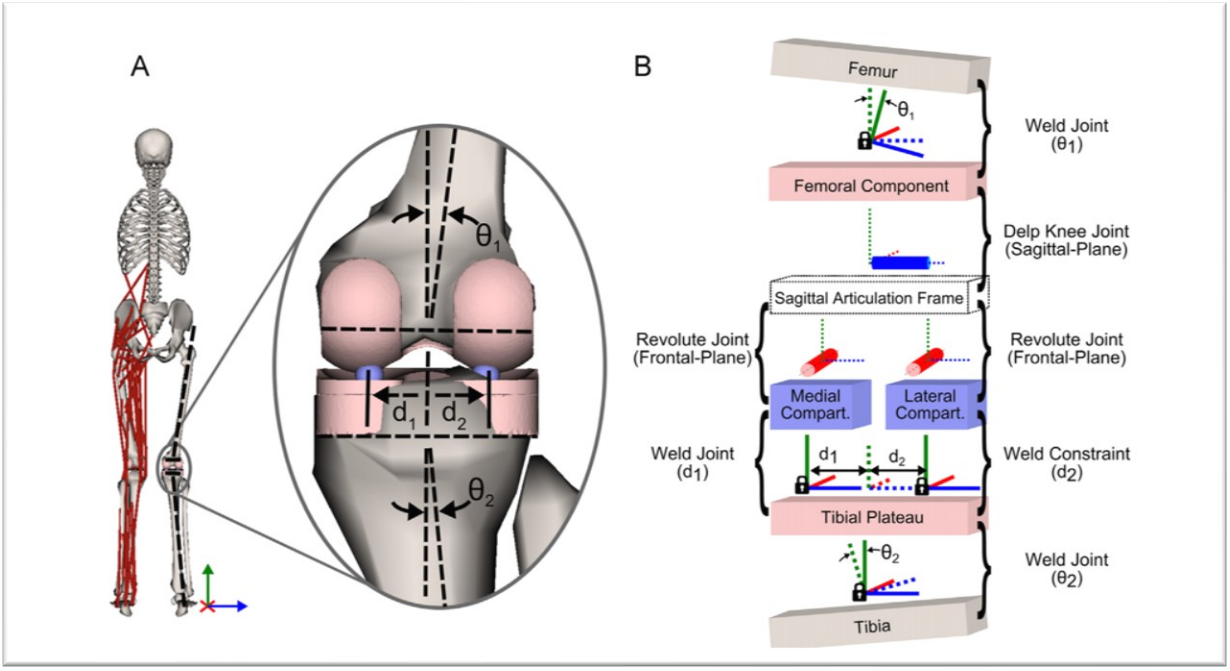

Figure 26 – Graphical (A) and schematic (B) visualization of the modified tibiofemoral joint structure. On the A side, the axis system is set as red axis perpendicular to the sagittal plane, green axis perpendicular to the transverse plane and blue axis perpendicular to the frontal-plane. On the B side, the combination of the weld joints defines the tibiofemoral alignment; the Delp knee joint allows the flexion-extension movement and is represented in blue; the red revolute joints compute the medial and lateral loads; the two weld joints on the tibial plateau define the contact point locations.

Lerner et al. developed a model of the tibiofemoral joint and incorporated it within DeMers' full-body model (67), comprised of 18 body segments and 92 muscle-tendon actuators, with a ball in socket joint between the third and the fourth lumbar vertebra and at each hip, revolute ankle and subtalar joint, and 6 degrees of freedom of the pelvis (61). As shown in *Figure*

26.B, the tibiofemoral model consists of a series of joints placed between a distal femoral component and a proximal tibial plateau. Through the weld joints, which fix the latter to the femur and the tibia, respectively, it is possible to configure frontal-plane tibiofemoral alignment, previously computed within HTO-RPlus software. The series of joints mentioned before allows to evaluate the knee kinematics and the load distribution between each compartment. Listed from the top there is:

- The Delp joint (68). It allows the flexion-extension movement and divides the femoral component from the sagittal articulation frame.
- Two revolute joints. They are oriented in the frontal plane and act in parallel to bear all loads between the two bones. In this way they compute the medial and lateral knee contact forces required to balance the net forces and moments acting in the tibiofemoral joint. The joints separate the sagittal articulation frame from the medial and lateral compartments.
- Two weld joints. They fix the two compartments to the tibial plateau.

The structure of the model also allows to define the contact points location by setting the distance between the two weld joints described above. This distance is 40 mm by default, with d_1 and d_2 both distant 20 mm from the midpoint of the tibial plateau. The points locations are different between subjects and have been demonstrated influencing knee contact forces (61). However, in these two theses we haven't been able to specify them due to lack of time and a specific calculation procedure. It will be the next step in the whole HTO project.

3.4 HTO-RPlus SOFTWARE

HTO-RPlus software was developed for HTO planning by using the open-source platform ALBA (Agile Library for Biomedical Applications) (70), which has been created inside the Bioengineering and Computing Laboratory (BIC) of Rizzoli Institute.

It has been tested and approved by surgeons involved in HTO project and it is currently adopted by clinicians in planning. By importing RX in DICOM format, HTO-RPlus allows to:

- Quantitatively evaluate tibiofemoral alignment/misalignment of the patient.
- Plan HTO surgery on panoramic weight-bearing RX, lateral RX and Rosenberg projection.
- Display the final correction, reporting all anatomical and mechanical angles.

The text “Principles of deformity corrections” by D. Paley was taken as reference in defining the articular points and the mechanical and anatomical axes of lower limbs inside the software (71).

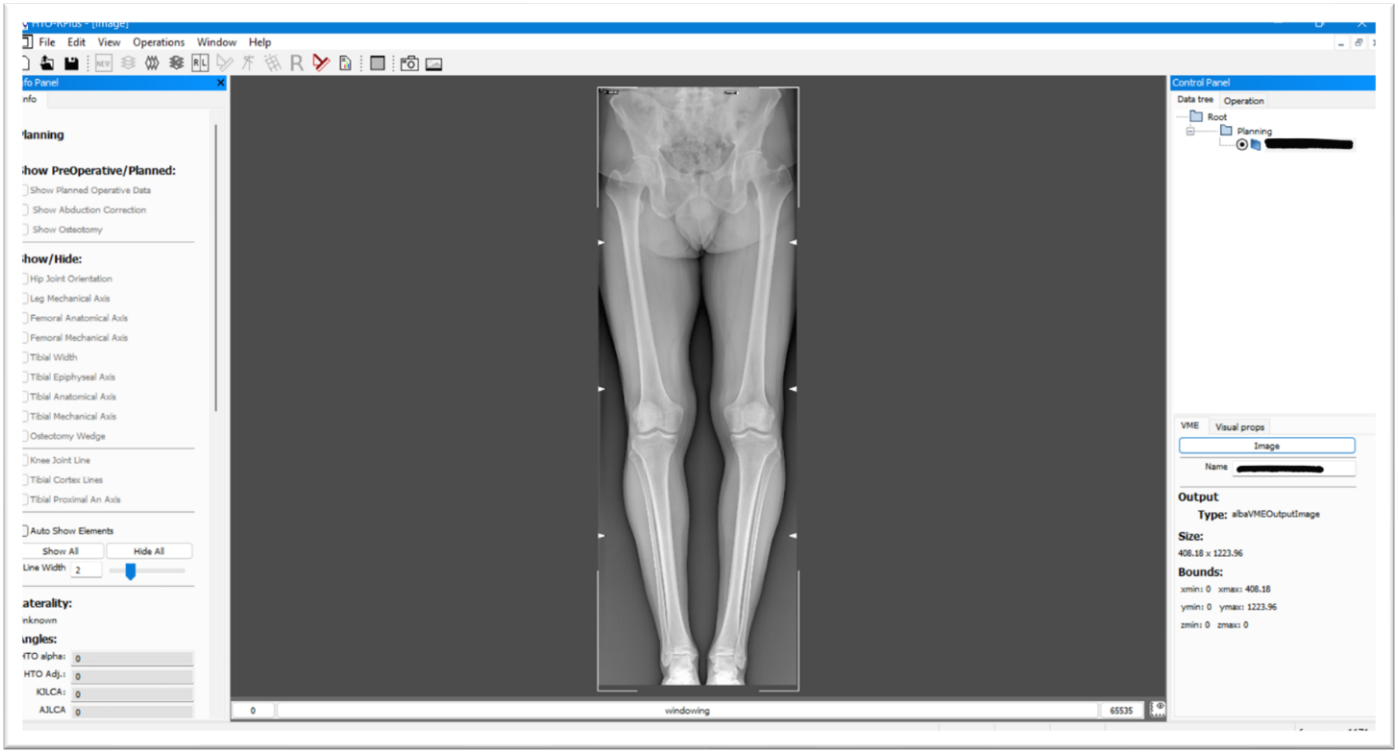

Figure 27 – Graphical User Interface

Figure 27 shows the Graphical User Interface (GUI) with the panoramic weight-bearing RX of a generic patient. The bar on top, reports the planning modalities, which differ according to the RX images; on the left the values of the angles, the “windowing” bar below allows to increase/decrease the contrast of the image. Moreover, the software is capable to process multiple images simultaneously, which are selected on the right panel and displayed in the central one. By using a panoramic weight-bearing RX image, the entire planning procedure is described below:

i. With the marked button in the top bar of *Figure 28*, the target limb is selected. In this thesis we evaluated both the target and the contralateral limbs to create a precise subject-specific model via OpenSim and to perform the statistical analysis.

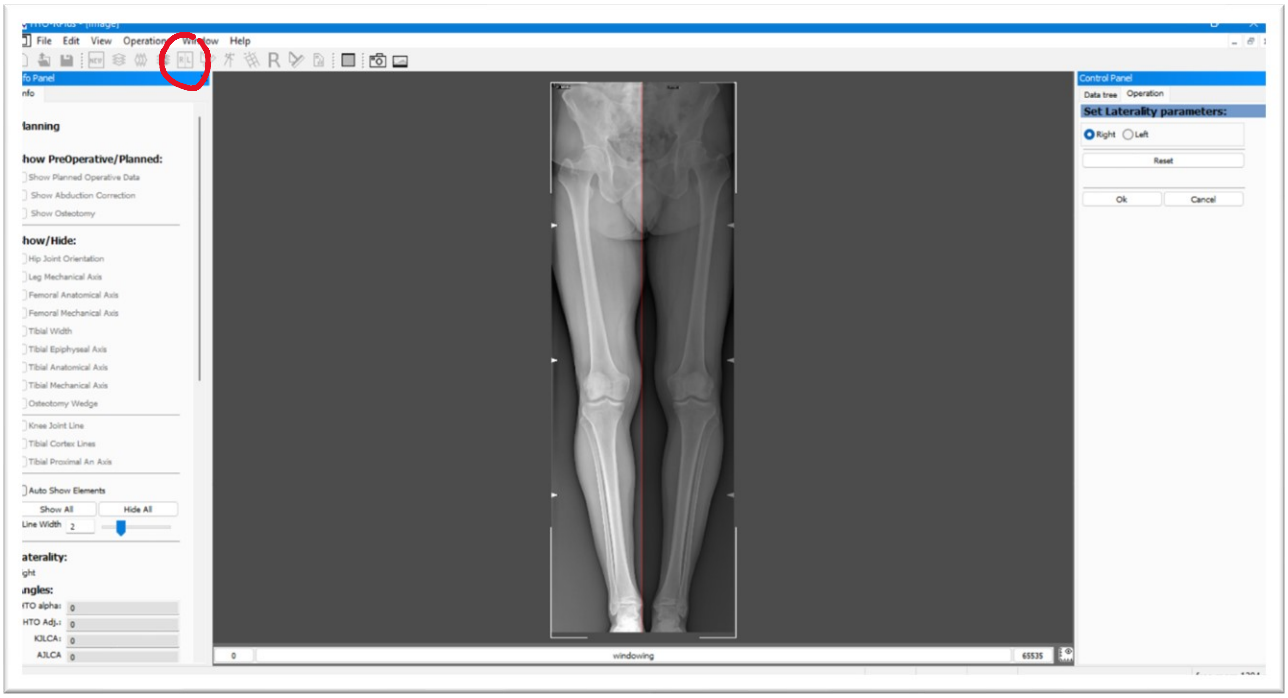

Figure 28 – Limb selection

ii. By selecting the circled button in *Figure 29*, we start the acquisition of the measures. The sequence is reported on the right side followed by a small illustrative explanation. The first step identifies the *Hip Joint Center,* defined as the center of the femoral head.

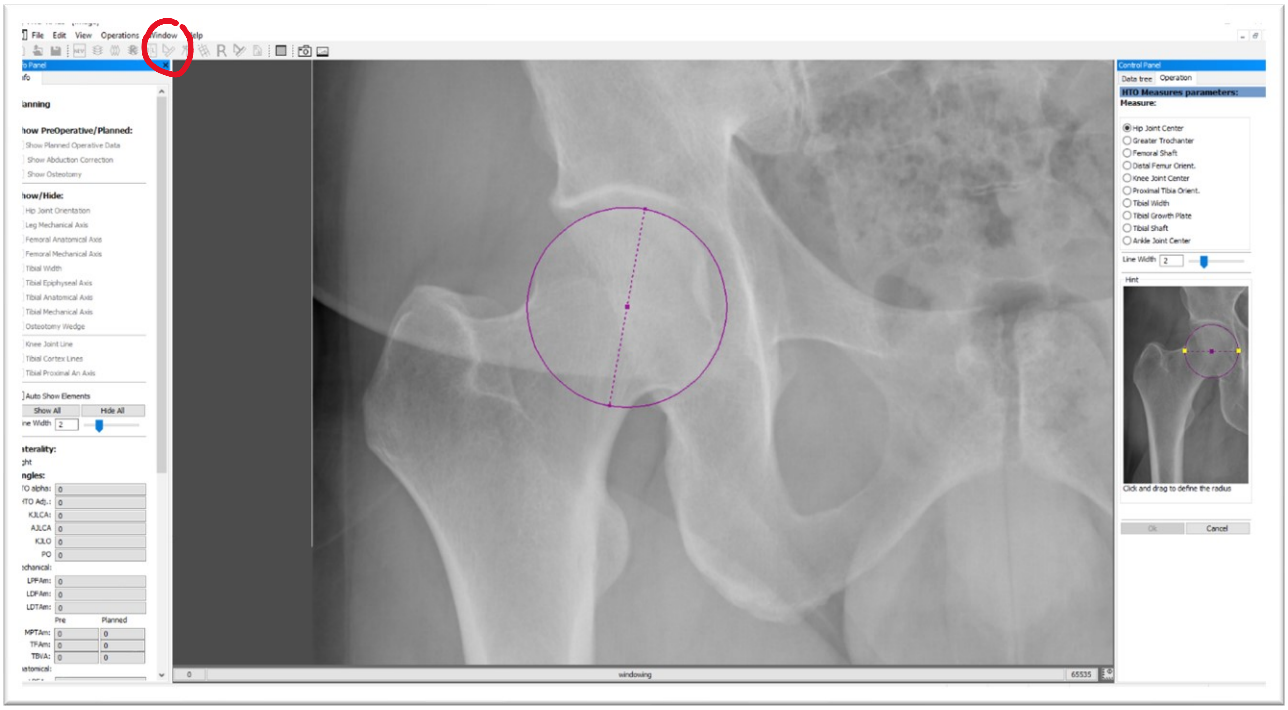

Figure 29 – Hip joint center

iii. The red point in *Figure 30* indicates the *Greater Trochanter*. In this case it can be useful to increase the contrast of the image to better define the point.

Figure 30 – Greater trochanter

iv. The identification of the *Femoral Shaft* in *Figure 31* allows to compute the femoral anatomical axis (8).

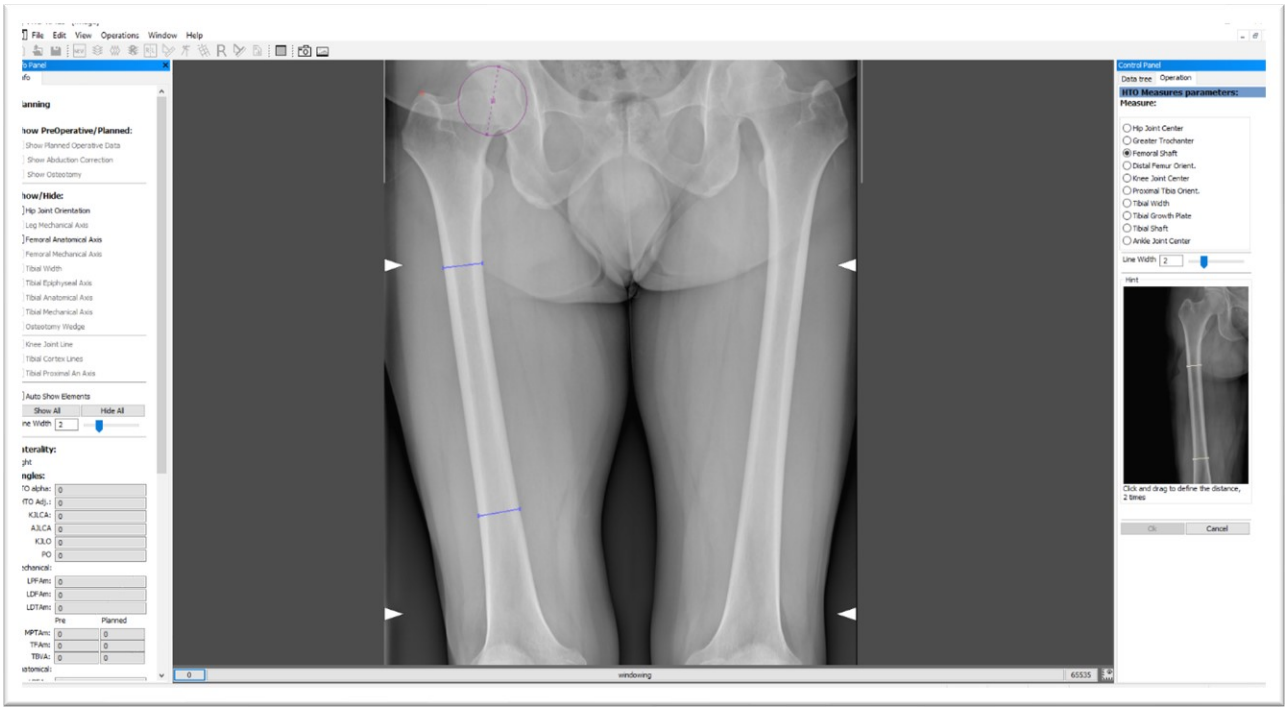

Figure 31 – Femoral shaft

v. The *Distal Femur Orientation* (*Figure 32*) is represented by a line passing through the two points located on the most distal part of the medial and lateral femoral condyles.

Figure 32 – Distal femur orientation

vi. The *Knee Joint Center* (*Figure 33*) identifies the midpoint between the medial intercondylar tubercle and the lateral intercondylar tubercle, also called tibial spines.

Figure 33 – Knee joint center

vii. The *Proximal Tibial Orientation* (*Figure 34*) returns the inclination of the tibial plateau.

Figure 34 – Proximal tibia orientation

viii. The *Tibial Width* (*Figure 35*) represents the width of the tibial plateau.

Figure 35 – Tibial width

ix. The *Tibial Growth Plate* (*Figure 36*). Growth plates are located near joints and are active in children and adolescents. Since they are not calcified yet, they do not appear on X-rays and once the maturity is reached, the growth plates close. Moreover, due to its softness, growth plates frequently fracture.

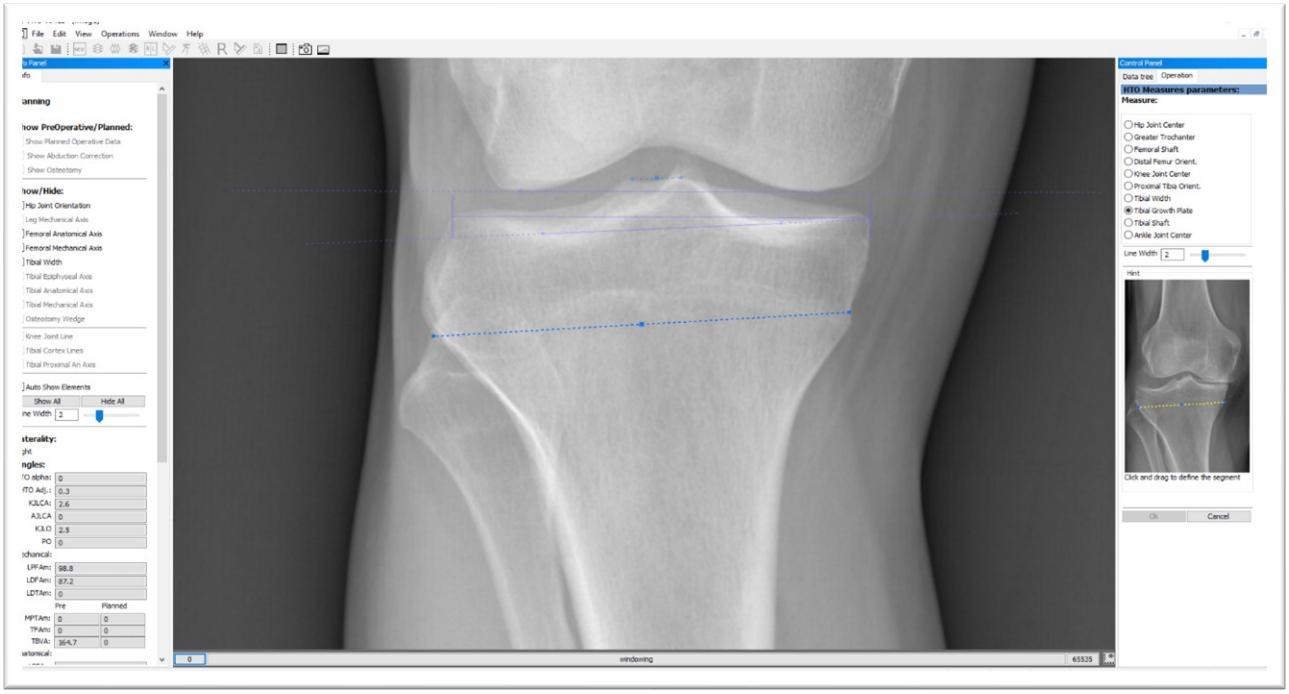

Figure 36 – Tibial growth plate

x. The *Tibial Shaft* (*Figure 37*), as in the femur case, allows to compute the tibial anatomical axis (8).

Figure 37 – Tibial shaft

xi. The *Ankle Joint Center* (*Figure 38*), as the midpoint of the proximal part of the talus.

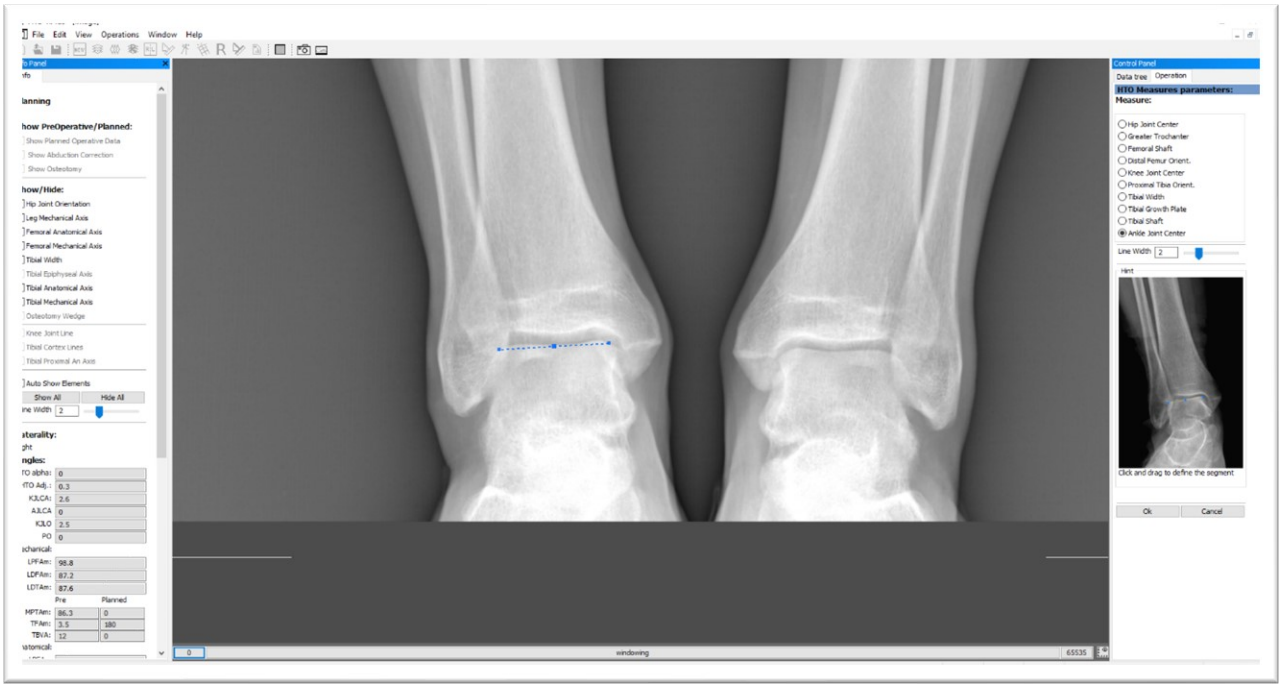

Figure 38 – Ankle joint center

Finally, we can observe in *Figure 39* the right leg mechanical axis (blue), the femoral and tibial mechanical axes (green) and the femoral and tibial anatomical axes (red). Hence, it is possible to evaluate the tibiofemoral malalignment both qualitatively and quantitatively. In particular, the value of *TFAm* (Mechanical Tibial Femoral Angle) is interesting to us. The others are very specific measures which are not needful for this thesis.

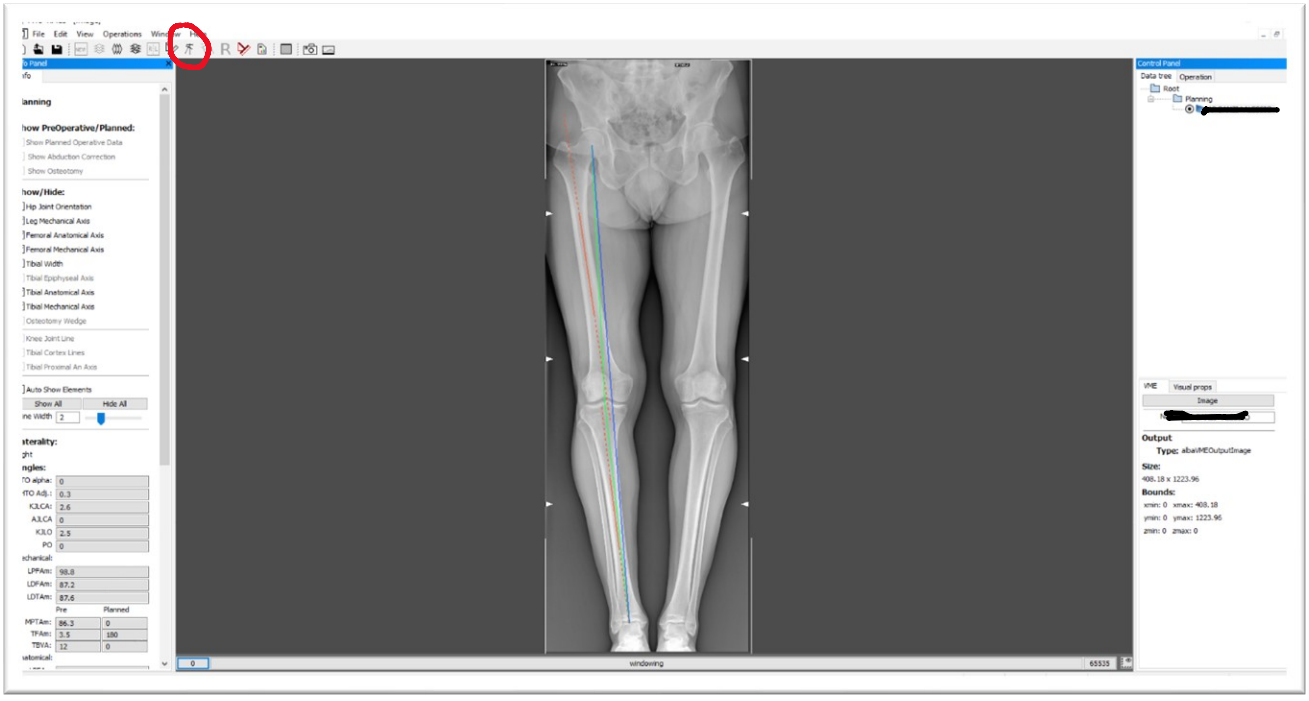

Figure 39 – Tibiofemoral malalignment

Now, all the measurements have been taken and by selecting the button circled in red in the *Figure 39*, we can visualize the steps of the HTO surgery planning, which are reported in the right panel of the figures below.

a) We define the *Cortical Point* as the intersection between the green line, which is given, and the lateral surface of the tibia (*Figure 40*).

b) We define the *Cutting Point* as reported in the instruction on the right. It corresponds to the point where the surgeon will perform the cut. Even in this case, the green line is given by the software (*Figure 41*).

c) Lastly, the software automatically generates the three green axes and the pink point displayed in *Figure 42* below, by using the data of the previous two steps. The pink point represents the *Hinge Point*, around which the osteotomy will rotate.

Figure 40 – Cortical point

Figure 41 – Cutting point

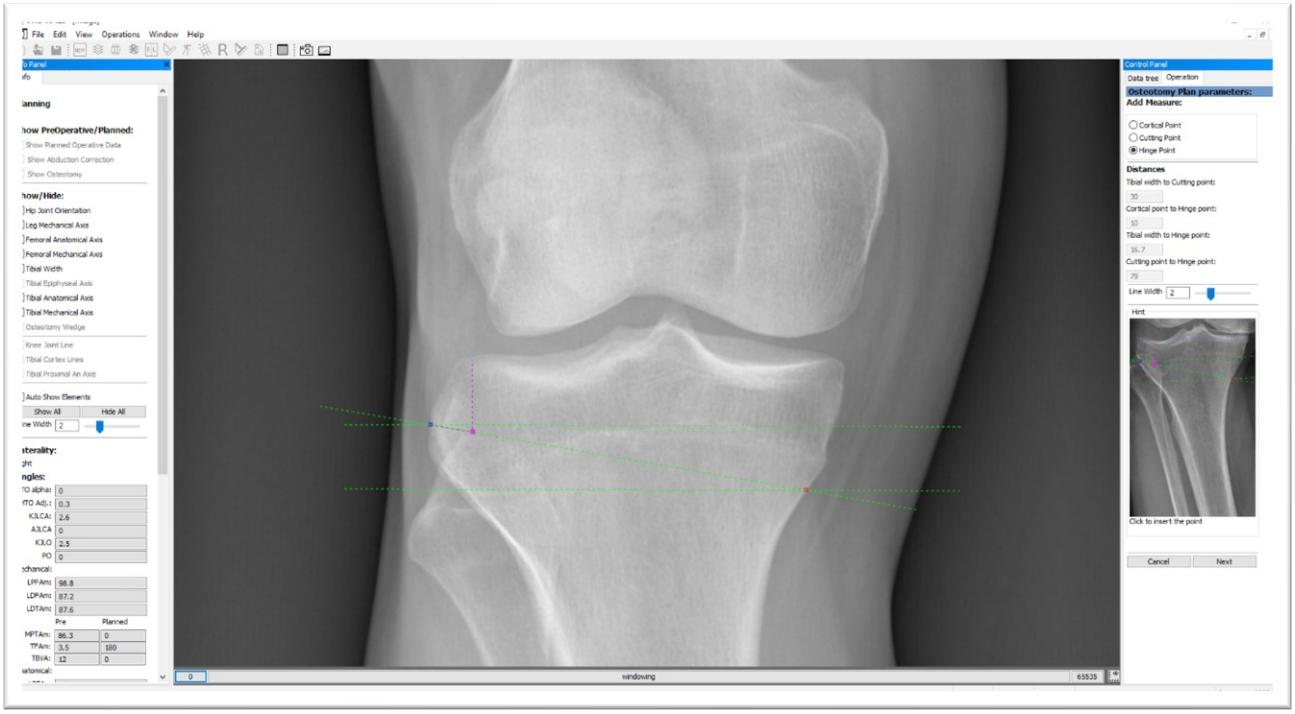

Figure 42 – Hinge point

It is now possible to graphically simulate the surgery by moving the midpoint of the talus. *Figure 43* represents the pre-operative phase. The tibiofemoral malalignment (*TFAm*) is reported on the left, while on the right are reported the correction angle and the mechanical axis – tibial width intersection, expressed in percentage.

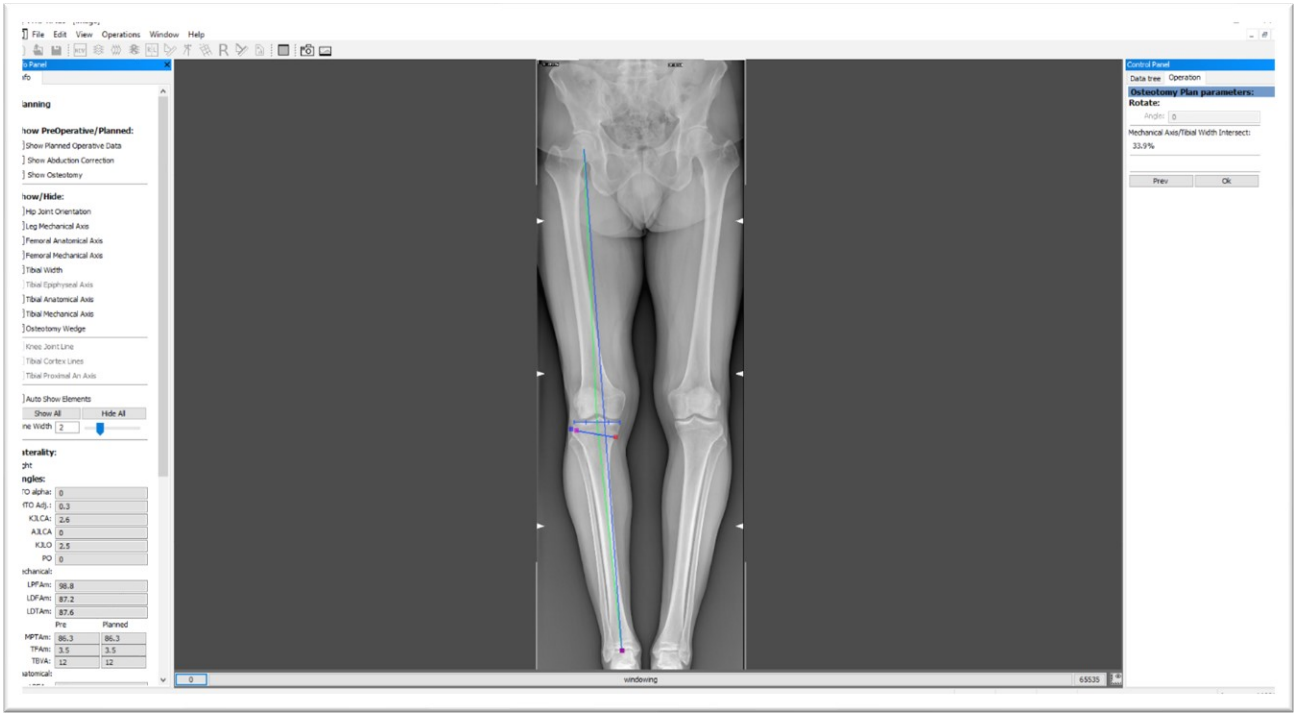

Figure 43 – Pre-operative phase

The operation outcome must be a perfect alignment between the femoral and tibial mechanical axes and the leg mechanical axis (8). Based on this, we rotate clockwise the midpoint of the talus until we graphically reach a perfect alignment of the green and blue axes. Otherwise, we can rotate the same point until the *TFAm* planned value on the left panel becomes null, leading to a more precise result. On the right panel it's reported the rotate angle in real time. *Figure 44A* and *Figure 44B* report the result of the surgery planning.

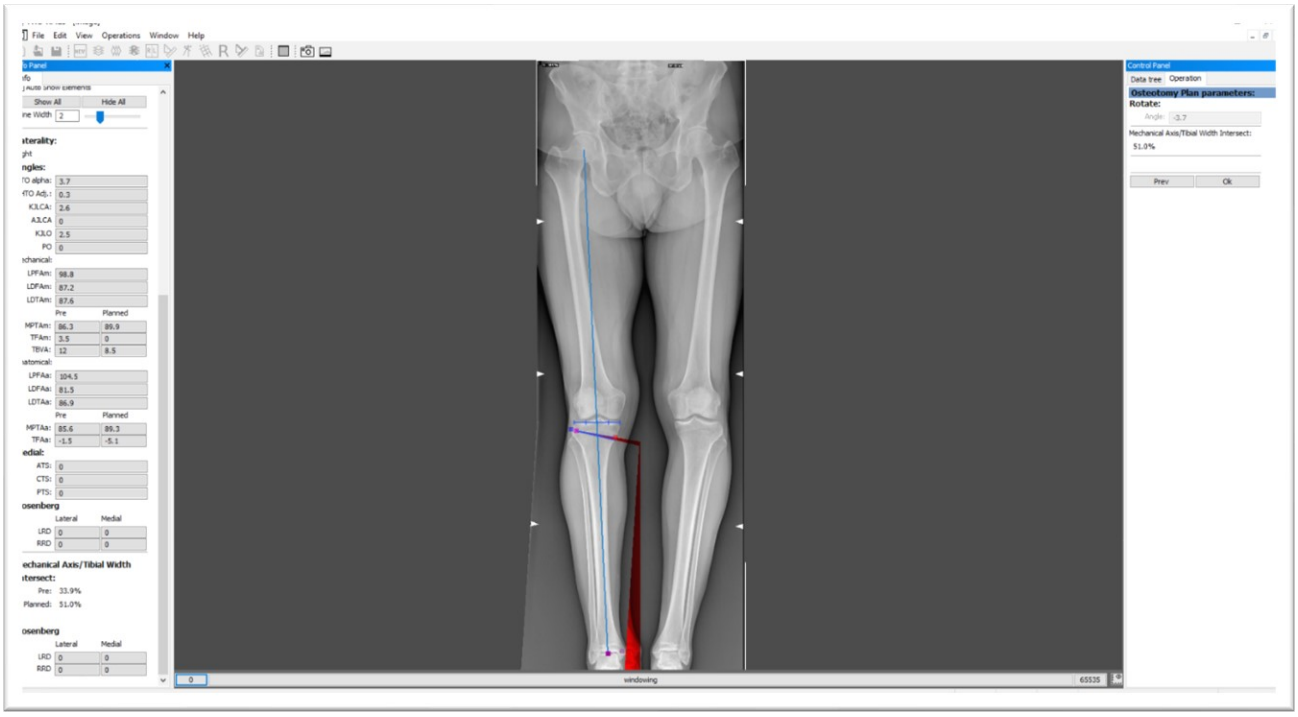

Figure 44A – HTO planning (general view)

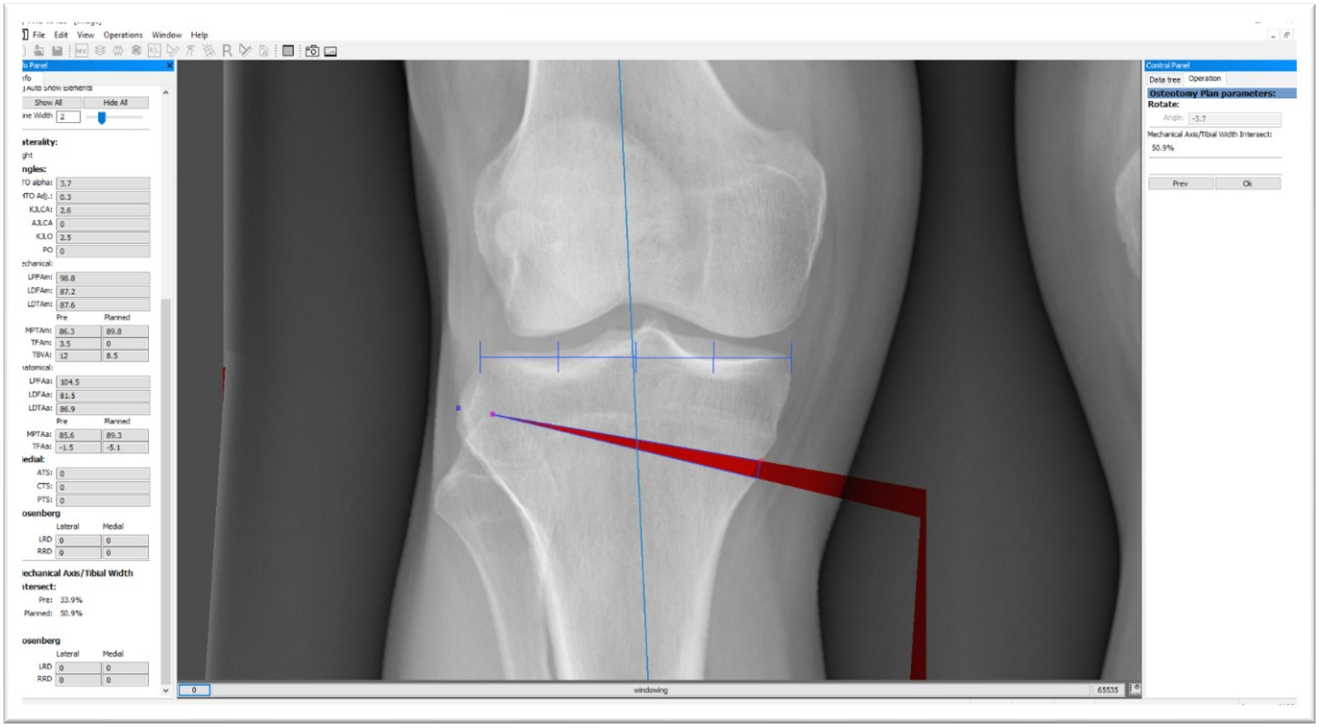

Figure 44B – HTO planning (tibial view)

Finally, the software allows to save into a file the planning outcome and all the measurements for each patient, which can be shown in the operating room. Moreover, this file can be used in a post-operative evaluation, by comparing the performed correction, with respect to the planned one.

3.5 OPENSIM WORKFLOW

OpenSim workflow schematized in *Figure 45* started turning the generic Lerner model into a subject-specific one. Since the software defined the angles in radians and the distances in meters, we converted the tibiofemoral angles calculated within HTO-RPlus software from degrees to radians and then we modified the frontal plane orientation of both target and contralateral knee joints, which combined the femoral and tibial weld joints angles in *Figure 26*.

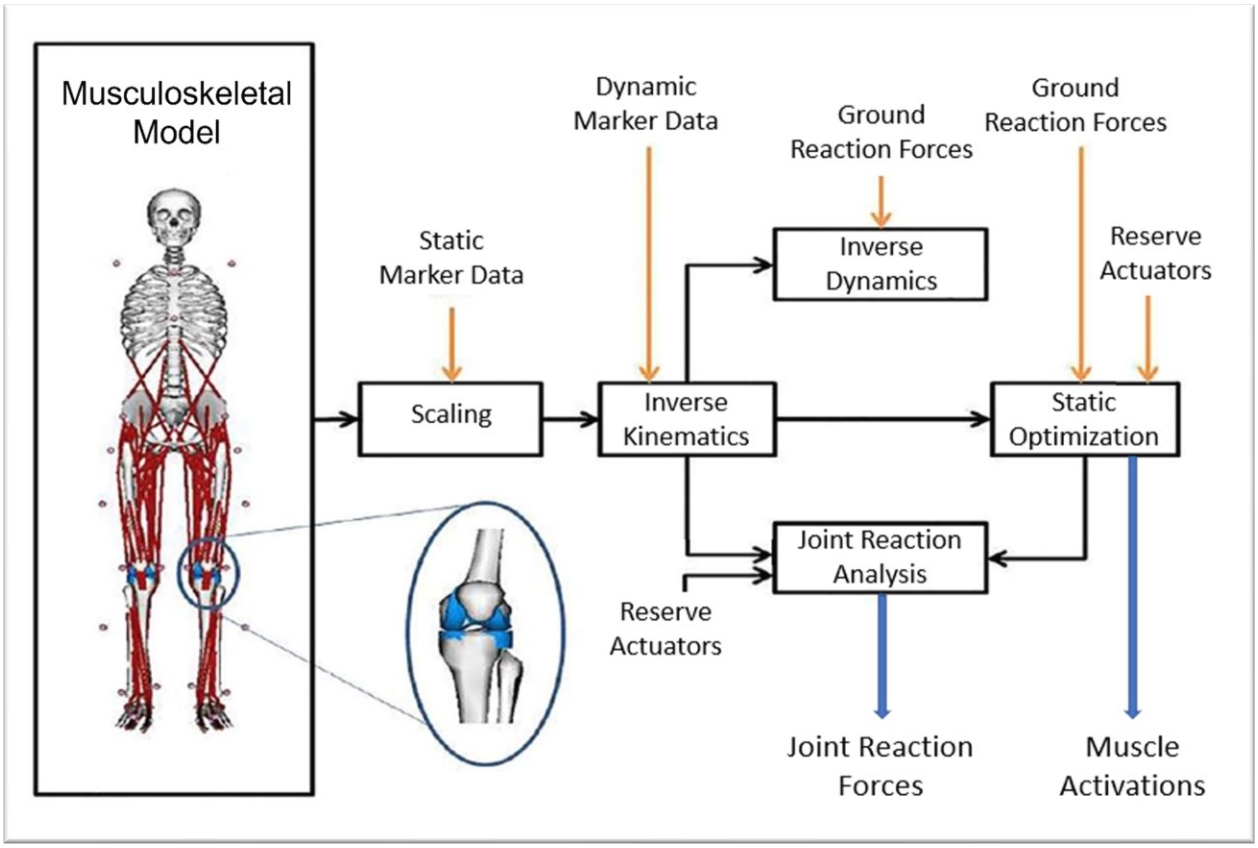

Figure 45 – OpenSim workflow for this thesis

Once defined the tibiofemoral alignment, the Scaling tool was used to minimize the errors between experimental markers in standing position and the IORgait set of corresponding virtual markers. We scaled model's geometry by computing the scaling factors using a measurement set, which was defined by differences between pairs of markers (*Figure 46*), and we scaled the masses and the inertial properties of the segments by specifying the subject's weight, which was calculated through the standing position on a single force platform. Moreover, by evaluating the scaling process of all the subjects, we found that unit markers weighting factors and the disabling of both the great trochanter (GT) markers, improved the scaling results. The latter was possibly due to the high BMI value of the patients. Lastly, in the "Messages" window we verified that the maximum marker error and an RMS error were less than 2 cm and 1 cm, respectively (53).

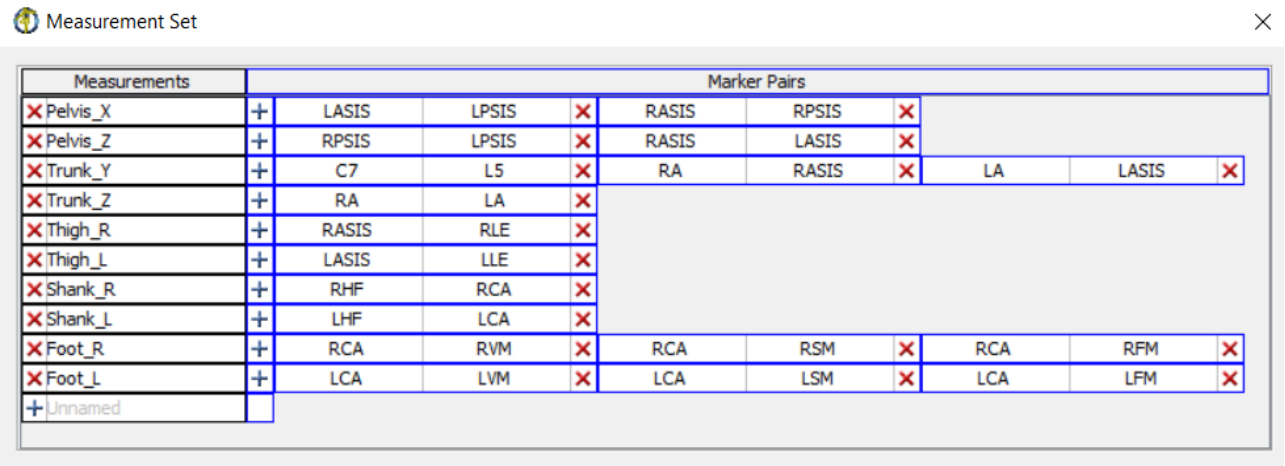

Figure 46 – Measurement set in scaling factors definition

Subsequently, Inverse Kinematics (IK) tool performed the same minimization operation of the previous step, but from a dynamic point of view and returned as outputs the joints angles and motion. We defined the time range of the simulation between the first heel strike of the right foot and the second heel strike of the left foot, in this way considering the whole gait cycle for both lower limbs, even if we considered only the stance phase during the evaluation of the results. Then we imported the markers trajectories for the specific trial. Differently from the scaling process, all markers were considered, but still keeping the weights of the values to one since no significant differences were noted in changing them. A maximum marker error and an RMS error respectively of 4 and 2 cm or less, were considered good results (53).

In the Inverse Dynamics (ID) step, we imported the motion file coming from the IK analysis and filtered the data. Subsequently, we fixed the same time range of the previous tool and the external loads by setting as input the ground reaction forces (GRF) of the same trial and the IK motion file mentioned before. External loads were defined for both the right and left sides and applied as point forces on the calcaneus of each foot as illustrated in *Figure 47*. The joints moments calculated in this step will be used to control the reserve actuators.

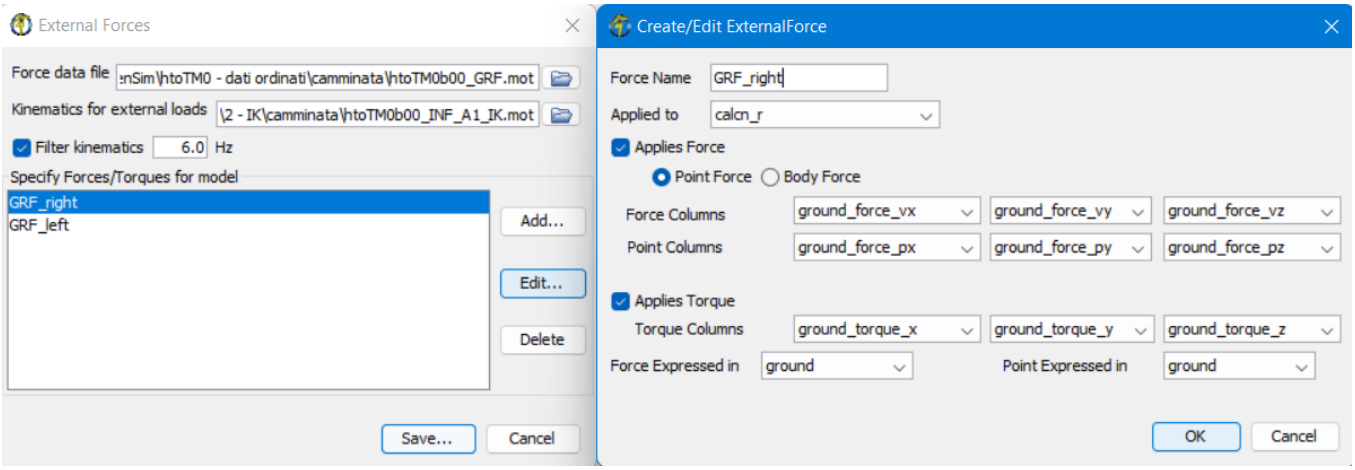

Figure 47 – External loads definition

Through the Static Optimization (SO) tool, we computed the muscle forces and activations, by importing the motion file from inverse kinematics, the external loads defined in ID analysis, and a set of actuators. These latter are divided into two categories: the residual actuators and the reserve actuators. The former are applicated to the first free joint of the model, in our case the pelvis, and resolve the dynamics inconsistency between the estimated model accelerations and the measured ground reaction forces, due to marker measurement error, differences between the geometry of the model and the subject, and inertial parameters (53). The latter are torques that are appended to each joint to increase the force of the actuators. The reserves are involved when an actuator cannot produce enough force to guarantee the movement, however, they should not exceed 5% of the relative maximum external moment magnitude (58). Then, we completed the SO analysis by fixing again the time range and filtering the input data.

Lastly, we performed a Joint Reaction Analysis (JRA) using as inputs the IK motion file, the external loads, the actuators file and the controls and force files coming from the SO analysis. We filtered the input data and fixed the time range. Then, differently from the project carried out by Nicolò, we extracted the hip contact forces from the output file for both target and contralateral limbs.

3.6 DATA POST-PROCESSING

In this phase we observed the interaction between different elements: the motion capture system, biomechanical software like Mokka (72) and OpenSim, and Matlab (73). For each trial and motor task, stereophotogrammetry outputs presented a *.c3d* and *.csv* extension which cannot be directly elaborated via OpenSim. For this reason, *.c3d* file could be processed via Mokka to obtain a *.trc* file, which contained the recorded markers trajectories. In this case the software resulted particularly useful since it directly displayed the patient's motion (*Figure 48*). Otherwise, *.csv* file could be imported and processed within Matlab, returning 4 different outputs:

- *.trc* file, which contained the same markers trajectories of the previous one.
- *.mot* file, which contained the ground reaction forces (GRF) recorded by the force platforms.
- *.mat* file, which contained the EMG data.

- *.mat* file, which contained the instances corresponding to the events of the gait cycle (first foot strike, toe off, second foot strike for both limbs).

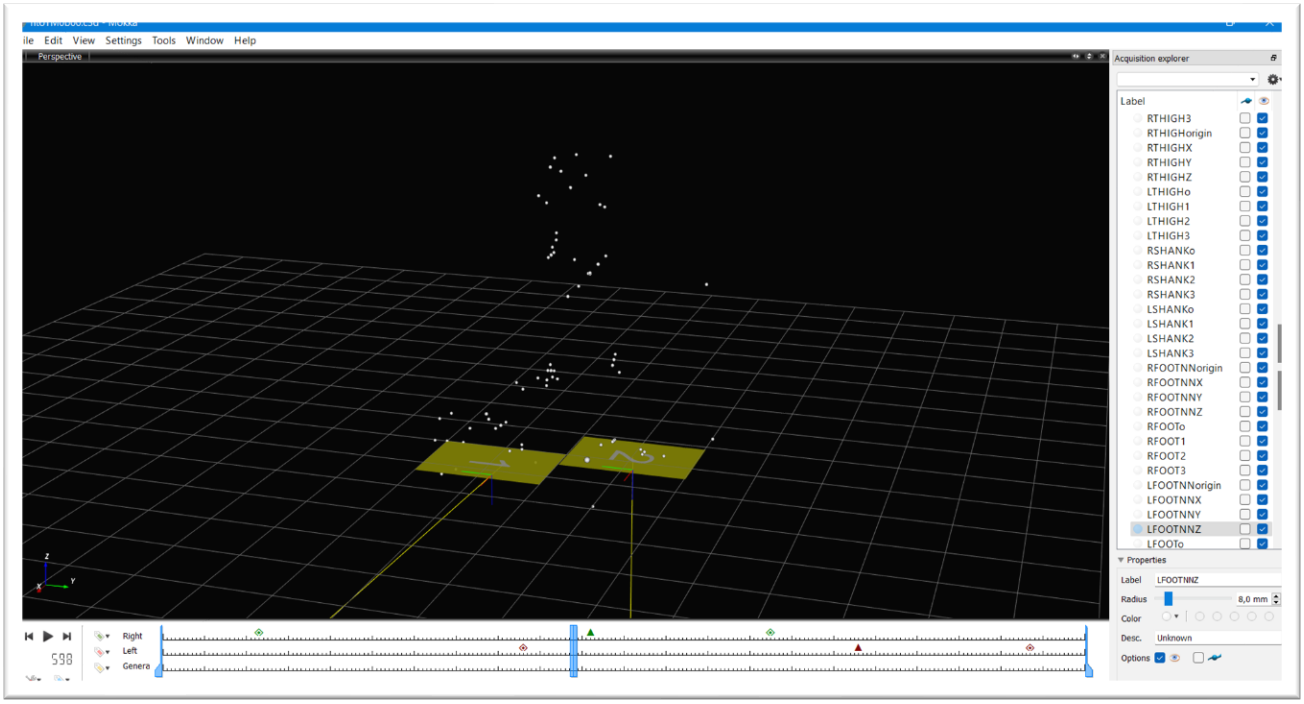

Figure 48 – Graphical User Interface (GUI) inside Mokka

Then, OpenSim took as input the *.trc* and the *.mot* files throughout the whole workflow, and returned outputs in *.mot* extension for the inverse kinematic and in *.sto* extension for the inverse dynamics, the static optimization and the joint reaction analysis, as described in the previous chapter.

Subsequently, these outputs were imported and elaborated in Matlab:

- *.mot* files containing the ground reaction forces were used to compute the subjects' weights in the standing position and to evaluate and visualize the mean and standard deviation GRF values for each task.
- *.mat* files of EMG data were compared to *.sto* files containing muscle activations in order to evaluate the OpenSim results.
- *.mat* files containing the events were used to create subject specific TimeIndex files with all-time indexes of all trials and tasks for each patient.
- . *sto* files from the joint reaction analysis were used to answer the research question of this thesis.

In particular, hip contact forces were loaded from *.sto* files, and computed as the Euclidean norm of the three directional components for both target and contralateral limb. Differently

from the previous thesis, here we focused only on the stance phase of each task, since we were only interested in the loading phase and in the forces peaks, which were much higher in the stance phase with respect to the swing one, as reported from the results. For this reason, hip contact forces, as well as muscle activations and GRF, were selected within this time interval, normalized to BW and stored in cells. Then, they were filtered with a lowpass 6^{th} order Butterworth filter and resampled in 100 samples long vectors, representing the percentage of the stance phase. These final cells contained the normalized, filtered and resampled hip contact forces organized in target and contralateral limb. Mean and standard deviation were also evaluated between the trials across all motor tasks for each subject and between all subjects for each motor activity.

3.7 STATISTICAL ANALYSIS

To evaluate our results and in particular the correlation between target tibiofemoral malalignment and contralateral hip contact forces, we run a statistical analysis in Matlab.

For each motor task, considering all the subjects and all the trials performed, we calculated mean, standard deviation, and mean difference for each frame to plot a comparison between target and contralateral limb and to obtain the maximum difference value between the means of the two limbs.

Then, differences in target and contralateral hip contact forces were evaluated using statistical parametric mapping (SPM). Performing a SPM nonparametric two-tailed unpaired t-test ($\alpha = 0.05$), they were considered statistically significant if they corresponded to at least 4% of the gait cycle (74).

Furthermore, we assessed a linear correlation (R, p-value) in three different combinations: peak contact forces and tibiofemoral malalignment in the target limb, peak contact forces and tibiofemoral malalignment in the contralateral limb, and peak contact forces in the contralateral limb and tibiofemoral malalignment in the target limb.

Finally, we evaluated the boxplot of peak contact forces in the target and the contralateral limbs for the specific motor task, and the boxplot of tibiofemoral malalignment angles in the two limbs. In both cases, the statistically significant difference between target and contralateral was tested using a Mann-Whitney U-test ($\alpha = 0.05$).

3.8 MODEL VALIDATION

The last step of this thesis concerned the model validation. This was carried out in Matlab by a comparison between EMG signals recorded during the gait analysis session, and the corresponding muscle activations taken from the outputs of the Static Optimization tool of OpenSim.

For this purpose, EMG signals were filtered with a Butterworth 6^{th} order filter at 1kHz and then rectified to obtain positive values. As reported in *Data Post-Processing* section, in this thesis we focused our attention only on the stance phase of the gait cycle, therefore EMG data were cut in the time range from heel strike to toe off and then resampled to 100 samples, representing the percentage of the considered interval.

Once selected the model's muscles corresponding to those recorded by EMG sensors, the cutting operation of the correct time range and the resampling process were applied to the muscle activations files as well. Finally, we normalized both vectors to better understand the comparison.

4. RESULTS

In this section we reported the results of our experience, which are then analysed and discussed in the next chapter. Differently from what Nicolò did in his thesis, where he focalized his attention on the medial and lateral compartment of the knee joint, here the clinicians asked us to investigate the correlation between the varus tibiofemoral malalignment in the target limb and the hip contact loads in the contralateral limb. The aim was to understand more deeply the biomechanical implications of this misalignment.

In our results we analysed not only the differences between the target and the contralateral limbs, but we also made a comparison with Nicolò's results, in particular with the knee medial compartment since it carried most of the joint load and thus more comparable values (15). As said in previous chapters, this study focused only on the stance phase of each lower limb, thus when the feet touched the corresponding force platforms.

The results included:

- Peak forces – varus angles linear correlation for each motor task, distinguishing the target limb from the contralateral one, but also the correlation between angles in target and forces in contralateral, which was our research question.
- Hip contact forces of both limbs, expressed in body weight and represented in the same figure with respect to the percentage of the stance phase, reporting the mean and SD values for each task. These plots were followed by the correspondent mean difference and statistical parametric mapping (spm).
- Boxplots of the force peaks for each task.
- Boxplot of the malalignment angle distribution in each limb.
- Mean and SD values of the ground reaction forces, comparing the target and the contralateral for each task.
- EMG validation, comparing muscles activation with EMG recorded signals.

4.1 PEAK FORCES-VARUS ANGLES CORRELATION

Walking

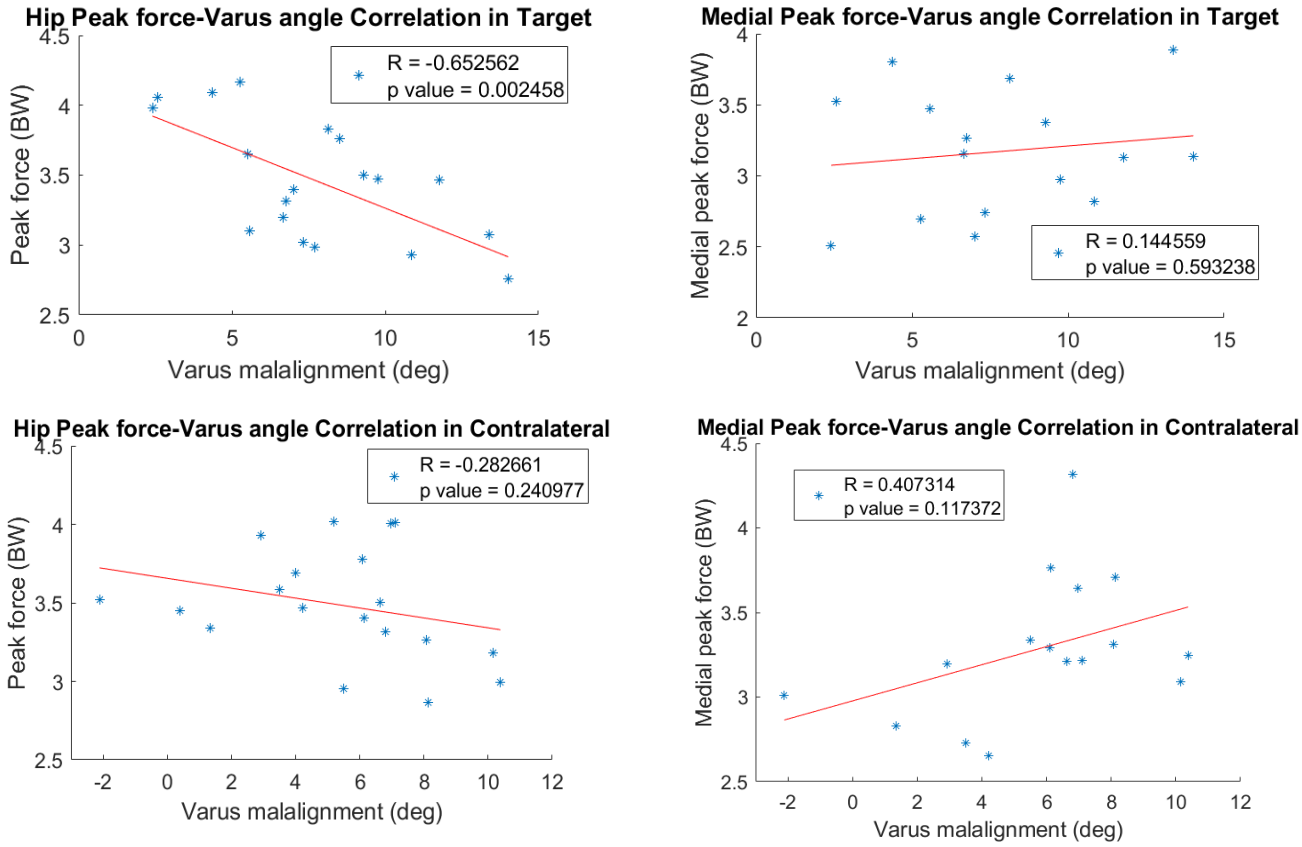

Figure 49 –WALKING. TOP-LEFT: hip peak force vs. tibiofemoral angle in target limb; TOP-RIGHT: peak force in medial compartment of knee joint vs. tibiofemoral angle in target limb; BOTTOM-LEFT: hip peak force vs. tibiofemoral angle in contralateral limb; BOTTOM-RIGHT: peak force in medial compartment of knee joint vs. tibiofemoral angle in contralateral limb.

In walking task, the hip joint reported weak correlation between contact forces and varus angles in the contralateral limb, as for the medial compartment of knee joint on the right. However, differently from Nicolò's results, a significant correlation was found in the target (p_value = 0.002458) with a coefficient of correlation R = - 0.652562. Moreover, while in medial compartment of knee joint there was a direct correlation between tibiofemoral angle and force peak (R > 0) in both limbs, hip joint stated a negative correlation (R < 0). Small differences between the target and contralateral limbs of the two joints also regarded the range of values, which was slightly higher on the hip joint (*Figure 49*).

Weak correlation was found between peak contact forces in contralateral limb and varus angles in target limb during walking (*Figure 50*).

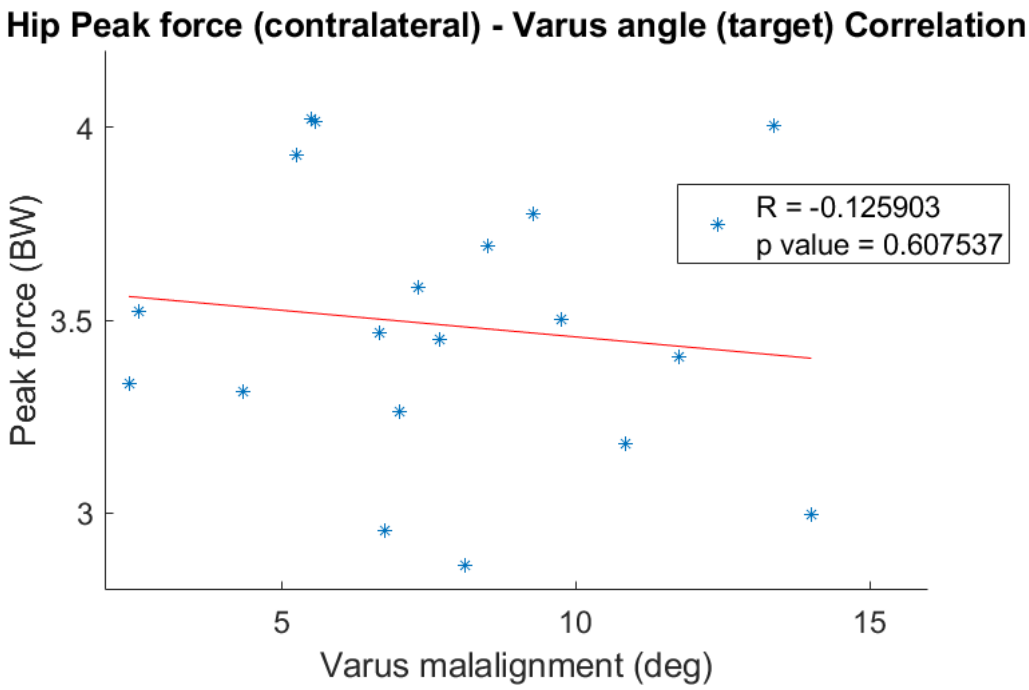

Figure 50 – WALKING. Hip peak force in contralateral limb vs. tibiofemoral angle in target limb

Stair Ascending

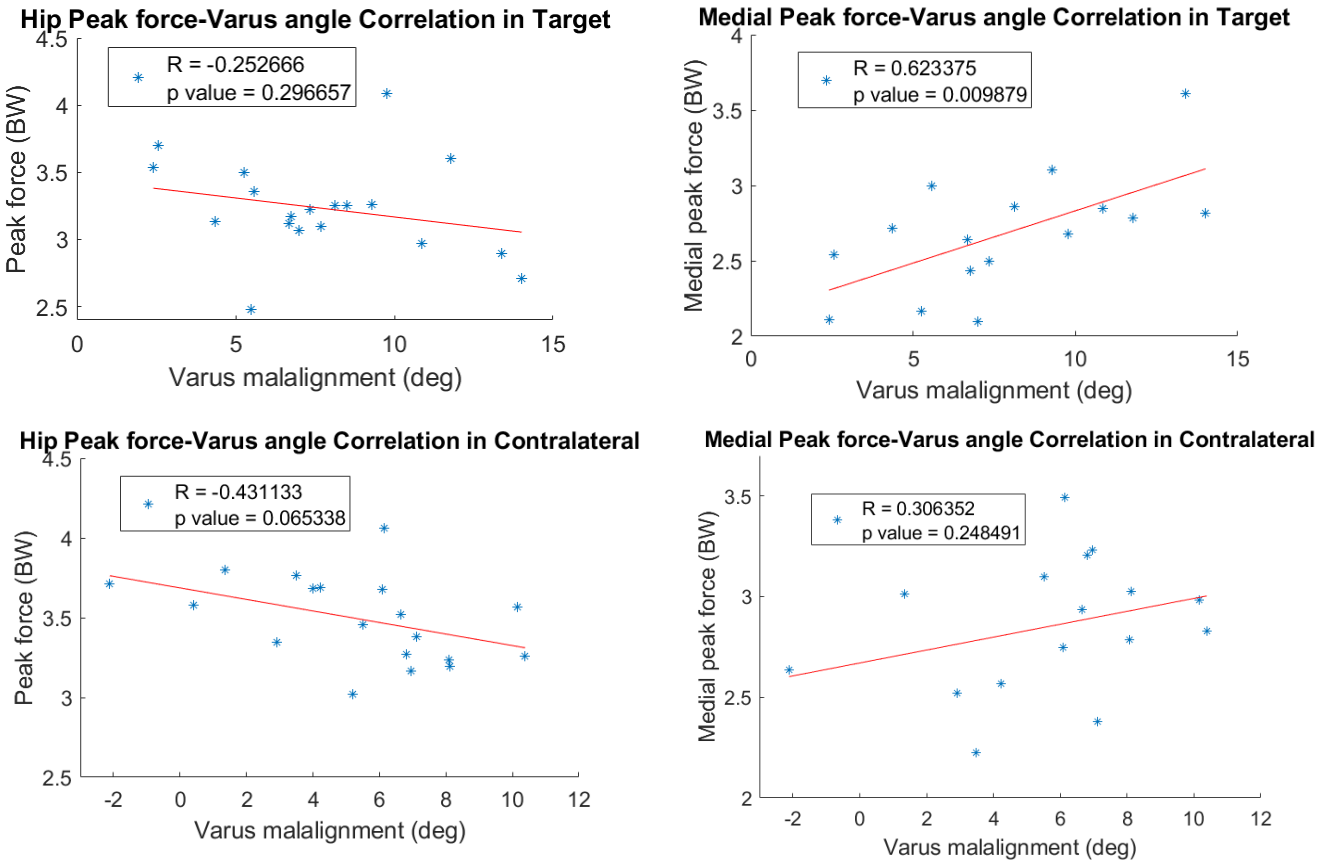

Figure 51 –STAIR ASCENDING. TOP-LEFT: hip peak force vs. tibiofemoral angle in target limb; TOP-RIGHT: peak force in medial compartment of knee joint vs. tibiofemoral angle in target limb; BOTTOM-LEFT: hip peak force vs. tibiofemoral angle in contralateral limb; BOTTOM-RIGHT: peak force in medial compartment of knee joint vs. tibiofemoral angle in contralateral limb.

In stair ascent, the hip joint didn't report any significant correlation between varus angle and peak force in both target and contralateral limbs, while a moderate correlation was found by Nicolò in the medial compartment of the target limb (R = 0.623375 and p-value = 0.009879). Again, contrary to the knee, a negative correlation was found in the hip joint (*Figure 51*).

In ascending task, hip peak forces in contralateral limb had a very weak correlation with varus angle in target limb (*Figure 52*).

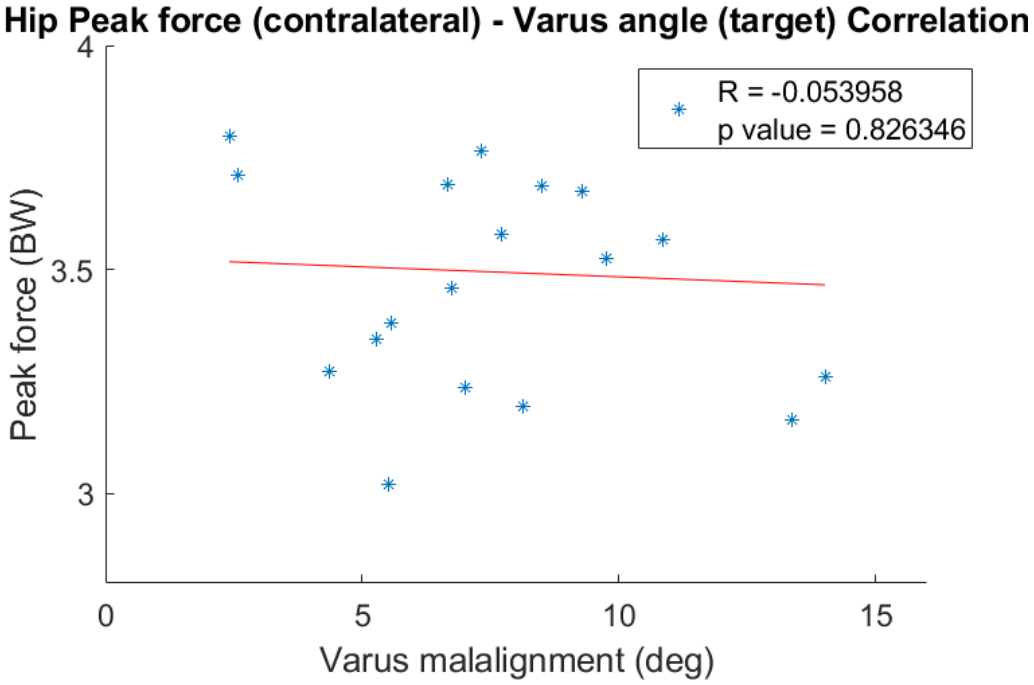

Figure 52 – STAIR ASCENDING. Hip peak force in contralateral limb vs. tibiofemoral angle in target limb

Stair Descending

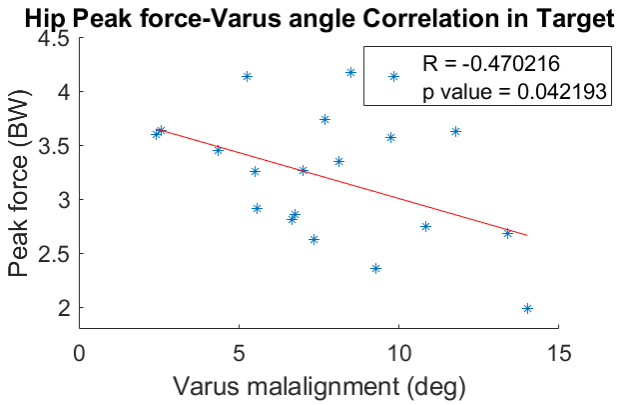

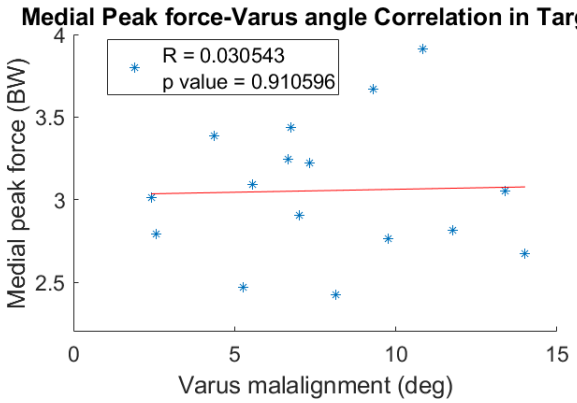

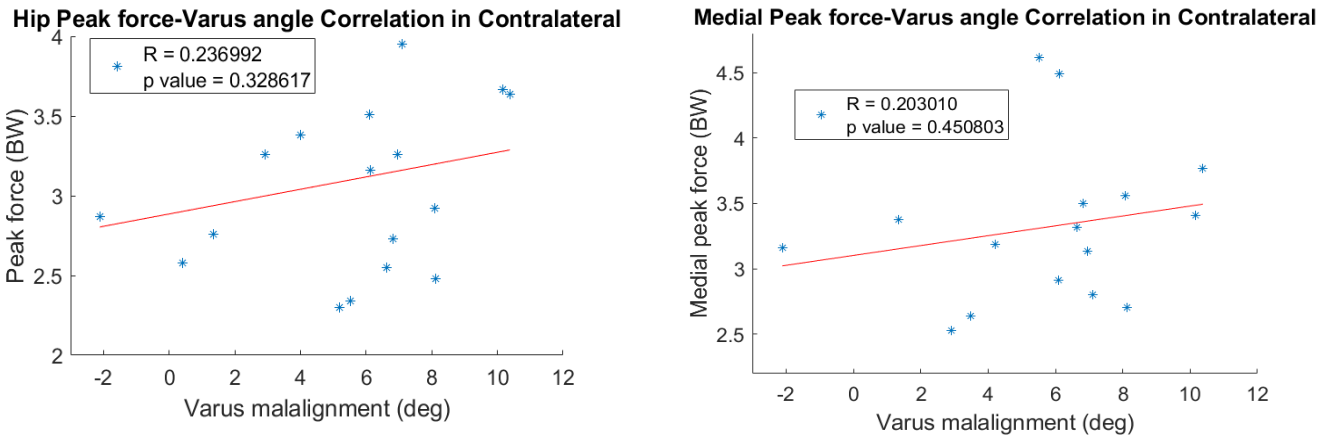

Figure 53 –STAIR DESCENDING. TOP-LEFT: hip peak force vs. tibiofemoral angle in target limb; TOP-RIGHT: peak force in medial compartment of knee joint vs. tibiofemoral angle in target limb; BOTTOM-LEFT: hip peak force vs. tibiofemoral angle in contralateral limb; BOTTOM-RIGHT: peak force in medial compartment of knee joint vs. tibiofemoral angle in contralateral limb.

In stair descending, we found a small significant inverse correlation only in the target, with a p_value = 0.042193 and a coefficient of correlation R = - 0.470216. Nicolò reported no strong correlation in both limbs for the medial compartment. Descending task confirmed the negative correlation in hip joint (*Figure 53*).

Very week correlation was found between peak force in contralateral limb and tibiofemoral angle in target limb, however, contrary to walking and ascending tasks, in this case there was a positive correlation (*Figure 54*).

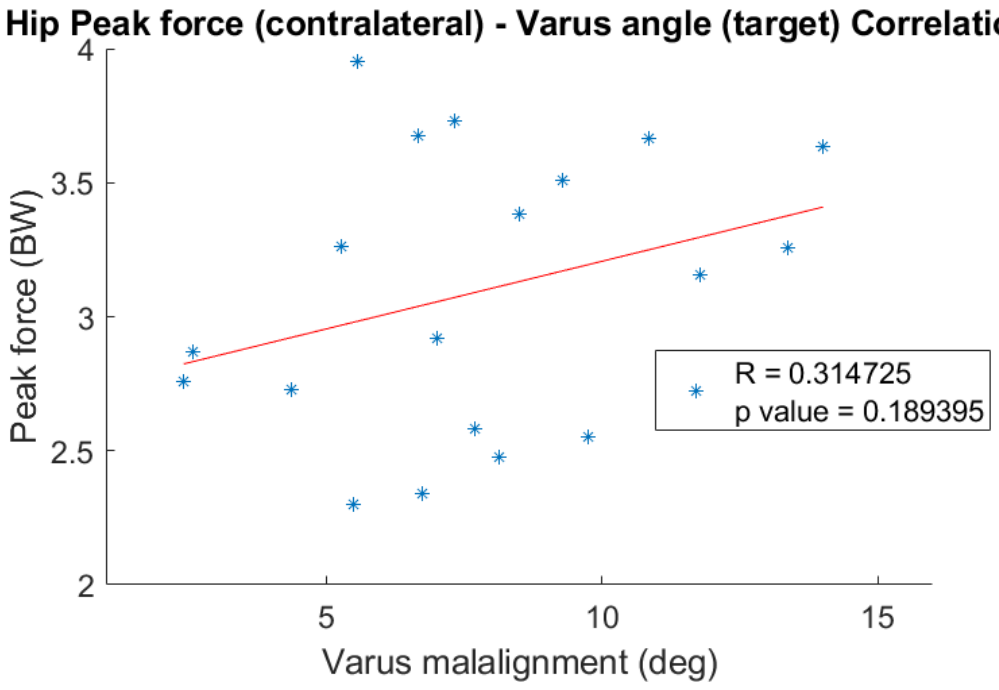

Figure 54 – STAIR DESCENDING. Hip peak force in contralateral limb vs. tibiofemoral angle in target limb

4.2 CONTACT FORCES ANALYSIS

Walking

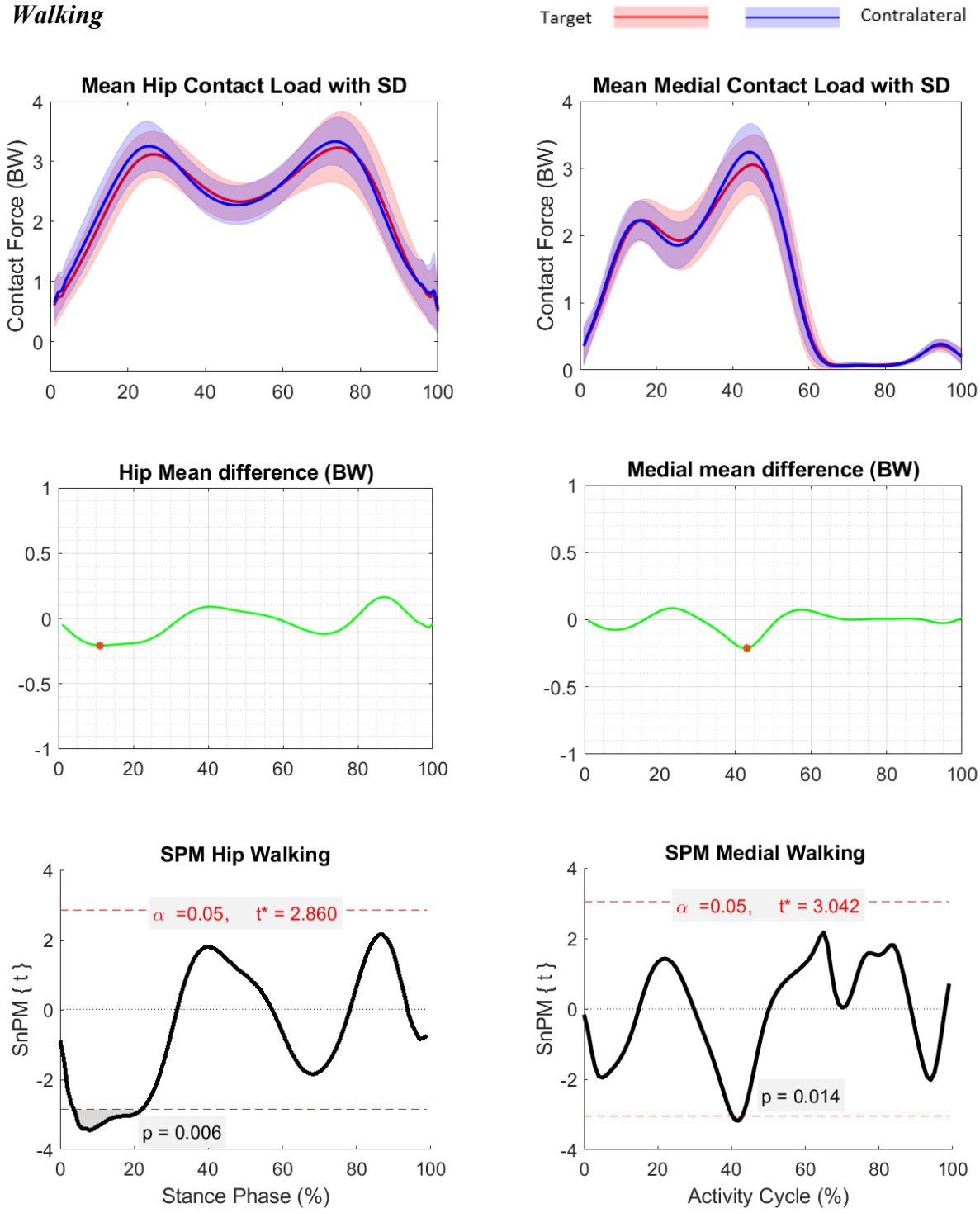

Figure 55 – WALKING. LEFT COLUMN: mean hip contact load (BW) between all patients vs. stance phase (%); hip mean difference (BW) between target and contralateral limb vs. stance phase (%); statistical parametric mapping (SPM) on hip joint; RIGHT COLUMN: mean medial contact load (BW) between all patients vs. gait cycle (%); medial mean difference (BW) between target and contralateral limb vs. gait cycle (%); statistical parametric mapping (SPM) on medial compartment of knee joint.

During walking trials, the hip contact forces were found to be higher in the contralateral limb, as it was for the medial compartment of the knee. In both joints a maximum difference of 0.2

BW was found in correspondence of the 10% of the stance phase for the hip, and in correspondence of the second peak of the gait double bump pattern for the knee. While the difference between contralateral and target limbs was not statistically significant in the latter joint, in the former SPM test reported significant differences for the first 20% of the stance phase, with a p_value = 0.006 (*Figure 55*).

Stair Ascending

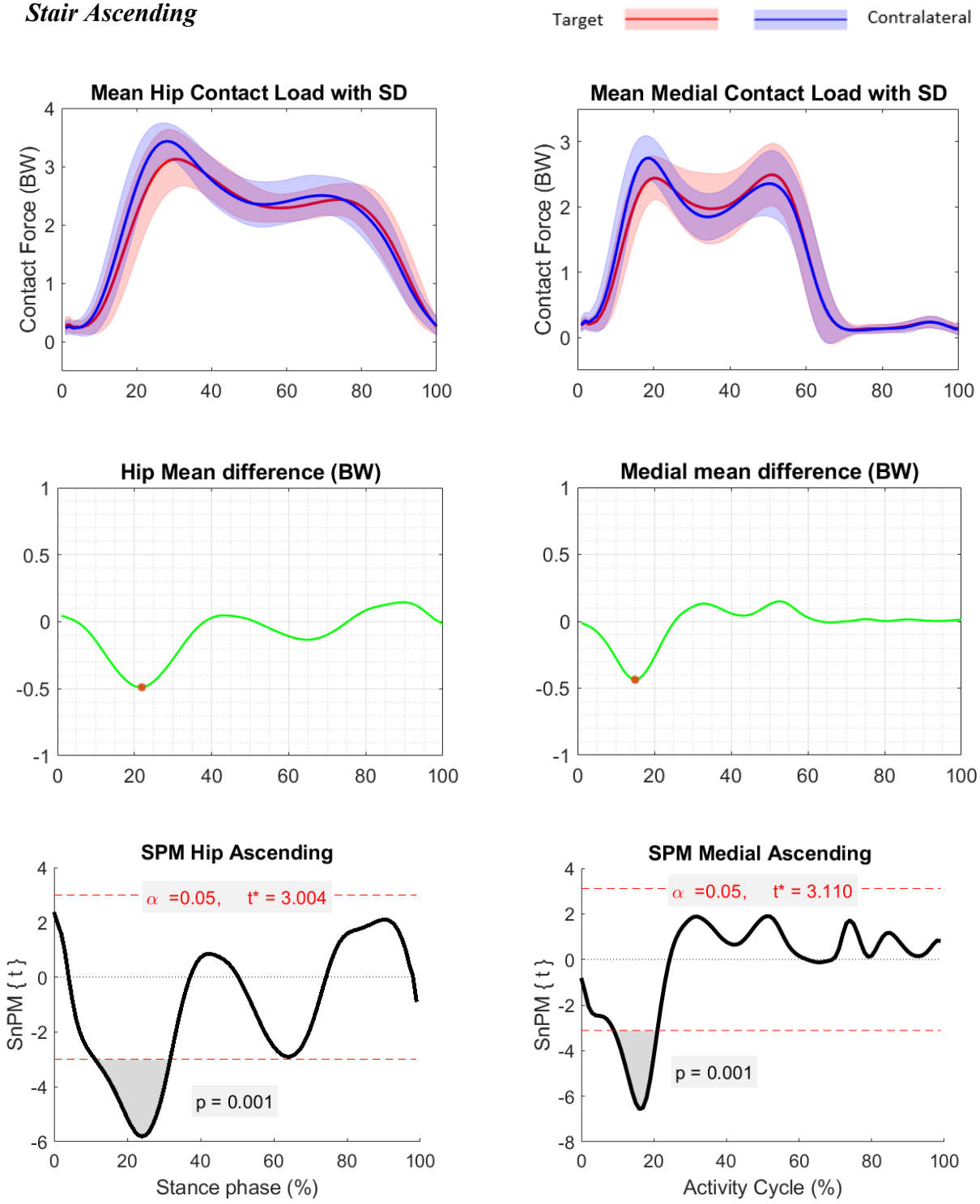

Figure 56 – STAIR ASCENDING. LEFT COLUMN: mean hip contact load (BW) between all patients vs. stance phase (%); hip mean difference (BW) between target and contralateral limb vs. stance phase (%); statistical parametric mapping (SPM)

on hip joint; RIGHT COLUMN: mean medial contact load (BW) between all patients vs. gait cycle (%); medial mean difference (BW) between target and contralateral limb vs. gait cycle (%); statistical parametric mapping (SPM) on medial compartment of knee joint.

In stair ascending, hip contact forces were higher in the contralateral limb for almost the entire period, while knee joint showed a more marked inversion of the trend. In both joints, mean difference reached a maximum value in the first peak of the curve, which was about 0.5 BW in the hip and 0.4 BW in the knee, in favor of the contralateral limb. Differences were statistically significant for about 20% of the stance phase in the hip (p_value = 0.001) and for over 10% of the activity cycle in the medial compartment of the knee (p_value = 0.001) (*Figure 56*).

Stair Descending

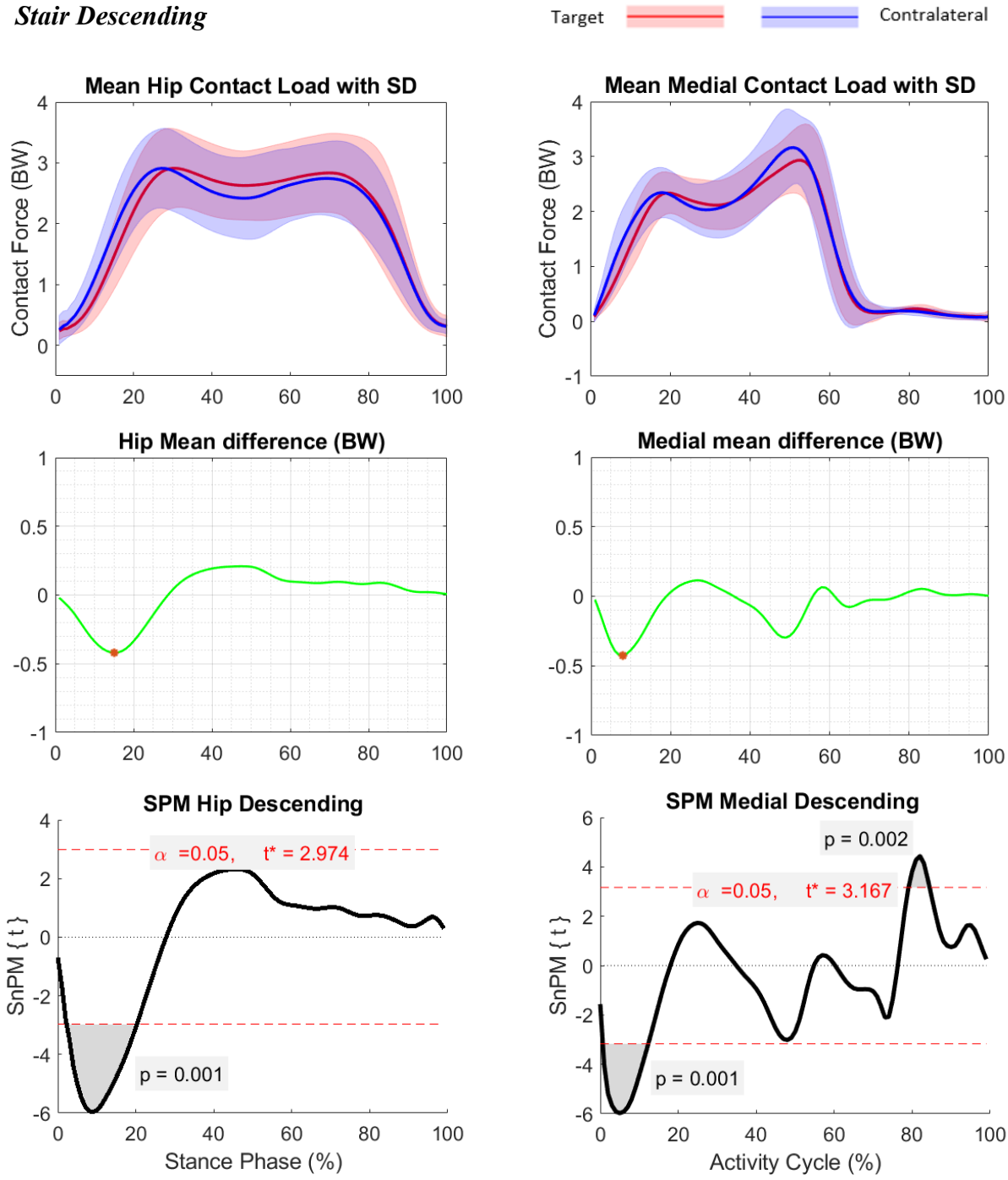

Figure 57 – STAIR DESCENDING. LEFT COLUMN: mean hip contact load (BW) between all patients vs. stance phase (%); hip mean difference (BW) between target and contralateral limb vs. stance phase (%); statistical parametric mapping (SPM) on hip joint; RIGHT COLUMN: mean medial contact load (BW) between all patients vs. gait cycle (%); medial mean difference (BW) between target and contralateral limb vs. gait cycle (%); statistical parametric mapping (SPM) on medial compartment of knee joint.

Contrary to the previous tasks, in stair descending hip contact forces were higher in the target limb, except the first quarter, where the trend was inverted, while medial contact forces showed higher values in the contralateral limb. In the first quarter, just before the first peak of the stance phase, both joints presented the maximum values of mean difference, in favor of the contralateral limb, which were also statistically significant for approximately 20% of the stance phase for the hip joint (p_value = 0.001), and for over 10% of the activity cycle for the knee joint (p_value = 0.001) (*Figure 57*).

4.3 PEAKS ANALYSIS

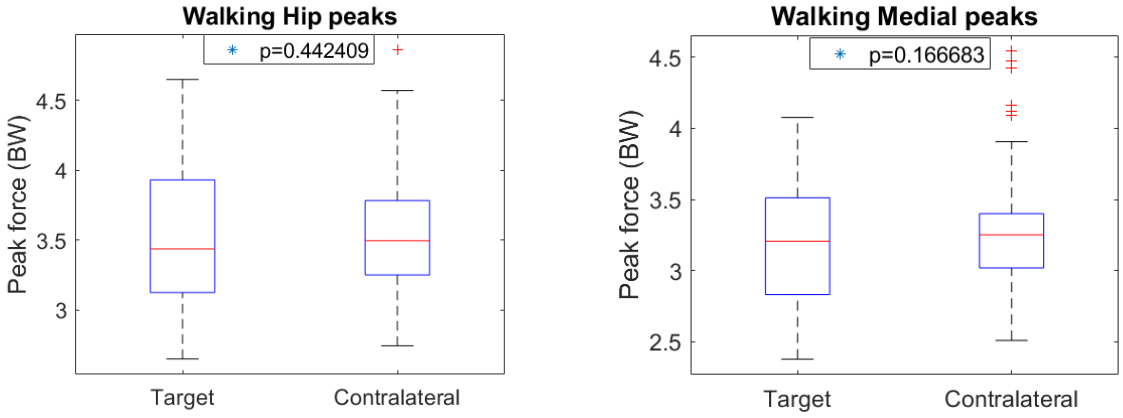

Figure 58 – WALKING. LEFT: distribution of the peak forces in target and contralateral limb in hip joint; RIGHT: distribution of the peak forces in target and contralateral limb in medial compartment of knee joint.

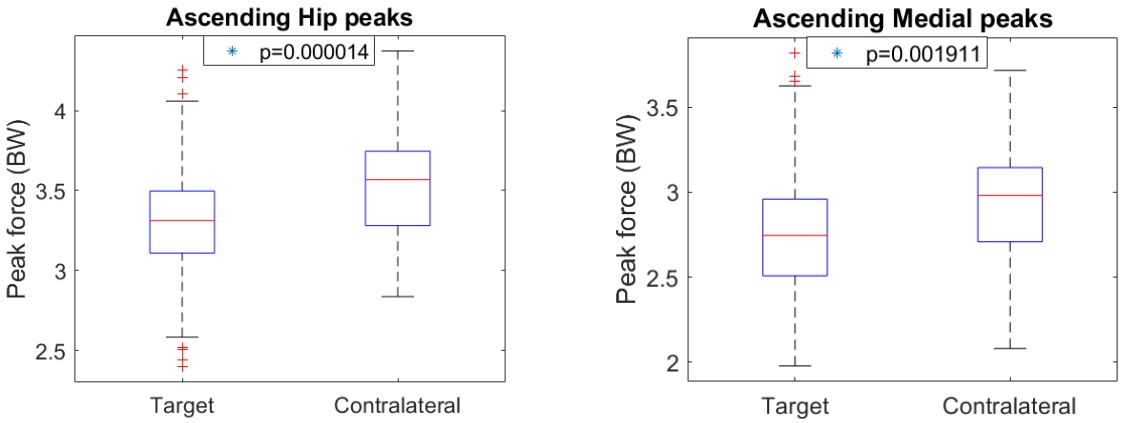

Figure 59 – STAIR ASCENDING. LEFT: distribution of the peak forces in target and contralateral limb in hip joint; RIGHT: distribution of the peak forces in target and contralateral limb in medial compartment of knee joint.

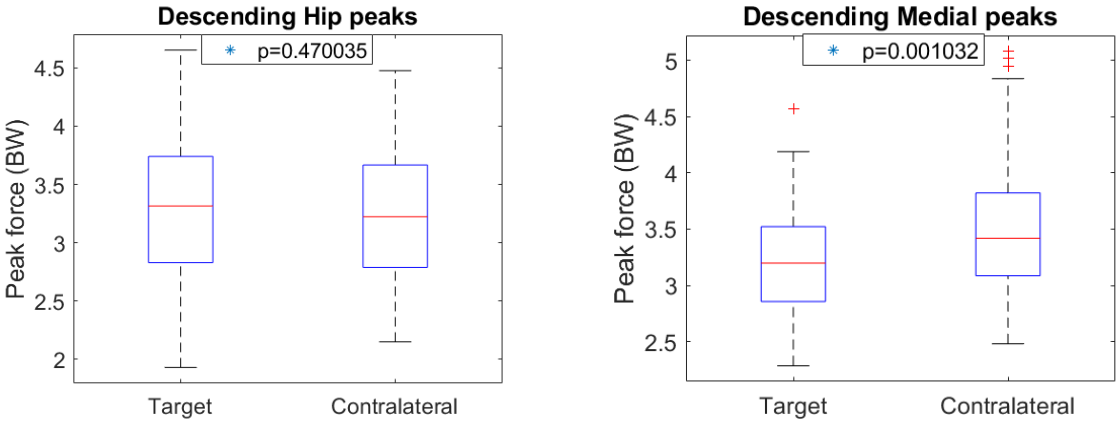

Figure 60 – STAIR DESCENDING. LEFT: distribution of the peak forces in target and contralateral limb in hip joint; RIGHT: distribution of the peak forces in target and contralateral limb in medial compartment of knee joint.

In walking task, the boxplot of peak force distribution (*Figure 58*) showed no statistically significant difference between target and contralateral limbs. Nicolò's results reported the same outcome.

Stair ascending showed a statistically significant difference in peaks distribution between the two limbs in both the hip joint and the medial compartment of the knee joint (*Figure 59*), in favor of the contralateral limb. The former reported p_value = 0.000014, the latter p_value = 0.001911.

In stair descending, contrary to the medial compartment of the knee joint, peaks distribution (*Figure 60*) was very similar in the target and contralateral limbs, thus no statistically significant difference was found in hip joint.

4.4 ANGLE DISTRIBUTION

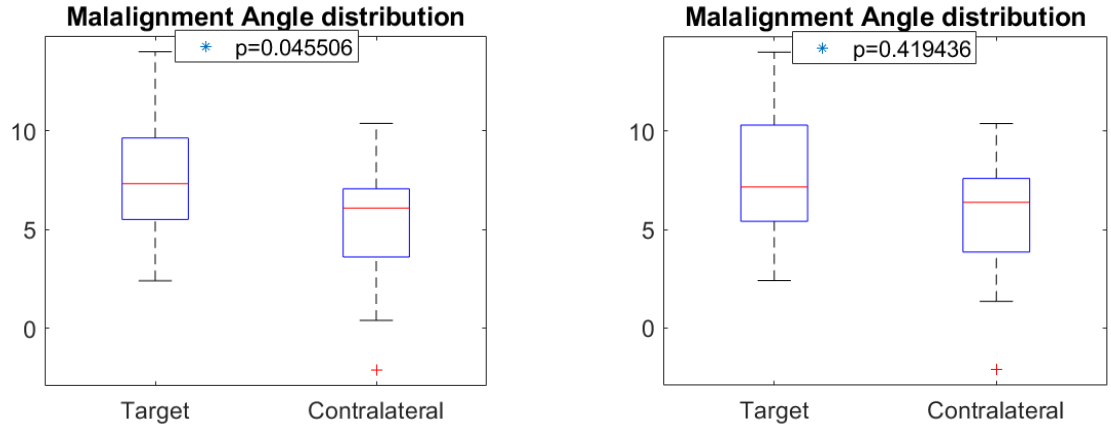

Figure 61 – Tibiofemoral angle distribution in target and contralateral limbs within this thesis (LEFT) and within Nicolò's thesis (RIGHT).

In this analysis 3 patients have been added to the study with respect to Nicolo's thesis, and this comported a modification on angle distribution boxplot (*Figure 61*): new values of mean angles were 7.7° +/- 3.2 and 5.3 +/- 3.2 in the target and contralateral, respectively, thus not so different from the previous ones, which were 7.8° +/- 3.5 and 5.7° +/- 3.2. However, the new boxplot highlighted a statistically significant difference between target and contralateral limb, with a p_value=0.045506.

In these last two sections, regarding ground reaction forces (GRF) and EMG, plots are an update of the Nicolo's ones, to state if the new patients comported some sort of changes as it happened for the tibiofemoral distribution.

4.5 GROUND REACTION FORCES

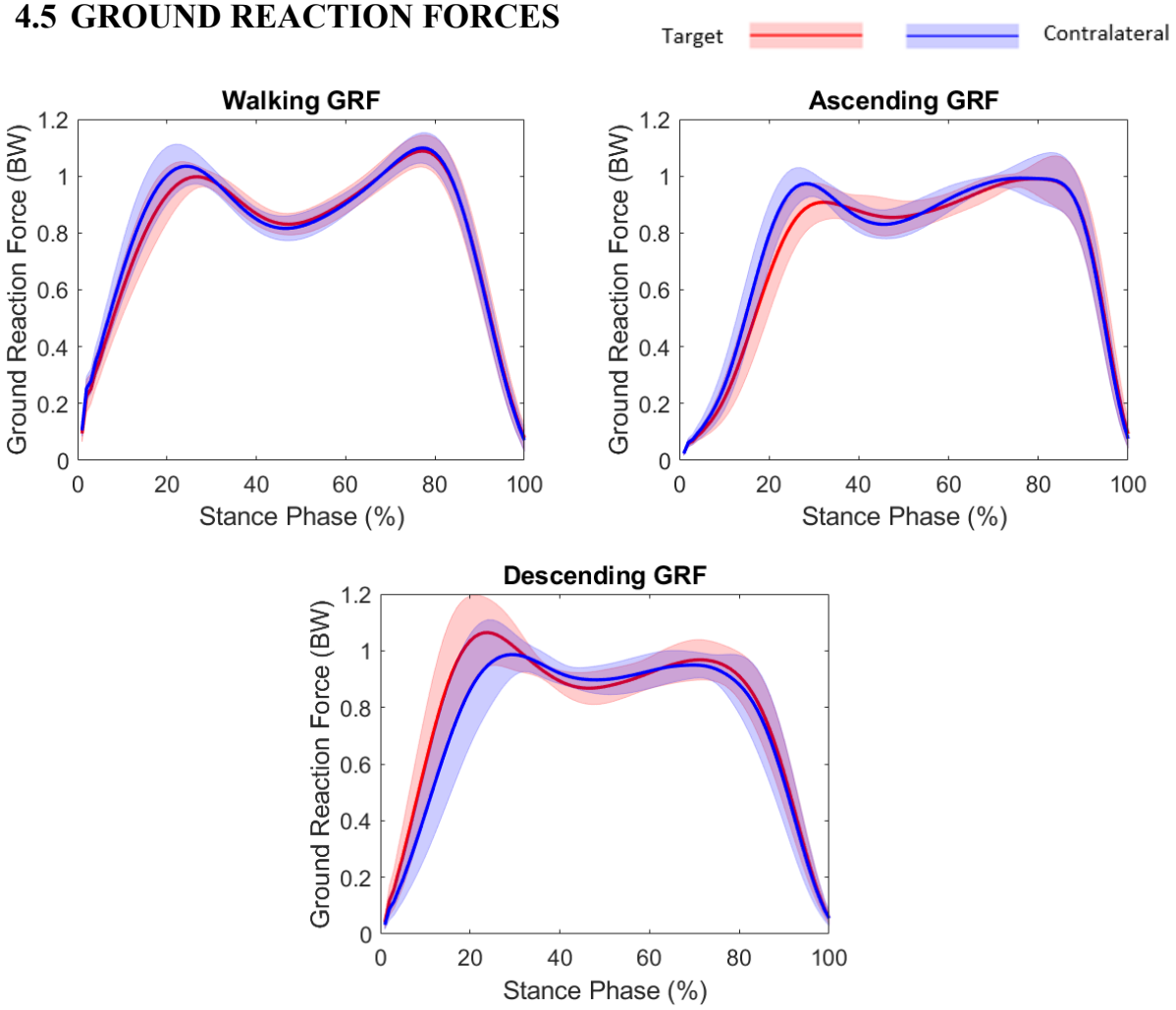

Figure 62 – TOP-LEFT: comparison of mean values of ground reaction forces in target and contralateral limbs during walking task; TOP-RIGHT: comparison of mean values of ground reaction forces in target and contralateral limbs during ascending task; BOTTOM: comparison of mean values of ground reaction forces in target and contralateral limbs during descending task

The analysis of the measured ground reaction forces was useful to evaluate if the predicted behaviour of the estimated hip contact forces related to the measured GRF. Target and contralateral limb showed similar patterns in all the GRF. Even in this case, it was represented only the stance phase in percentage.

In walking trials (*Figure 62 – TOP-LEFT*), the two peaks highlighted a higher value in the contralateral limb showing a similar trend with the hip contact loads. No differences were found with respect to nicolo's results by adding the new patients.

Stair ascending (*Figure 62 – TOP-RIGHT)* was similar to the previous one, with contralateral values higher than the target ones in both peaks. Here we noticed some differences with the corresponding plot of the hip contact forces, where the first peak, for both target and contralateral, sowed to be higher than the second peak, contrary to what seen in GRF plot. Results were equal to nicolo's ones.

In stair descending (*Figure 62 - BOTTOM*) the trend was inverted, thus ground reaction forces in target were higher in both the peaks of the stance phase. The corresponding plot of hip contact forces was slightly different in the first half.

The next three pages report the EMG validation, thus the comparison between the EMG signals recorded during gait analysis sessions, and the muscle activations estimated via OpenSim. The validation was executed for all the motor tasks: walking, stair ascending and stair descending.

4.6 EMG VALIDATION

Walking

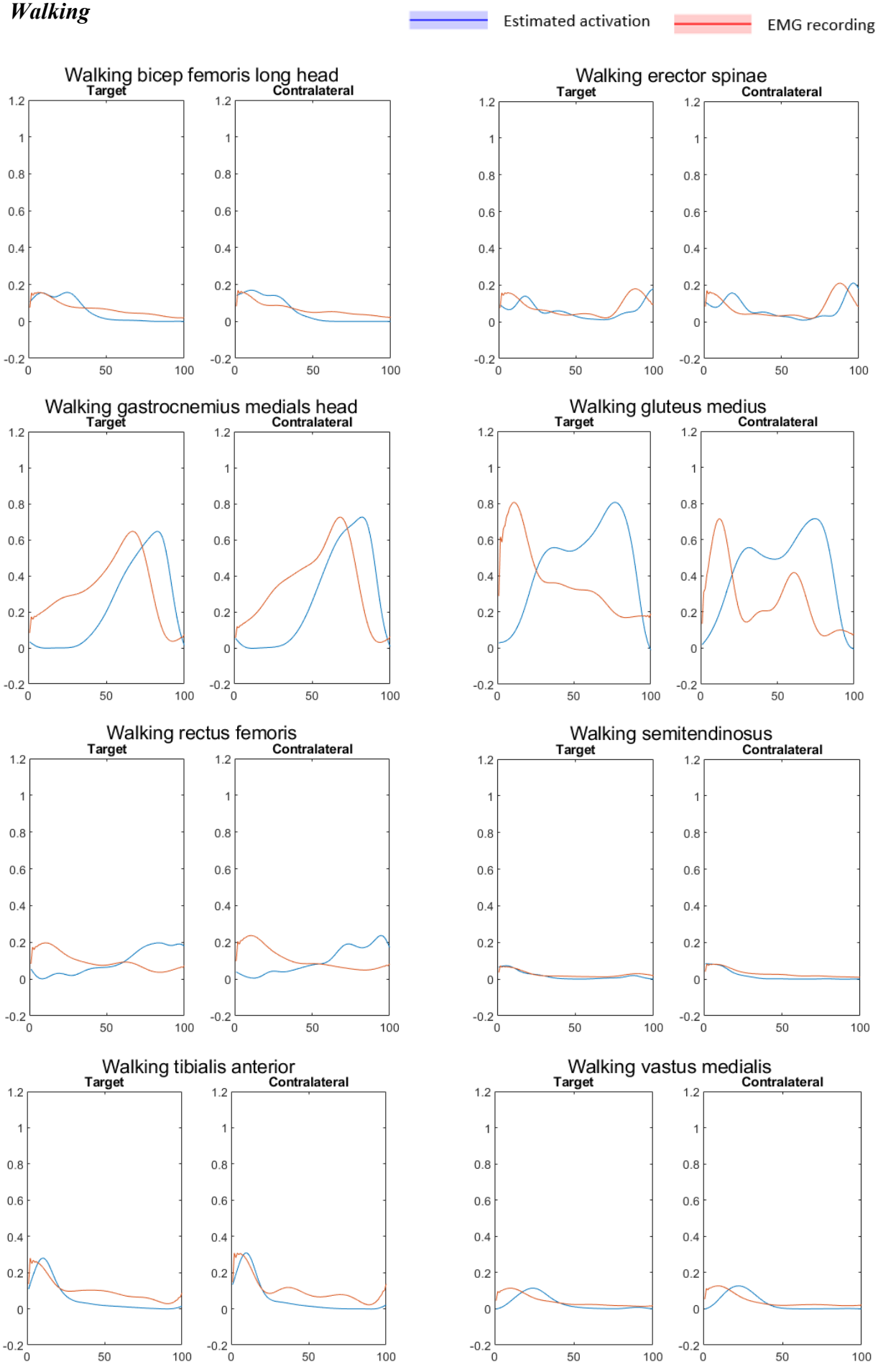

Stair Ascending

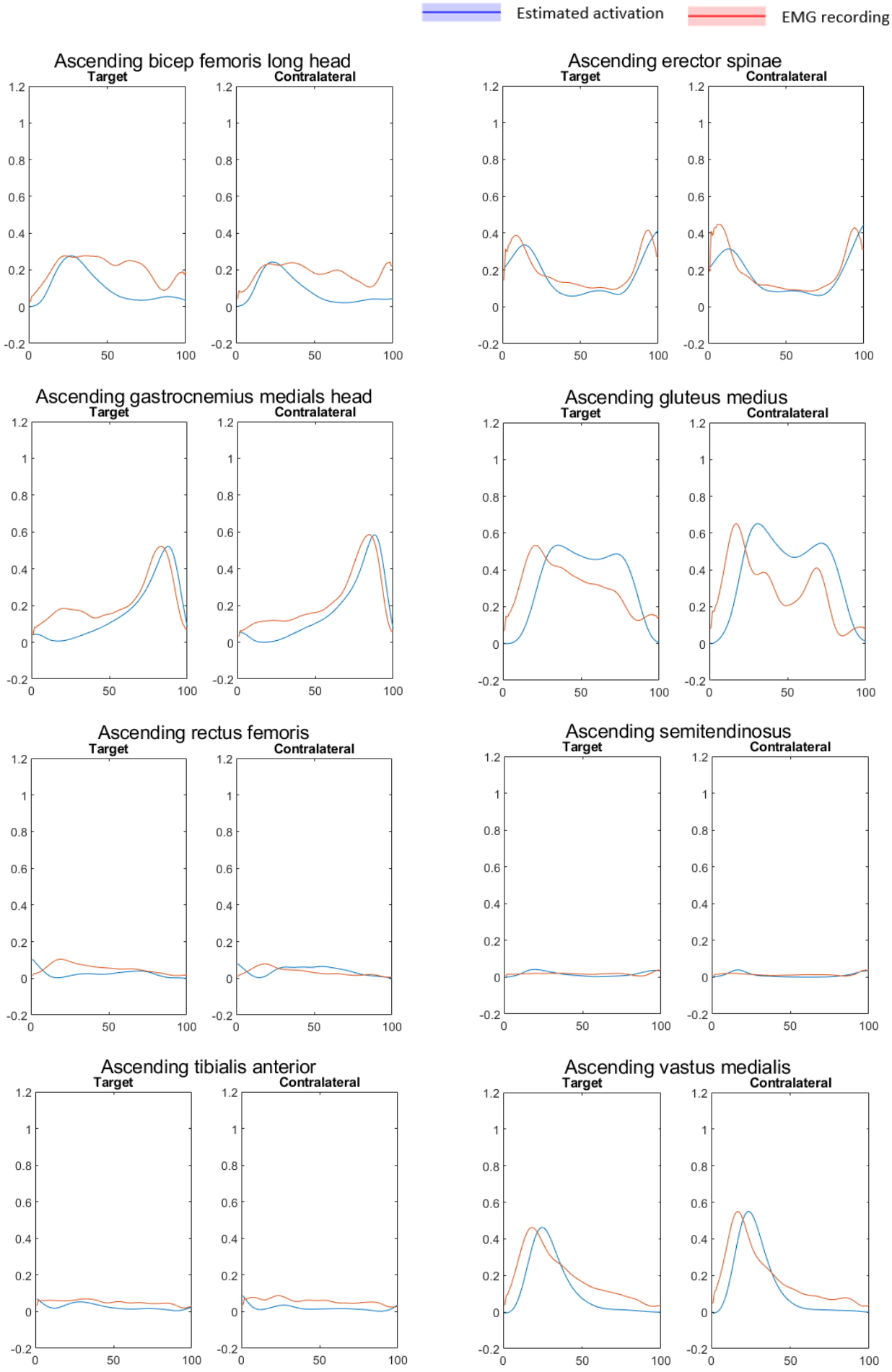

Stair Descending

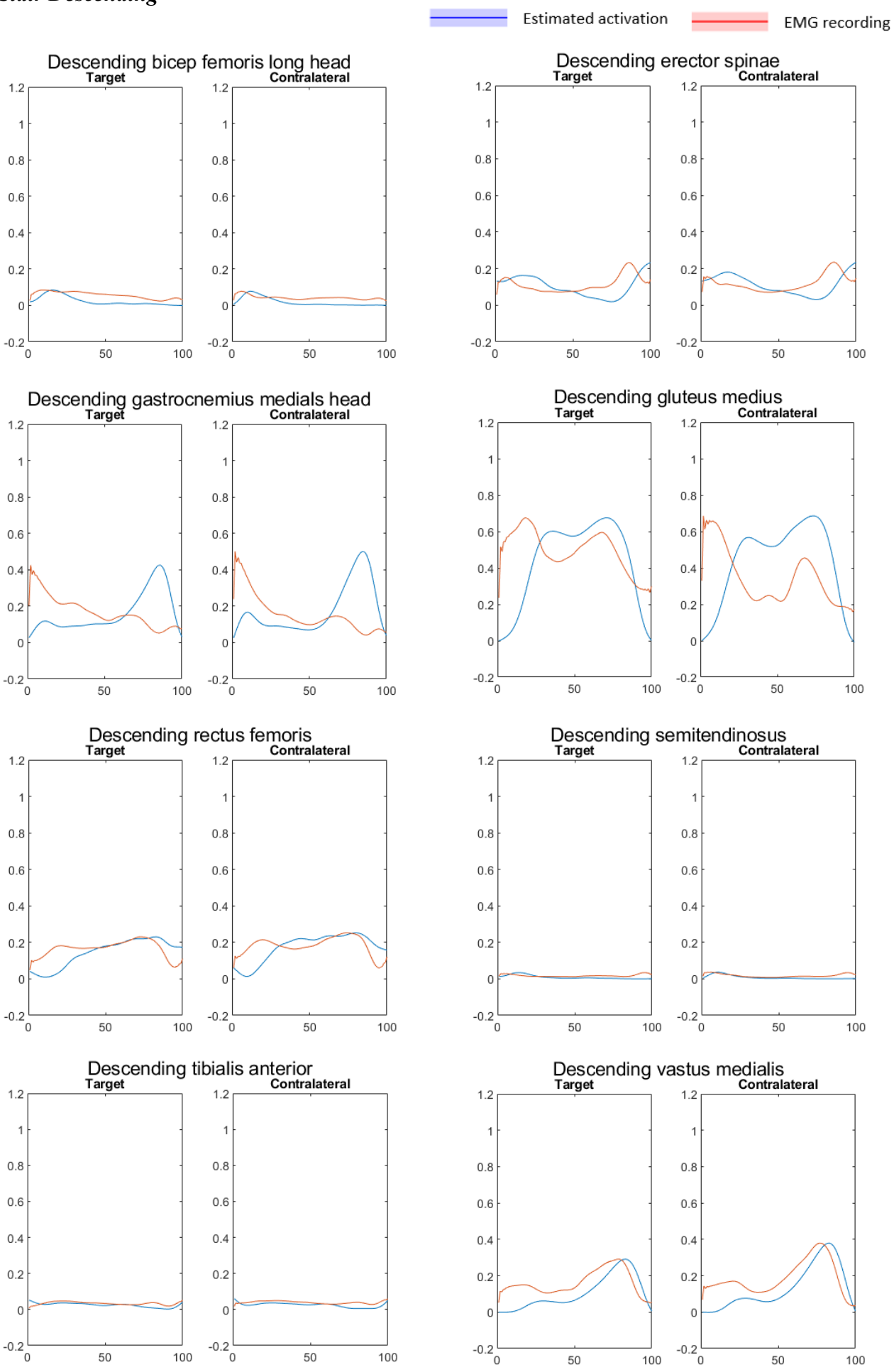

Figure 63 – Validation of the results through the comparison between recorded EMG signals and estimated muscle forces in walking (FIRST PAGE), stair ascending (SECOND PAGE) and stair descending (THIRD PAGE).

In accordance with all the analyses conducted so far, EMG validation took into consideration the only stance phase, expressed as percentage.

All the comparisons reported an activation offset between the estimated muscle activations and the EMG recordings, with values between 10% and 15% of the stance phase which corresponded to a few tens of hundredths of a second.

In general, all comparisons conducted to good outcomes (*Figure 63*), except for the *rectus femoris,* which showed higher values of delay between the recorded signals and the estimations in both walking and stair ascending, while in stair descending the percentage difference was within the range of values indicated above. Moreover, the *gluteus medius* and the *gastrocnemius medials head* did not match perfectly in walking and descending tasks, respectively.

Finally, the results confirmed with no significant differences what obtained by Nicolò in the previous thesis.

5. DISCUSSION

Within this thesis, hip contact forces were calculated and analysed to study the biomechanical consequences of symptomatic early-stage osteoarthritis localized in the medial compartment of knee joint, which was due to a genu varus condition in both patients' limbs. In particular, the research question given by the clinicians focalized the attention on the correlation between the tibiofemoral malalignment in the target limb and the hip contact loads in the contralateral limb. Moreover, the elaborate carried out a comparison with the results obtained in a previous thesis carried out in the same laboratory by Nicolò Caredda, who studied the correlation between the tibiofemoral angle and the knee contact forces, by distinguishing the medial and the lateral component. Both experiences are part of a wider project whose aim is to evaluate the effect of high tibial osteotomy (HTO) in preventing the worsening of the disease and maybe reversing it. Here, musculoskeletal modelling plays a fundamental role since it allows to compute those biomechanical quantities not directly measurable on the subjects, like joint contact forces, muscle forces and activations. Moreover, it permits to evaluate not only a wide range of clinical cases, but also different surgical operations, by varying model's parameters and thus avoiding a direct consequence on the patient. In this case, the creation of subject-specific models and analyses is indispensable to have more reliable and precise outcomes.

In the first part of this section, we focused on the research question, thus if hip peak forces in contralateral limb and varus angle in target limb were significantly correlated. Then we discussed the similarities and dissimilarities with Nicolò's results regarding the medial compartment of the knee joint, by considering the two limbs separately. Finally, we evaluated the recorded ground reaction forces and the model validation.

From the analysis of the hip contact forces, we found a very weak correlation between peak forces in contralateral limb and varus angle in target limb in all the motor tasks, with a slight increase in the stair descending, but far from being statistically significant (p_value = 0.189395). Moreover, while the latter was characterized by a positive correlation, walking and stair ascending reported a negative correlation, thus an increasing varus angle comported decreasing peak forces (Section 4.1). Considering the two lower limbs separately, hip contact loads and tibiofemoral angle highlighted an inverse correlation in all the occasions, with the exception of the contralateral limb in descending task, which showed a direct one. In the end, a few statistically significant correlations were found in the target limb in walking (p_value = 0.002458) and in stair descending (p_value = 0.042193), but in no occasion in the contralateral limb. In the other hand, Nicolo' reported direct correlations in all the tasks, for

both the target and contralateral limbs, which were statistically significant only in the target limb during stair ascending (p_value = 0.009879) (Section 4.1). These very weak correlations were probably due to the fact that muscles sustained almost the entire load during motor tasks, thus a variation of the tibiofemoral angle didn't report a significant variation in joint loads. Moreover, the positive and negative correlations between the two quantities were again related to the action of muscles in supporting the joint. In the other hand, weak correlations could also be associated to not physically demanding motor tasks and to the fact that all the patients in the HTO project presented an early-stage osteoarthritis which didn't interfere too much with the activities. Thus, more difficult tasks and more advanced stages of the disease could show more significant correlation between hip (and knee) contact forces and tibiofemoral angle.

In contact forces analysis (Section 4.2), hip loads were generally higher in the contralateral limb, except for the stair descending. We found statistically significant mean difference values in all motor tasks, which corresponded to 10% of the stance phase in walking, and 20% of the stance phase in both stair ascending and stair descending. These percentages were located before the first peak of the double bump pattern and they were always in favor of the contralateral limb, with a maximum value of 0.2 BW in walking, 0.4 BW in stair descending and 0.5 in stair ascending. The medial compartment of the knee showed similar results, except for the walking task where the maximum mean difference value was located in the second peak of the stance phase, but it was not statistically significant. In general, greater values of joint contact forces in the contralateral limb were explained by symptomatic pain in the target limb which led to a modification of patients' movements. Moreover, we noticed generally higher values in the hip joint with respect to the medial compartment of the knee, but this was probably due to the exclusion of the lateral compartment of the joint from this analysis.

In Section 4.3 we analysed the distribution of the hip peak force in target and contralateral limbs for each task. The results confirmed what stated in the previous section, that was higher peak values in the contralateral limb during walking and stair ascending, and higher peak values in the target limb during stair descending. However, a statistically significant difference between the two limbs was found only in ascending task (p_value = 0.000014). On the contrary, the medial peaks reported significant differences in both stair ascending and stair descending. As said before, the higher values in the contralateral limb were probably due to compensatory techniques of the patient to alleviate the pain in the target limb, and this gap increased as the task became more demanding. This explained the statistically significant differences only in stair ascending and descending.

The boxplots of the malalignment angle distribution showed an interesting outcome. Within his thesis, Nicolò didn't find a statistically significant difference in angle distribution between target and contralateral (p_value = 0.419436), with mean values of 7.8° +/- 3.5 and 5.7° +/- 3.2, respectively. However, the addition of three more patient within this elaborate, changed mean values to 7.7° +/- 3.2 in the target limb and 5.3 +/- 3.2 in the contralateral limb, and led to a statistically significant difference in malalignment angle distribution. This meant that while in the former thesis patients were characterized by a more painful target limb but probably in a similar medial osteoarthritis condition of the contralateral one, in this thesis the added subjects may presented a big difference between the angles in the two limbs, implying that the target limb was subjected not only to a greater symptomatic pain, but probably also to a more advanced stage of the disease, however we had not the clinical confirmation.

The compensatory techniques adopted by the patients as pain relief, and thus the shift of the load to the contralateral limb, can be also evaluated in the plots of the ground reaction forces in Section 4.5. During the stance phase of walking and ascending tasks, force platforms registered higher values in the contralateral limb, while in stair descending the trend was inverted. However, the two limbs showed generally similar curves and force values through all the tasks, with the differences that increased as the task became more demanding. This confirmed that the patients of the study presented an early-stage medial osteoarthritis and thus no big differences were reported between the two limbs. As said before, more difficult tasks and a more advanced stage of the osteoarthritis could probably emphasize our outcomes.

EMG validation (Section 4.6) allowed us to validate our models through a comparison between estimated muscle activations and recorded EMG signals, verifying our results' reliability. In this case, but also in the ground reaction forces analysis, we didn't compare our outcomes with those obtained by Nicolò, but we updated them, and observed if some of the new patients comported a significant change. In the end, all comparisons conducted to good outcomes, except for the *rectus femoris* in both walking and stair ascending, the *gluteus medius* in walking task and the *gastrocnemius medials head* in descending task. Since the recorded EMG signals reflected the trend of those in literature, these errors derived from the estimation of muscle activation via OpenSim and we didn't find a precise explanation for that. In the other hand, the activation offset of 10/15% of the stance phase found confirmation in the literature (75) and was probably due to the time difference between fiber recruitment and actual force generation, or to the crosstalk effect, which can improve the outcomes if taken into consideration (76). In conclusion, no significant differences were found with Nicolò's results, thus confirming a good matching between EMG signals and muscle activations.

In this thesis, the research question was focused on the correlation between the tibiofemoral varus angle in the target limb and the hip contact loads in the contralateral limb. Although we didn't find other works which confirmed or refused our findings in this specific contest, we compared the peaks of the hip contact forces, expressed in BW, in all the motor activities, with the correspondent values in healthy subjects studied by Valente et al. (80) and Wesseling et al. (81), finding similar results. This proved that the variation of tibiofemoral angle within our patient cohort, didn't lead to a significant variation in hip biomechanics, thus maintaining physiological values.

In the other hand, we can make our results more reliable and precise considering future comparisons and insights. In fact, within these two studies we didn't exploit the whole potential of Lerner's musculoskeletal model (61), in particular the definition of the contact point locations in the knee, which both Zeighami (77) and Saliba (78) have shown to improve the accuracy of the knee contact forces, and thus probably of the hip joint. Moreover, even if we simulated the High Tibial Osteotomy procedure within the HTO-RPlus software, the identification of some parameters was not unique and absolute (Section 3.4), thus leading to inter- and intra-operator variability in the definition of the tibiofemoral angle, with a consequent uncertainty on the values of the joint contact forces (78). Finally, the use of a scaled generic model causes uncertainties, too, due to the large inter-subject variability (79) which influence marker location, muscle and limbs geometry and properties, and limbs alignment.

6. CONCLUSION

The aim of this thesis was to evaluate, through daily life activities, the correlation between the tibiofemoral malalignment in the target limb and the hip contact loads in the contralateral limb in 19 patients with an early-stage medial osteoarthritis due to genu varus condition. The study is part of a wider project whose purpose is to evaluate the impact of High Tibial Osteotomy (HTO) in slowing down and maybe reversing the osteoarthritic process. For this reason, we scaled a generic musculoskeletal model with subject-specific anthropometric data, in particular we computed the tibiofemoral angle within the software HTO-RPlus, which was developed inside the BIC Laboratory of the Rizzoli Institute to simulate the HTO surgical operation starting from the antero-posterior weight-bearing RX of the patient. Then, through OpenSim we simulated the motion data collected through gait analysis sessions and we isolated the hip contact loads. In the last part of this thesis, we post-processed via Matlab the output data from OpenSim, to perform a statistical analysis and the model validation.

At the end of the project, our research question found a negative outcome. In both walking and stair ascending there was a very weak inverse correlation between target tibiofemoral angle and contralateral hip contact forces, while in stair descending there was a direct but not statistically significant correlation. This may lead to the conclusion that there's not correlation between varus tibiofemoral angle and hip contact loads, however, in this study we also investigated the two limbs separately, each of them with the correspondent angle and hip loads. In this case we found significant correlations on few occasions, thus showing that a correlation between the two quantities was indeed present. As reported in the previous chapter, muscles play a crucial role in sustaining most of the load during a motor task, therefore making it difficult to find a possible meaningful correlation. Unfortunately, the absence of articles in literature describing these correlations, did not allow us to clarify the correctness of our results.

Nevertheless, future developments of the HTO project should focus on:

- More demanding tasks, to evaluate if greater correlations between tibiofemoral angle and joint contact loads will occur
- A major overview of the literature, focusing on the correlation between tibiofemoral alignment and hip contact loads to compare and analyse the results obtained in this work
- The definition of knee contact points locations, leading to more precise and reliable outcomes
- Greater accuracy in defining the quantities within the software HTO-RPlus

- The comparison between pre- and post-intervention

In conclusion, an accurate study of internal joints biomechanics, may help the planning of an ideal HTO surgery which reduces and eventually reverses the progression of medial knee osteoarthritis, with consequent improvements in bone and cartilage quality. In this way, this technique could represent the first choice for young and fit patients, leading to a better quality of life and the return to high impact activities, maintaining at the same time the original joint.

BIBLIOGRAPHY

1 - Soames R, Palastanga N. Anatomy and human movement: structure and function [Internet]. 2019 [cited 2022 Mar 9] (https://nls.ldls.org.uk/welcome.html?ark:/81055/vdc_100065003707.0x000001).

2 - "Cartilage". Encyclopaedia Britannica. Retrieved 2021-06-23.

3 - Normal Anatomy and Biomechanics of the Knee Fred Flandry, MD, FACS*w and Gabriel Hommel, MD*.

4 - Hopkins Medicine. Knee ligaments and repair, Johns Hopkins Medicine (from https://www.hopkinsmedicine.org/health/treatment-tests-and-therapies/knee-ligament-repair).

5 - Platzer, Werner (2004). Color Atlas of Human Anatomy, Vol. 1: Locomotor System (5th ed.). Thieme. pp. 26, 192-252.

6 - How to prevent and treat knee injuries (from https://www.medicalnewstoday.com/articles/299204).

7 - https://www.physio-pedia.com/Knee.

8 - Cherian, Jeffrey J et al. “Mechanical, Anatomical, and Kinematic Axis in TKA: Concepts and Practical Applications.” *Current reviews in musculoskeletal medicine* vol. 7,2 (2014): 89-95. doi:10.1007/s12178-014-9218-y

9 - J. M. Sikorski, ‘’Alignment in total knee replacement’’, The Journal of Bone and Joint Surgery. British volumeVol. 90-B, No. 9, 2008 (https://online.boneandjoint.org.uk/doi/full/10.1302/0301-620X.90B9.20793)

10 - Hsu RW, Himeno S, Coventry MB, Chao EY. Normal axial alignment of the lower extremity and load-bearing distribution at the knee. *Clin Orthop Relat Res.* 1990; 255:215

11 - Bellemans J, Colyn W, Vandenneucker H, Victor J. The Chitranjan Ranawat award: is neutral mechanical alignment normal for all patients? The concept of constitutional varus. *Clin Orthop Relat Res.* 2012; 470:45. doi: 10.1007/s11999-011-1936-5.

12 - Fahlman L, Sangeorzan E, Chheda N, Lambright D. Older adults without radiographic knee osteoarthritis: knee alignment and knee range of motion. *Clin Med Insights Arthritis Musculoskelet Disord.* 2014; 7:1. doi: 10.4137/CMAMD.S13009.

13 - Najefi AA, Malhotra K, Goldberg A. Mechanical and anatomical axis of the lower limb in total ankle arthroplasty. Foot (Edinb). 2020 Sep; 44:101666. doi: 10.1016/j.foot.2020.101666. Epub 2020 Feb 4. PMID: 32172139.

14 - Krackow KA. The Measurement and Analysis of Axial Deformity of the Knee. Homer Stryker Center; 2008.

15 - Halder A, Kutzner I, Graichen F, Heinlein B, Beier A, Bergmann G. Influence of limb alignment on mediolateral loading in total knee replacement: in vivo measurements in five patients. J Bone Joint Surg Am. 2012 Jun 6;94(11):1023-9. doi: 10.2106/JBJS.K.00927. PMID: 22637208.

16 - Li OL, Pritchett S, Giffin JR, Spouge ARI. High Tibial Osteotomy: An Update for Radiologists. AJR Am J Roentgenol. 2022 Apr;218(4):701-712. doi: 10.2214/AJR.21.26659. Epub 2021 Nov 24. PMID: 34817194.

17 - Black M. S., d'Entremont A. G., McCormack R. G., Hansen G., Carr D., Wilson D. R. The effect of wedge and tibial slope angles on knee contact pressure and kinematics following medial opening-wedge high tibial osteotomy. *Clinical Biomechanics.* 2017; 51:17–25. doi: 10.1016/j.clinbiomech.2017.10.021.

18 - Brinkman JM, Lobenhoffer P, Agneskirchner JD, Staubli AE, Wymenga AB, van Heerwaarden RJ. Osteotomies around the knee: patient selection, stability of fixation and bone healing in high tibial osteotomies. J Bone Joint Surg Br. 2008 Dec;90(12):1548-57. doi: 10.1302/0301-620X.90B12.21198. PMID: 19043123.

19 - Sun H., Zhou L., Li F., Duan J. Comparison between closing-wedge and opening-wedge high tibial osteotomy in patients with medial knee osteoarthritis: a systematic review and meta-analysis. *The Journal of Knee Surgery.* 2017;30(2):158–165. doi: 10.1055/s-0036-1584189.

20 - Aglietti P., Rinonapoli E., Stringa G., Taviani A. Tibial osteotomy for the varus osteoarthritic knee. *Clinical Orthopaedics and Related Research.* 1983;(176):239–251. doi: 10.1097/00003086-198306000-00035.

21 - Murray, Ryan et al. "High Tibial Osteotomy for Varus Deformity of the Knee." *Journal of the American Academy of Orthopaedic Surgeons. Global research & reviews* vol. 5,7 e21.00141. 9 Jul. 2021, doi:10.5435/JAAOSGlobal-D-21-00141

22 - Cao Z., Mai X., Wang J., Feng E., Huang Y. Unicompartmental knee arthroplasty vs high tibial osteotomy for knee osteoarthritis: a systematic review and meta-analysis. *Journal of Arthroplasty.* 2017;33(3):952–959. doi: 10.1016/j.arth.2017.10.025.

23 - Liu, Xiaoyu et al. "High Tibial Osteotomy: Review of Techniques and Biomechanics." *Journal of healthcare engineering* vol. 2019 8363128. 2 May. 2019, doi:10.1155/2019/8363128

24 - Kutzner I., Bender A., Graichen F., et al. "Mediolateral force distribution at the knee joint shifts across activities and is driven by tibiofemoral alignment." *The Bone & Joint Journal.* 2017;99(6):779–787. doi: 10.1302/0301-620x.99b6.bjj-2016-0713.r1.

25 - McNamara I, Birmingham TB, Fowler PJ, Giffin JR. High tibial osteotomy: evolution of research and clinical applications--a Canadian experience. Knee Surg Sports Traumatol Arthrosc. 2013 Jan;21(1):23-31. doi: 10.1007/s00167-012-2218-9. Epub 2012 Sep 28. PMID: 23052112.

26 - Hoorntje A., Witjes S., Kuijer P. P. F. M., et al. High rates of return to sports activities and work after osteotomies around the knee: a systematic review and meta-analysis. *Sports Medicine.* 2017;47(11):2219–2244. doi: 10.1007/s40279-017-0726-y.

27 - Hofmann S, Lobenhoffer P, Staubli A, Van Heerwaarden R. Osteotomien am Kniegelenk bei Monokompartmentarthrose [Osteotomies of the knee joint in patients with monocompartmental arthritis]. Orthopade. 2009 Aug;38(8):755-69; quiz 770. German. doi: 10.1007/s00132-009-1458-y. PMID: 19629433.

28 - Wright JM, Crockett HC, Slawski DP, Madsen MW, Windsor RE. High tibial osteotomy. J Am Acad Orthop Surg. 2005 Jul-Aug;13(4):279-89. doi: 10.5435/00124635-200507000-00007. PMID: 16112984.

29 - Takeuchi R., Umemoto Y., Aratake M., et al. A mid-term comparison of open wedge high tibial osteotomy vs unicompartmental knee arthroplasty for medial compartment osteoarthritis of the knee. *Journal of Orthopaedic Surgery and Research.* 2010;5(1): p. 65. doi: 10.1186/1749-799x-5-65.

30 - Hantes ME, Natsaridis P, Koutalos AA, Ono Y, Doxariotis N, Malizos KN: Satisfactory functional and radiological outcomes can be expected in young patients under 45 years old after open wedge high tibial osteotomy in a long-term follow-up. *Knee Surg Sports Traumatol Arthrosc* 2018; 26:3199-3205

31 - Berruto M, Maione A, Tradati D, Ferrua P, Uboldi FM, Usellini E: Closing-wedge high tibial osteotomy, a reliable procedure for osteoarthritic varus knee. *Knee Surg Sports Traumatol Arthrosc* 2020; 28:3955-3961.

32 - Duivenvoorden T, Brouwer RW, Baan A, et al.: Comparison of closing-wedge and opening-wedge high tibial osteotomy for medial compartment osteoarthritis of the knee: A randomized controlled trial with a six-year follow-up. *J Bone Joint Surg Am* 2014; 96:1425-1432.

33 – Osteoarthritis – symptoms and causes (https://www.mayoclinic.org/diseases-conditions/osteoarthritis/symptoms-causes/syc-20351925)

34 – Knee Osteoarthritis; Hunter Hsu; Ryan M.Siwiec (https://www.ncbi.nlm.nih.gov/books/NBK507884/)

35– https://www.webmd.com/osteoarthritis/ostearthritis-of-the-knee-degenerative-arthritis-of-the-knee

36 - Joseph A. Buckwalter, James A. Martin, *Osteoarthritis*, Advanced Drug Delivery Reviews, Volume 58, Issue 2, 2006, Pages 150-167, ISSN 0169-409X

37 - https://www.physio-pedia.com/Knee_Osteoarthritis

38 - J.A. Buckwalter, D.R. Lappin, The disproportionate impact of chronic arthralgia and arthritis among women, Clin. Orthop., 372 (2000), pp. 159-168

39 - Cui A, Li H, Wang D, Zhong J, Chen Y, Lu H. Global, regional prevalence, incidence and risk factors of knee osteoarthritis in population-based studies. EClinicalMedicine. 2020 Dec;29–30:100587.

40 - Reyes Carlen et al. “Association Between Overweight and Obesity and Risk of Clinically Diagnosed Knee, Hip, and Hand Osteoarthritis: A Population-Based Cohort Study.” *Arthritis & rheumatology (Hoboken, N.J.)* vol. 68,8 (2016): 1869-75. doi:10.1002/art.39707

41 - King LK, March L, Anandacoomarasamy A. Obesity & osteoarthritis. *Indian J Med Res.* 2013;138:185–93.

42 – Man, G. S., and G. Mologhianu. “Osteoarthritis pathogenesis – a complex process that involves the entire joint”. *Journal of medicine and life* vol. 7,1 (2014): 37-41.

43 - Heijink A, Gomoll AH, Madry H. Biomechanical considerations in the pathogenesis of osteoarthritis of the knee, Knee Surgery, Sports Traumatology, *Arthroscopy.* 2012;20:423–435.

44 - Basilio Pueo, 'Application of motion capture technology for sport performance analysis', July 2017, Retos: Nuevas Tendencias en Educación Física, Deporte y Recreación 2017(32):241-247

45 - "Character Motion Systems", SIGGRAPH 94: Course 9

46 - Celik Y, Stuart S, Woo WL, Godfrey A. Gait analysis in neurological populations: Progression in the use of wearables. Med Eng Phys. 2021 Jan;87:9-29. doi: 10.1016/j.medengphy.2020.11.005. Epub 2020 Nov 13. PMID: 33461679.

47 - Correa TA, Baker R, Graham HK, Pandy MG. Accuracy of generic musculoskeletal models in predicting the functional roles of muscles in human gait. J Biomech. 2011 Jul 28;44(11):2096-105. doi: 10.1016/j.jbiomech.2011.05.023. Epub 2011 Jun 23. PMID: 21703627.

48 - Codina M, Navarrete M, Rezaee A, Castells-Rufas D, Torrelles MJ, Burkard S, Arndt H, Drevet S, Boudissa M, Tonetti J, Marque I, Moreau-Gaudry A, Castillejo A, Carrabina J. Gait Analysis Platform for Measuring Surgery Recovery. Stud Health Technol Inform. 2021 Oct 27;285:199-204. doi: 10.3233/SHTI210598. PMID: 34734874.

49 - Y Moon, J Sung, R An, ME Hernandez, JJ Sosnoff, Gait variability in people with neurological disorders: a systematic review and meta-analysis, Hum Mov Sci, 47 (2016), pp. 197-208

50 - States RA, Krzak JJ, Salem Y, Godwin EM, Bodkin AW, McMulkin ML. Instrumented gait analysis for management of gait disorders in children with cerebral palsy: A scoping review. Gait Posture. 2021 Oct;90:1-8. doi: 10.1016/j.gaitpost.2021.07.009. Epub 2021 Aug 3. PMID: 34358847.

51 - di Biase L, Di Santo A, Caminiti ML, De Liso A, Shah SA, Ricci L, Di Lazzaro V. Gait Analysis in Parkinson's Disease: An Overview of the Most Accurate Markers for Diagnosis and Symptoms Monitoring. Sensors (Basel). 2020 Jun 22;20(12):3529. doi: 10.3390/s20123529. PMID: 32580330; PMCID: PMC7349580.

52 - Bulat M, Korkmaz Can N, Arslan YZ, Herzog W. Musculoskeletal Simulation Tools for Understanding Mechanisms of Lower-Limb Sports Injuries. Curr Sports Med Rep. 2019 Jun;18(6):210-216. doi: 10.1249/JSR.0000000000000601. PMID: 31385836.

53 - OpenSim Documentation; site: https://simtk-confluence.stanford.edu:8443/display/OpenSim/User%27s+Guide

54 - Rajagopal A, Dembia CL, DeMers MS, Delp DD, Hicks JL, Delp SL. Full-Body Musculoskeletal Model for Muscle-Driven Simulation of Human Gait. IEEE Trans Biomed Eng. 2016 Oct;63(10):2068-79. doi: 10.1109/TBME.2016.2586891. Epub 2016 Jul 7. PMID: 27392337; PMCID: PMC5507211.

55 - Seth, A., Sherman, M., Reinbolt, J. A. & Delp, S. L. OpenSim: A musculoskeletal modelling and simulation framework for in silico investigations and exchange. Procedia IUTAM 2, 212–232 (2011).

56 - Blemker SS, Asakawa DS, Gold GE, Delp SL. Image-based musculoskeletal modeling: applications, advances, and future opportunities. J Magn Reson Imaging. 2007 Feb;25(2):441-51. doi: 10.1002/jmri.20805. PMID: 17260405.

57 - Delp SL, Anderson FC, Arnold AS, Loan P, Habib A, John CT, Guendelman E, Thelen DG. OpenSim: open-source software to create and analyze dynamic simulations of movement. IEEE Trans Biomed Eng. 2007 Nov;54(11):1940-50. doi: 10.1109/TBME.2007.901024. PMID: 18018689.

58 - Hicks JL, Uchida TK, Seth A, Rajagopal A, Delp SL. Is My Model Good Enough? Best Practices for Verification and Validation of Musculoskeletal Models and Simulations of Movement. J Biomech Eng. 2015 Feb 1;137(2):020905.

59 - Cappozzo A, Catani F, Leardini A, Benedetti MG, Croce UD. Position and orientation in space of bones during movement: experimental artefacts. Clin Biomech (Bristol, Avon). 1996 Mar;11(2):90-100. doi: 10.1016/0268-0033(95)00046-1. PMID: 11415604

60 - Leardini A, Sawacha Z, Paolini G, Ingrosso S, Nativo R, Benedetti MG. A new anatomically based protocol for gait analysis in children. Gait Posture. 2007 Oct;26(4):560-71. doi: 10.1016/j.gaitpost.2006.12.018. Epub 2007 Feb 8. PMID: 17291764.

61 - Lerner ZF, DeMers MS, Delp SL, Browning RC. How tibiofemoral alignment and contact locations affect predictions of medial and lateral tibiofemoral contact forces. J

Biomech. 2015 Feb 26;48(4):644-650. doi: 10.1016/j.jbiomech.2014.12.049. Epub 2015 Jan 5. PMID: 25595425; PMCID: PMC4330122.

62 - Kainz H, Wesseling M, Jonkers I. Generic scaled versus subject-specific models for the calculation of musculoskeletal loading in cerebral palsy gait: Effect of personalized musculoskeletal geometry outweighs the effect of personalized neural control. Clin Biomech (Bristol, Avon). 2021 Jul;87:105402. doi: 10.1016/j.clinbiomech.2021.105402. Epub 2021 Jun 1. PMID: 34098149.

63 - Song K, Anderson AE, Weiss JA, Harris MD. Musculoskeletal models with generic and subject-specific geometry estimate different joint biomechanics in dysplastic hips. Comput Methods Biomech Biomed Engin. 2019 Feb;22(3):259-270. doi: 10.1080/10255842.2018.1550577. Epub 2019 Jan 20. PMID: 30663342; PMCID: PMC6478547.

64 - Lenaerts G, Bartels W, Gelaude F, Mulier M, Spaepen A, Van der Perre G, Jonkers I. Subject-specific hip geometry and hip joint centre location affects calculated contact forces at the hip during gait. J Biomech. 2009 Jun 19;42(9):1246-51. doi: 10.1016/j.jbiomech.2009.03.037. Epub 2009 May 21. PMID: 19464012.

65 - Akhundov R, Saxby DJ, Diamond LE, Edwards S, Clausen P, Dooley K, Blyton S, Snodgrass SJ. Is subject-specific musculoskeletal modelling worth the extra effort or is generic modelling worth the shortcut? PLoS One. 2022 Jan 25;17(1):e0262936. doi: 10.1371/journal.pone.0262936. PMID: 35077508; PMCID: PMC8789151.

66 - Valente G, Crimi G, Vanella N, Schileo E, Taddei F. nmsBuilder : Freeware to create subject-specific musculoskeletal models for OpenSim. Comput Methods Programs Biomed. 2017 Dec;152:85–92.

67 - Demers MS, Pal S, Delp SL. Changes in tibiofemoral forces due to variations in muscle activity during walking. J Orthop Res. 2014 Jun;32(6):769-76. doi: 10.1002/jor.22601. Epub 2014 Feb 26. PMID: 24615885; PMCID: PMC4409006.

68 - Delp SL, Loan JP, Hoy MG, Zajac FE, Topp EL, Rosen JM. An interactive graphics-based model of the lower extremity to study orthopaedic surgical procedures. IEEE Trans Biomed Eng. 1990 Aug;37(8):757–67.

69 - Vicon. Vicon Motion Systems Ltd UK - https://www.vicon.com/.

70 - https://github.com/IOR-BIC/ALBA

71 – D. Paley “Principles of deformity corrections”, 1st ed. 2002. Corr. 3rd printing 2005, Springer-Verlag Berlin Heidelberg GmbH

72. Mokka. Mokka, Motion Kinematic and Kinetic Analyzer - https://biomechanical-toolkit.github.io/mokka/index.html.

73. Matlab r2021b, Natick, Massachusetts: The mathworks Inc.; 2021.

74 - Wesseling M, Meyer C, Corten K, Desloovere K, Jonkers I. Longitudinal joint loading in patients before and up to one year after unilateral total hip arthroplasty. Gait Posture. 2018 Mar;61:117-124. doi: 10.1016/j.gaitpost.2018.01.002. Epub 2018 Jan 5. PMID: 29324297.

75 - Melzner M, Engelhardt L, Simon U, Dendorfer S. Electromyography-Based Validation of a Musculoskeletal Hand Model. J Biomech Eng. 2022 Feb 1;144(2):021005.

76 - Jungtaubl D, Aurbach M, Melzner M, Spicka J, Suss F, Dendorfer S. EMG-Based Validation of Musculoskeletal Models Considering Crosstalk. In: 2018 International Conference BIOMDLORE [Internet]. Bialystok: IEEE; 2018 [cited 2022 Mar 13]. p. 1–4. Available from: https://ieeexplore.ieee.org/document/8467211/

77 - Zeighami A, Aissaoui R, Dumas R. Knee medial and lateral contact forces in a musculoskeletal model with subject-specific contact point trajectories. J Biomech. 2018 Mar;69:138–45.

78 - Saliba CM, Brandon SCE, Deluzio KJ. Sensitivity of medial and lateral knee contact force predictions to frontal plane alignment and contact locations. J Biomech. 2017 May;57:125–30.

79 - Dumas R, Zeighami A, Aissaoui R. Knee Medial and Lateral Contact Forces Computed Along Subject-Specific Contact Point Trajectories of Healthy Volunteers and Osteoarthritic Patients. In: Ateshian GA, Myers KM, Tavares JMRS, editors. Computer Methods, Imaging and Visualization in Biomechanics and Biomedical Engineering [Internet]. Cham: Springer International Publishing; 2020 [cited 2022 Mar 14]. p. 457–63. (Lecture Notes in Computational Vision and Biomechanics; vol. 36).

80 - Valente G, Pitto L, Stagni R, Taddei F. Effect of lower-limb joint models on subject-specific musculoskeletal models and simulations of daily motor activities. J Biomech. 2015 Dec 16;48(16):4198-205. doi: 10.1016/j.jbiomech.2015.09.042. Epub 2015 Oct 23. PMID: 26506255.

81 - Wesseling M, Meyer C, Corten K, Simon JP, Desloovere K, Jonkers I. Does surgical approach or prosthesis type affect hip joint loading one year after surgery? Gait Posture. 2016 Feb;44:74-82. doi: 10.1016/j.gaitpost.2015.11.009. Epub 2015 Nov 23. PMID: 27004636.